A REVIEW OF PHENOMENOLOGICAL MODELS FOR PION PRODUCTION ON NUCLEI WITH PROTONS INCIDENT AT INTERMEDIATE ENERGIES

by

DIANA JOYCE LIM

B.Sc., University of Western Ontario, 1974

A THESIS SUBMITTED IN PARTIAL FULFILLMENT

OF THE REQUIREMENTS FOR THE DEGREE OF

MASTER OF SCIENCE

in the department

of

Physics

We accept this thesis as conforming

to the normal standard

[redacted]

University of Victoria

August 1977

ABSTRACT

Supervisor: Dr. Charles Picciotto

Phenomenological models for single pion production from proton collisions with nuclei at rest are reviewed. The incident energies considered are from threshold to approximately 800 MeV. Due to the short range of the strong interaction at these energies, compared with internucleon distances in the nuclei, the scattering with a nucleus is highly incoherent, and the production is predominantly the single nucleon-nucleon interaction (ie. the impulse approximation). Modifications of the free nucleon-nucleon interaction due to the nuclear medium, such as the inclusion of the Fermi motion of the target nucleon, multiple scattering effects and nuclear potentials, are included in an ad hoc manner. The upper energy limit of 800 MeV for the models considered, restricts the dominant production mechanism to the formation of the $\Delta(1236)$ isobar in the intermediate state.

Due to the limited available data, the models considered are concerned only with the characteristics of the emerging pion, and the final state of the nucleus is ignored. This often results in one or more free parameters which may give reasonably good fits to experimental data,

but this correlation may have little physical meaning. Certain aspects of the production mechanisms and of nuclear structure can, however, be investigated successfully with these models. More success can be expected with models in which the final state of the nucleus is taken into account.

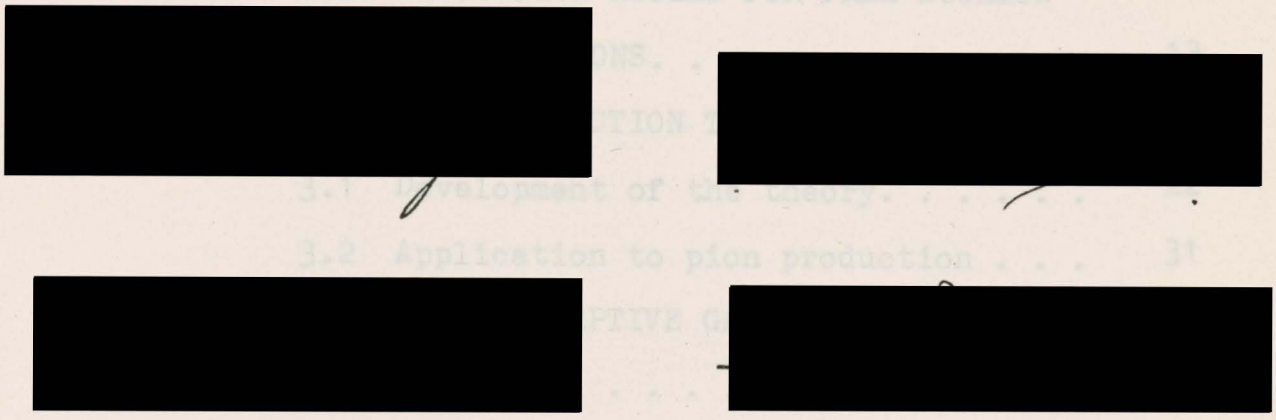

TABLE OF CONTENTS

		Page
ABSTRACT		ii
LIST OF TABLES		vi
LIST OF FIGURES		vii
ACKNOWLEDGEMENTS		xi
CHAPTER 1	INTRODUCTION	1
CHAPTER 2	PION PRODUCTION MODELS FOR FREE NUCLEON-NUCLEON COLLISIONS	13
CHAPTER 3	MULTIPLE DIFFRACTION THEORY	22
	3.1 Development of the theory	22
	3.2 Application to pion production	31
CHAPTER 4	CLASSICAL ABSORPTIVE GAS MODEL: BEDER AND BENDIX	34
CHAPTER 5	GEOMETRICAL MODELS	49
	5.1 Importance of the nuclear geometry in pion production	49
	5.2 Geometrical models with no nuclear corrections	53
	5.3 Geometrical models with nuclear corrections	65
	5.4 Extension to include multiple scattering with and without nucleon recoil	81
CHAPTER 6	SUMMARY AND CONCLUSIONS	87

Page

REFERENCES 140

APPENDIX A THE NUCLEON-NUCLEON INTERACTION 144

APPENDIX B ISOTOPIC SPIN WAVE FUNCTIONS FOR πN SYSTEMS 146

LIST OF TABLES

TABLE		Page
II.1	Partial wave analysis of $pN \rightarrow NN\pi^i$	98
II.2	Reactions for $NN \rightarrow NN\pi$ in terms of isotopic spin cross sections.	99
II.3	Experimental results for π production on free nucleons and complex nuclei	100
II.4	The isobar model for $pN \rightarrow NN\pi$	101
II.5	The isobar model and Fermi statistical weights for $pN \rightarrow NN\pi$.	102
II.6	Partial Wave analysis of $pp \rightarrow \pi NN$ for the Mandelstam model	103
III.1	Effective nucleon number for various targets for various.	104
IV.1	Averaged production rates in μb/MeV.sr	105
IV.2	Effective nucleon number	105
V.1	Results for total $\pi^{\pm}$ production cross sections (mb)	106
V.2	Origins of produced pions sorted into six nuclear bins according to Fig. 5.13.	106
V.3	Effects of the various nuclear corrections (one at a time) on production cross sections for Pb	107
V.4	Effects of nuclear corrections (an improvement on Table V.3)	108

LIST OF FIGURES

FIGURE		Page
1.1	The total and the elastic cross sections in the pp interaction. Total cross sections are taken from Lock and Measday (1970).	108
1.2	The total and the elastic cross sections in the np interaction.	108
2.1	The total cross section for the T=1/2 and T=3/2 isotopic spin states of the πN interaction. . . .	109
2.2	Comparison of the total π^+p cross section (full line) and $8\pi\lambda^2$ (dashed line) to illustrate that it is probably the J=3/2 angular momentum state that is resonating.	109
2.3	The π^+p mass distribution from the reaction $\pi^+ p \rightarrow \pi^0 \pi^+ p$ at 979 MeV. The curve is the prediction of the isobar model.	110
3.1	Diagram showing the definition of the transverse components s_j of the nucleon co-ordinate vectors.	111
3.2	Contributions of the various multiple scattering terms to the amplitude for elastic scattering of protons by He. The intersections are indicated by arrows and determine the momentum transfers near which the angular distribution has zeros . .	112
3.3	T(B) is the integral of the nucleon density function along the straight line path given by the impact parameter b. $T(B)=A\int_{-\infty}^{\infty}\int(\rho(b+\frac{E}{\|E\|}z)dz$.	113
3.4	The shape of the nuclear density function and thickness function for Cu are shown in the upper curves. The lower one shows the way in which the contributions to quasi-elastic scattering by Cu depend on the impact parameter .	114
3.5	Contributions of multiple quasi-elastic scattering of protons by Cu. The results derived for momentum transfer outside the region of diffraction region, $-t>0.1(GeV/c)^2$, have been extrapolated to t=0.	115
3.6	Comparison of experiment and theory for the effective number of nucleons $N_1(A)$ which scatters quasi-elastically in a nucleus A.	116

3.7 Comparison with experiment of the theoretical distibution for quasi-elastic scattering of protons by Cu. 117

3.8 The cross sections for positive pion production T_p=600 MeV. 118

3.9 The cross sections for negative pion production T_p=600 MeV. 118

3.10 The effective nucleon number $N_{\downarrow}$ for incoherent quasi-elastic processes. The Woods-Saxon density has a radius $c=1.07A^{1/3}$fm and surface thickness t=2.4fm. The sum of the cross sections (at 0°.8 and 21°.5) for π^+ production in the pp interaction is taken to be 36 b/MeV.sr. 119

4.1 The real part V_R and the imaginary part V_I of the potential well depth for pion nucleus scattering. . 120

4.2 Phase space calculations 121

4.3 Differential cross sections for 21°.5, 600 MeV protons 121

4.4 Sensitivity to Fermi averaging. 122

4.5 Two nucleon absorption coefficient a and charge exchange cross section σ_{CE}(both Fermi averaged. . . 122

4.6 Results for 21°.5 , 600 MeV protons on ^{12}C. 123

4.7 Results for 21°.5 , 600 MeV protons on ^{208}Pb 123

5.1 Model geometry for the case ϕ=0. In general, the pion is produced at r=(b,z,ϕ) and goes out at an angle θ to the incident z direction. The path lengths in the nucleus for the proton and pion are d_p and d_π, respectively. 124

5.2 The pion absorption cross section $\sigma_{\pi,abs}$ as fitted to the 15° Pb data, for various values of the proton absorption cross section $\sigma_{p,abs}$. 125

5.3 The scaled total production cross section $\sigma(\pi^+)/Z^{1/3}$ versus A. Experimental points are taken from Cochrane et al. (1972) 126

5.4 The scaled production cross section $\sigma(\pi^-)/N^{2/3}$ versus A. Experimental points are taken from Cochran et al. (1972). 126

5.5 The angular distributions $d\sigma/d\Omega$ in mb/sr for π^+ production from C, Cu and Pb. The solid lines connect the calculated values. 127

5.6 The angular distributions $d\sigma/d\Omega$ in mb/sr for π^- production from C, Cu and Pb. The solid lines connect the calculated values. 127

5.7 The π^+ spectra $d^2\sigma/dTd\Omega$ in μb/MeV.sr for C, Cu and Pb at $\theta=30^\circ$, 90° and 135°. The calculated points are connected by solid lines 128

5.8 The π^- spectra $d^2\sigma/dTd\Omega$ in μb/MeV.sr for C, Cu and Pb at $\theta=30^\circ$, 90° and 135°. The calculated points are connected by solid lines. 129

5.9 The phase space model predictions for the pion spectrum in the reaction NN πNN at $\theta=15^\circ$ and $T_p=740$ MeV: (a) reaction on free nucleons; (b) effect of averaging over Fermi motion; (c) effect of Fermi averaging and potential for the incident nucleon. $k_F=250$MeV/c, B=8MeV and $V_1=26$MeV. 130

5.10 Effects of the pion potential on pion kinematics (a) function of f(x); (b) $p_{\pi,in}$ and $p_\pi=(E^2-\mu^2)^{1/2}$ versus T; (c) effective mass squared, $\mu^{*2}=E_\pi^2-p_\pi^2$, in in units of μ^2. 131

5.11 Pion charge exchange cross sections as functions of pion energy: (a) both pion and nucleon free; (b) effects of Fermi averaging and Pauli Exclusion Principle, $k_F=250$ MeV/c; (c) same as (b) with the pion potential. 132

5.12 Fits to $\sigma_{\pi,abs}(T)$: (a) full calculation with nuclear corrections; (b) fits with no nuclear corrections (Fig. 5.2) with $\sigma_{N,abs}=30$mb. ; (c) same as (a) with $\sigma_{N,abs}=30$mb rather than 5.6 mb. (d) Beder's prediction from Fig. 4.5 132

5.13 Division of the nucleons into bins. The case of Pb is illustrated: $r(90\%)=5.6$fm and $r(0.3\%)=9.7$fm. . . .133

5.14 Pion absorption cross sections deduced from pPb with and without Fermi averaging of $\sigma_{\pi,abs}$. Error bars are from the pPb data. 134

5.15 The best fit to the pion absorption cross section $\sigma_{\pi,abs}$ as fitted to the $d\sigma^+/dT$ for Pb. 134

5.16 Comparison of the π^+ spectrum $d\sigma^+/dT$ in three models using the pion absorption cross section from Adler's model 135

5.17 Comparison of the π^- spectrum $d\sigma^-/dT$ in three models using the pion absorption cross section from Adler's model 135

5.18 Comparison of the π^+ angular dependence $d\sigma^+/d\Omega$ in three models 136

5.19 Comparison of the π^- angular dependence $d\sigma^-/d\Omega$ in three models 137

5.20 Calculated and measured $d\sigma/dT$. Experimental data are taken from Cochran et al. (1972) 138

5.21 Calculated and measured $d\sigma^+/d\Omega$. Data from Cochran et al. (1972). 139

5.22 Calculated and measured $d\sigma^-/d\Omega$. Data from Cochran et al. (1972) 140

ACKNOWLEDGEMENTS

The author would like to express her thanks to Dr. C. E. Picciotto for his guidance and his patience during the preparation of this thesis.

The author would also like to thank Mr. Joachim Klingermann for all his encouragement.

CHAPTER 1

INTRODUCTION

Much of the work done in studying collisions of two hadrons (e.g. nucleons) has been concentrated on collisions in which there are only two particles in the final state. This may include either elastic scattering in which the final particles are the same as the initial particles or exchange processes in which the final particles differ from the initial pair by certain quantum numbers, such as isospin. In recent years, increased interest has been shown in production processes in which there are three or more particles in the final state. It is expected from both a theoretical and an experimental standpoint that the production processes would be more difficult to deal with than would be the two particle final state cases. This can be seen from a consideration of the dimensionality of the two cases. For a particle incident upon a target at rest, which results in n particles in the final state, there will be $3n$ momentum components limited by only 4 energy-momentum constraints leaving $3n-4$ independent variables for each production event. This gives only two independent variables for a two body process ($n=2$) which are normally taken to be the incident particle momentum

and the scattering angle. For single particle production, where n=3, there are 5 independent variables, and 8 for double particle production, where n=4. For simplicity, only single particle production will be considered in these models.

The problem of dimensionality for production processes is compounded by the difficulty in the application of quantum field theory to strongly interacting particles. This results from a perturbation expansion in terms of the coupling constant for the interaction; this has been a successful approach for the electromagnetic interaction where the coupling constant is small ($\div 1/137$), but not for the strong interaction which has a large coupling constant (≥ 1). A field-theoretical approach has been successful only in giving a qualitative picture of the strong interaction.

The picture which emerges from quantum field theory is that the interactions between elementary particles occur through exchanges of "virtual" or "off-the-mass-shell" particles. They are virtual in the sense that they are not observable, and they do not obey the Einstein condition that the suare of the rest mass of a particle equals the square of its four-momentum. The quantization of the electromagnetic field indicates that the electomagnetic field is composed of virtual photons, and an electromagnetic interaction between particles is interpreted as the exchange of one or more photons. Analogously, quantization of the

strong field predicts that the strong interaction is equivalent to the exchange of one or more virtual mesons. The type and number of mesons exchanged will depend on the magnitude of the interaction.

If strongly interacting particles have sufficient relative kinetic energy, this energy can be used to change one or more virtual mesons into real, i.e. observeable, mesons which obey the Einstein condition. The seven possible reactions for single pion production from nucleon-nucleon collisions are given by

$$pp \rightarrow \pi^+ pn \qquad (1.1a)$$

$$pp \rightarrow \pi^o pp \qquad (1.1b)$$

$$pn \rightarrow \pi^+ nn \qquad (1.2a)$$

$$pn \rightarrow \pi^o pn \qquad (1.2b)$$

$$pn \rightarrow \pi^- pp \qquad (1.2c)$$

$$nn \rightarrow \pi^o nn \qquad (1.3a)$$

$$nn \rightarrow \pi^- pn \qquad (1.3b)$$

(Note that proton collisions include only Eq.(1.1) and (1.2).)

The theoretical threshold for single pion production from nucleon-nucleon collisions is easily calculated using standard relativistic kinematics. At threshold, by definition, all particles are at rest in the centre-of-mass frame. For single pion production for a nucleon incident upon another nucleon at rest, the threshold involves an initial kinetic energy of approximately 290 MeV.

It might seem that with only a qualitatively successful idea of the two nucleon interaction, it might be futile to consider production processes in which there are more than two final particles. It is felt by many, however, that an understanding of nucleon dynamics, and hadron dynamics in general, may come from a combined study of the 2-body and the n-body processes. It is likely that the dynamics of the two types of processes possess many similarities. It is hoped that a study of production processes may offer information for models for 2-body scatterings. In terms of available data alone, the importance of considering production processes can be seen. Above threshold, the p-p inelastic cross section rises quickly, and comprises 50% of the total cross section by 900 MeV. The same is true for n-p collisions (Figs. 1.1 and 1.2).

Production processes are, however, not merely an extension of 2-body processes, but also possess characteristics which are unique to production. This is seen, for example, in the formation of intermediate resonant states which subsequently decay to form the final particles, including the "produced" particle(s).

The formulation of a theoretical model for pion production from nucleon-nucleon or nucleon-nucleus collisions may be attempted using a field-theoretical or a phenomenological approach. As mentioned, field-theoretical

calculations have had limited success for strong interactions. Although not a complete theory, a phenomenological model offers insight into the mechanisms of the processes involved and yields a strong theoretical foothold for the explanation of experimental data. Increasing experimental data will allow the development of increasingly sophisticated phenomenological models, and a better understanding of the dynamics involved will, hopefully, result.

The first phenomenological model for pion production was developed by Watson and Brueckner (1951) in order to analyze recently obtained data for production near threshold for free nucleon-nucleon collisions. They found that the data could be easily analyzed, at low energies, using an angular momentum analysis of the scattering matrix, and applying conservation of angular momentum, parity and isotopic spin. An angular momentum analysis was a natural approach. Near threshold most of the incident energy goes into the rest mass of the pion, implying large momentum transfers. This, in turn, implies a range of interaction for the production process ($\div \hbar/Q$, where Q is the momentum transfer) which is very small compared to the range of the nuclear force. The short range of the interaction and the low kinetic energies involved both motivated the angular momentum analysis.

Rosenfeld (1954) extended the angular momentum analysis to incident energies of about 400 MeV. An extensive angular

momentum and isotopic spin analysis, valid up to 600-650 MeV, was derived by Mandelstam (1958); this was extended, by Vovchenko (1966), to energies of about 700-800 MeV. Above these energies, there are too many angular momentum states, and a partial wave decomposition becomes too complicated.

The most significant feature to emerge from the angular momentum and isotopic spin analysis of pion production was that, above threshold and up to 800MeV, the pion and one of the final state nucleons are in a resonant $J=T=3/2$ state (where J is the total angular momentum, and T is the total isotopic spin). This was recognized by Rosenfeld as a result of his analysis, and was supported by π-p scattering experiments.

The discovery of a pion-nucleon resonant state was the basis for the Isobar Model, postulated by Lindenbaum and Sternheimer (1958), in which pion production from nucleon-nucleon collisions takes place via an intermediate state which consists of an isobar, or a resonant state, and a nucleon. The isobar then decays to a pion and a nucleon. This is given schematically by

$$\begin{array}{l} N+N \rightarrow \Delta+N \\ \qquad\quad \searrow \\ \qquad\quad \pi+N \end{array} \qquad (1.4)$$

The final states of the particles are, thus, not determined purely by statistical weights, as predicted by Fermi (1950), but there exist preferred final states which are determined by the requirement that the final πN state have a fixed angular momentum and isotopic spin. At the energies with

which we are concerned, this is a J=T=3/2 state, also called the $\Delta(1236)$; at higher energies, different isobars will be formed.

The concepts behind these free nucleon models, and the models themselves, are directly useful for constructing models for nucleon-nucleus collisions. This is due to the fact that, for nucleon-nucleus collisions at incident nucleon energies which are above the single pion production threshold for nucleon-nucleon collisions, the interaction with the nucleus is highly incoherent. This is easily seen by noting that the de Broglie wavelength (h/p, where p is the particle momentum) for a 500 MeV proton is 0.2 fm., while a typical internucleon distance is 1.9 fm. At energies relevant to this thesis, the incident nucleon will tend to interact with only one target nucleon at a time, as described by the impulse approximation, so that the pion production process will be a result, predominantly, of free nucleon-nucleon interactions.

The number of nucleon-nucleon interactions assumed to occur within the nucleus will be a variable of the model used, but due to the strong absorption within the nucleus, the assumption of only a single scattering of each incident nucleon is not unrealistic. This latter assumption greatly simplifies the calculations involved; very lengthy and complicated computations are a main difficulty of multiple scattering models. Indeed, it is found by Yang, Sparrow, Holstein and Sternheim (1976), that results from multiple

scattering models are no better than simpler single scattering models with the same parameters. Ignoring higher order scattering tends to underestimate the number of low energy, large angle pions produced, but the total cross sections are not expected to be affected..

An alternative to multiple scattering calculations for the scattering of particles off nuclei is multiple diffraction theory, developed by Glauber (1952 and 1958), which treats the nucleus as an optically diffracting medium. It is a high energy calculation, but it is also applicable to the intermediate energy range which is of interest here. The impulse approximation is assumed, and each target nucleon acts as an independent diffracting centre. Its applicability to intermediate energies is limited by the assumption of only forward scattering. The advantage of multiple diffraction theory over multiple scattering theory is that it results in an expansion of different orders of scattering off the target nucleons; the n-th order scattering term gives the contribution from scattering of the incident nucleon off n target nucleons.

Glauber theory was applied directly to pion production by Margolis (1968) and Kolbig and Margolis (1968) in which the formation of the intermediate (3/2,3/2) resonant πN state is assumed. Only the first term in Glauber's expansion for incoherent, quasi-elastic scattering is used, that is to say, only single scattering is assumed. Although Kolbig and

Margolis were able to obtain information on nuclear density distributions, an outstanding limitation to their calculation was their neglect of many nuclear effects which greatly alter the free production rate.

These effects are included, to varying degrees, in papers by Beder and Bendix (1971) and by Sternheim and Silbar (1972 and 1973); they also account for the angular distribution of the exiting pions. Their models assume the impulse approximation, and are thus mathematically equivalent to Glauber theory for incoherent, quasi-elastic scattering, but are conceptually and computationally much easier to deal with. Both models assume that the free nucleon-nucleon production reaction proceeds via the (3/2,3/2) resonance: Beder and Bendix use a free production cross section based upon Mandelstam's T-matrix and Sternheim and Silbar use, directly, the experimentally measured cross section for the reaction $pp \rightarrow \pi^+pn$. The free production cross sections are then modified to account for the nuclear effects.

There are three important modifications of the free production cross section which are necessary when considering production from nucleons bound in a nucleus. These modifications account for the Fermi energy of the target nucleons, the Pauli Principle which will forbid some collisions, and secondary scatterings which include absorption (attenuation) of the incident nucleon and exiting pion as well

as charge exchange processes.

Target nucleons within a nucleus are constrained by the Pauli Exclusion Principle, since they are fermions in a bound system, to certain energy levels within the nucleus. This gives each a certain nonzero energy within the rest frame of the nucleus which is the Fermi energy of that particle. This results in a total energy of the bound nucleon-nucleon system which is greater than that for the free nucleon-nucleon system, and pion production is possible at lower incident nucleon energies in collisions with nuclei than with free nucleons. Pion production has been observed with incident energies as low as 185 MeV (Cohen et al. 1963).

The Pauli Exclusion Principle enters not only through the Fermi motion of the target nucleons, but also in considering the allowed final states of the nucleons. It will forbid those collisions which leave the final nucleons with energies which correspond to states of the nucleus which are occupied by other nucleons.

Both the incident nucleon and the exiting pion undergo strong attenuation by the nuclear medium. For this reason, it is expected that most of the pions will be produced in the surface of the nucleus, in particular, in a ring normal to the direction of the incident nucleon momentum. This implies a dependence of the production cross section on the geometry of the nucleus from which nuclear surface information may

be obtained. This, as mentioned, supports the assumption of only single scattering.

The charge exchange processes will include pion charge exchange given by $\pi^+ n \rightarrow \pi^o p$ and $\pi^- p \rightarrow \pi^o n$ and nucleon charge exchange given by $pn \rightarrow np$. The pion charge exchange processes have an especially important effect; neglecting them was a major weakness of the models of Kolbig and Margolis. It will be seen that the exchange processes affect the relative numbers of the three charge states of the pions; for production from incident protons, charge exchange will tend to decrease the π^+/π^- ratio. The charge exchange process, since it is a secondary scattering, will tend to increase the number of pions, particularly π^-'s, predicted at large angles and low energies.

The various nuclear effects are accounted for in an ad hoc manner, usually relying heavily on experimental data, in particular, on two particle data. This is done very differently by the various authors.

By chapter, the above models will be discussed in detail: Chapter 2 gives a brief outline of the development of the Isobar Model of the pion-nucleon interaction and its application to the angular momentum analyses of pion production. In Chapter 3, Section 3.1, Glauber's multiple diffraction theory is developed and in Section 3.2 its application to nuclear pion production by Kolbig and Margolis

is shown. Chapter 4 describes and gives the results of the "absorptive gas" model of Beder and Bendix for π^+ production from proton collisions on nuclei. Chapter 5, Section 5.1 discusses the important connection of nuclear geometry to nuclear pion production; Sections 5.2 and 5.3 discuss the "geometrical" models of nuclear pion production of Sternheim and Silbar; Section 5.4 describes and extension of the Sternheim and Silbar models to include multiple scattering with and without nucleon recoil. Chapter 6 compares the successes and the failures of the above models and indicates the future direction of models for nuclear pion production.

CHAPTER 2

PION PRODUCTION MODELS FOR FREE NUCLEON-NUCLEON COLLISIONS

Since the basis of the production mechanism for the nucleon-nucleus collisions at intermediate energies is the free nucleon-nucleon scattering interaction, it is important to first consider this basic interaction. The models for free nucleon-nucleon scattering form a foundation for the construction of models for the nucleon-nucleus case.

The possible reactions with single pion production are given in Eqs. (1.1), (1.2) and (1.3); the proton induced collisions are represented in the first two equations.

Brueckner (1951) and Watson and Brueckner (1951) developed the first phenomenological model for pion production from nucleon-nucleon collisions using an angular momentum analysis of the scattering matrix, valid near threshold. The matrix element for the cross section is then held constant, which is true for a sufficiently small energy range, except for a factor due to the final state nucleon-nucleon interaction. As was pointed out by Brueckner (1951) and Watson (1952), the reaction cross section of pion production is greatly affected by the strong interaction of the final nucleons, which occurs while within the range of the pion production interaction, i.e. the impact parameter for the pion production reation is

less than that of the nuclear forces. This is due to the existence of a bound state at nearly zero energy.

The use of a partial wave analysis of the scattering matrix provides a good means for a partial wave analysis of newly-acquired experimental data to be made. It allowed a comparison of the energy spectrum and the angular distributions of the pions, and the excitation functions of the different cross sections with the available data for $pp \to np\pi^+$.

In the partial wave analysis, the final state nucleons are assumed to be in a relative S-state (zero relative angular momentum). This is supported by the experimental pronounced high energy for the pions produced. Calculations indicate that the pion will be in an s- or a p-state relative to the nucleons. This is valid for energies up to only 400 MeV. Inclusion of a final NN P-state would extend the validity to 600 MeV.

The contributions from the different states means a different predicted angular distribution for the pion:

$$\begin{aligned} (S,s) &\propto 1 \\ (S,p(\mathrm{sym})) &\propto q^2 \\ (S,p(\cos^2\theta)) &\propto q^2\cos^2\theta \end{aligned} \qquad (2.1)$$

where q is the momentum of the pion and θ is the exit angle of the pion (between q and p , the relative momentum of the initial two-nucleon system). For an S-state final nucleon, the angular distribution of the pions will by given by Eq. (2.1), while if

there is a nucleon-nucleon P-wave contribution, there will be an extra p'^2 factor.

The angular distributions are fitted to the data with proper adjustment of the multiplicative numerical factors to determine the cross section. Of interest here, however, is not the calculation of the cross section, itself, but only the angular momentum analysis of the $NN \rightarrow \pi NN$ interaction.

By applying the Pauli Principle and the conservation of angulare momentum, isotopic spin and parity, there are only four possible transitions when the final nucleons are in a relative S-state and the pion is in either an s- or a p-state relative to the final NN system. The transitions are:

$$\begin{aligned} {}^3P_1 &\rightarrow {}^3S_1 s_1 \\ {}^1S_0 &\rightarrow {}^3S_1 p_0 \\ {}^1D_2 &\rightarrow {}^3S_1 p_2 \\ {}^3P_0 &\rightarrow {}^1S_0 s_0 \end{aligned} \qquad (2.2)$$

These reactions can be written in terms of three cross sections, σ_{31}, σ_{10} and σ_{11}, where the subscripts are the total isotopic spins of the initial and the final NN systems. (Table II.1). It is useful to note that $\sigma_{10} = \sigma_{10}(np) + \sigma_{10}(d)$ where the first term refers to production of an unbound T=0 np system and the latter refers to production of a bound deuteron state; an np system may have T=0 or T=1, but for a deuteron T=0 only. Note that σ_{00} would violate conservation of isotopic spin for the production of a T=1 pion.

Comparison of experiment (Table II.3) with partial wave analysis predictions show that there is a contradiction if the pion is emitted predominantly in an s-state; it is expected from Table II.1 that if the pion is in an s-state that $\sigma(pp \rightarrow \pi^0) \div \sigma(pn \rightarrow \pi^-) \div \sigma(pn \rightarrow \pi^+)$. On the other hand, it is predicted that if the pion is predominantly in a p-state, then $\sigma(np \rightarrow \pi^0) \div \sigma(np \quad \pi^+) + 1/2\ \sigma(pp \rightarrow \pi^+)$ which is consistent with the data. Also from Table II.1 it is expected that if the pion is in a p-state then $pp \rightarrow \pi^0$ is forbidden which is also consistent with the experiment.

The angular distributions also agree with a $\cos^2\theta$ distribution, which is compatible with a p-state pion, and nucleons in a final S-state.

By 1954, there was sufficient data available for Rosenfeld (1954) to do an extensive partial wave analysis comparing the phenomenological theory of Watson and Brueckner to the data. Data had become available for np as well as for pp collisions; reactions were studied to energy down to only 10 MeV above threshold where s-state pions become important, and cross sections up to 50 MeV above threshold. Rosenfeld, again, by using charge independence (ie. conservation of isotopic spin) expresses the single pion production reaction in terms of the three independent cross sections σ_{10}, σ_{01}, and σ_{11}. It was well recognized by 1954 that at such low energies there was a strong attractive S- state interaction between

nucleons, in contrast to a relatively weak P-state interaction. This would allow the enhancement of the low energies observed for the final state nucleons; most of the energy is made available to the pion. It is expected, and observed, that the final state interactions in order of dominance will, in general be Sp, Ss, Pp and Ps. Consider the Sp interactions.

It is expected that the anisotropic reaction $^1D_2 \rightarrow {}^3S_1P_2$ will dominate over the $^1S_0 \rightarrow {}^3S_1P_1$ since it is favoured by a statistical factor of $2J+1=5$. It also dominates over all other Sp and Ss reactions by a factor of at least $2J+1/2j+1 = 5/3$. For this reason, it is expected that σ_{10} would dominate over the other cross sections σ_{01} , σ_{11} . For σ_{10} , only, the final nucleons are in a triplet, rather than a singlet state which allows for deuteron formation, and this roughly doubles the cross section. Another extremely significant factor is that it had been recently determined by πp scattering, at intermendiate energies, there exists a strong interaction between a pion and a nucleon in a state with angular momentum and isotopic spin of 3/2. Of the six possible reactions for Sp and Ss final states, only the reaction (which is associated only with σ_{10}) allows this (3/2,3/2) πN state. This (3/2,3/2) interaction is also possible in Ps and Pp final states which are constituents of σ_{10} and σ_{11} . There is no possibility of a πN state with T=3/2 for σ_{01} , since combination of this with another

nucleon (T=1/2) cannot result in a total isotopic spin of zero.

Thus the $^1D_2 \rightarrow {}^3S_1 p_2$ reaction is favoured both statistically and by the (3/2, 3/2) interaction.

The realization of the resonant (3/2,3/2) πN interaction was an important development in the theory of pion production and is the basis of the phenomenological models discussed.

As mentioned, this resonant nature had previously been indicated from πp scattering experiments; all cross sections (elastic, inelastic, charge exchange) contained sharp peaks which indicated resonances, the most striking appearing at a pion energy of 180 MeV. This resonance nature was possible, in terms of isotopic spin, to be either in a total T=1/2 or T=3/2 state (pion with T=1 and nucleon with T=1/2). In Figure 2.1 can be seen the pure T=1/2 and 3/2 isotopic spin cross sections; except near threshold, it is the T=3/2 resonance which is dominant up to pion energies of 900 MeV. The peaks, seven of which are easily identifiable, are well separated which allows for easy identification. The resonances are normally classed according to their masses, $m_\Delta = m_\pi + m_N + T_{\text{centre-of-mass}}$; the (3/2,3/2) resonance which is of interest here is normally referred to as $\Delta(1236)$.

One can compare the πp cross sections with the cross section predicted from scattering theory for a resonance state denoted by J and l, the total and orbital angular momenta. From scattering theory it is known that $\sigma(J) = 2\pi\lambda^2(2J+1)$

so that $\sigma(\frac{3}{2}) = 8\pi\lambda^2$. Figure 2.2 compares the πp cross section with $\sigma(\frac{3}{2}) = 8\pi\lambda^2$ which clearly indicates that the peak is due to the J=3/2. resonanace. Another method is to make a plot of the invariant mass of the πp pair from πp scattering reactions. Figure 2.3 shows such a result for an initial pion pair for an initial pion energy of 979 MeV, which clearly indicates a baryon of mass 1236 MeV.

This indicates that pion production from πN collisions is a two stage process, the intermediate stage being a resonant state of mass 1236 MeV, and a pion. The resonance then decays into a pion and a nucleon, ie.

$$\pi^+ p \rightarrow \Delta^{++} \pi^o \searrow \pi^+ p$$
$$\rightarrow \Delta^{+} \pi^+ \searrow \pi^o p$$

This is the basis of the isobar model first suggested by Lindenbaum and Sternheimer (1958).

Using an isotpic spin decomposition based on the isobar model for pion production, the Clebsch-Gordon coefficients were calculated by Peaslee (1954) (Table II.4). For pp collisions, the ratio for the three pion charge states are $\pi^+ : \pi^o : \pi^- = 5/6 : 1/6 : 0$. For np collisions, the ratios are 1/6:2/3:1/6. For nn collisions, the ratios are 0:1/6:5/6.

The ratios for the isobar model are very different from those predicted by the Fermi statistical weights (Table II.5)

Mandelstam (1958) extended Rosenfeld's partial wave analysis to 650-700 MeV by the assumption that the pion is in a (3/2,3/2) resonant state with one of the final nucleons, while the second nucleon is in either an S- or a P-state with respect to the centre-of-mass (referred to as S-state or P-state production). The matrix element for each transition is constant with respect to energy except for factors due to the final state nucleon-pion and nucleon-nucleon interaction; the latter is felt after the resonance production.

Table II.6 indicates the possible partial waves for the initial NN states, the intermediate ΔN states and the equivalent final πNN states. There are 8 possible transitions for P-wave production and only 1 for S-wave production. From lack of data, Mandelstam was obliged to neglect the $^3F_2$ and the $^3F_3$ transitions, which leaves one parameter for S-wave production and five complex parameters for P-wave production. The neglect of the transitions from initial F states limits the upper bound of validity to incident proton energies of 600-700 MeV.

The remaining five parameters for P-state production were made equal through careful choices sot that it was possible to fit the experimental data with only three real parameters. The resulting fits to the data were good. In some cases, the fits were obtained without any free parameters; in other cases, fits were obtained using two free parameters for the cross section, and it is pointed out that equally

good fits were obtained with these cross sections even when assumptions of the formation of the resonant state were ignored.

Standard expressions for the πN and NN interactions are used to formulte a phenomenological T matrix. The calculation of the π^+ and π^o production is then accomplished by an analysis in terms of the angular momentum and isotopic spin.

A later paper by Vovchenko (1966) extended Mandelstam's model to higher energies. Phase shift analyses of pp scattering indicated that from 630-660 MeV, that transitions from $^3F_2$ and $^3F_3$ initial states, ignored by Mandelstam, also contributed to inelastic scatterings. To do this three parameters are necessary: the S-state production parameter and two nonzero P-state parameters (one of these was set to zero by Mandelstam). The inclusion of the production from F states substantially improves the agreement with experiment.

CHAPTER 3

MULTIPLE DIFFRACTION THEORY

3.1 Development of the theory

As previously discussed, due to the large momentum transfers involved in the pion production even at the intermediate energy range which shows in the strong forward peaking, especially of the π^+, and the short range of the nuclear force compared to the mean free path of the Δ resonance, one can assume that nuclear pion production essentially occurs on single ("free") target nucleons and nuclear effects are only modifications of this interaction. Certain high energy approximations can be applied with reasonable validity even at the intermediate energy range considered. In this way, Glauber's theory of multiple diffraction for high energy inelastic collisions of elementary particles with nuclei can be applied to nuclear pion production.

Glauber (1958 and 1967) extended the Fraunhofer diffraction amplitude formula to a scattering amplitude $f(\vec{k}-\vec{k}')$ for collisions with momentum transfer $\hbar q$, given by:

$$f(q) = \frac{ik}{2\pi}\int e^{i\vec{q}\cdot\vec{b}}\left\{1-e^{i\chi(b)}\right\}d^2b \qquad (3.1)$$

where $\vec{b}$ is the impact parameter vector, which lies in the plane perpendicular to $\vec{k}$, the propagation vector of the

incident particle,

$\vec{k}'$ is the propagation vector of the exiting particle, d^2b is an area element in the impact vector plane. Note that $kb = \ell + \frac{1}{2}$ where ℓ is the angular momentum of the partial wave, so that at lower energies the integral in Eq. (3.1) becomes a discrete sum over ℓ, or b. $\chi(b)$ is a phase shift function defined by $\chi(b) = 2\delta_\ell$ where δ_ℓ is the phase shift of the corresponding ℓ^{th} partial wave. The profile function $\Gamma(b)$ is defined by

$$\Gamma(b) = 1 - e^{i\chi(b)} \tag{3.2}$$

and is just the Fourier transform of the scattering amplitude

$$f(\vec{q}) = \frac{ik}{2\pi} \int e^{i\vec{q}\cdot\vec{b}} \Gamma(b)\, d^2b \tag{3.3}$$

and thus

$$\Gamma(b) = \frac{1}{2\pi i k} \int e^{-i\vec{q}\cdot\vec{b}} f(\vec{q})\, d^2q \tag{3.4}$$

where d^2q is a two dimensional element in a plane perpendicular to $\vec{k}$. If the scattering amplitude is known, then one can obtain the profile function.

The interaction region is treated as a medium with an appropriate refractive index and the incident nucleon undergoes absorption and refraction due to the interaction region. For multiple scatterings in the nucleus, it is found that the use of diffraction theory, with certain assumptions, is much less complicated than multiple

scattering theory. Multiple diffraction theory for particles colliding with nuclei assumes that, as in optics, when a wave passes through more than one interaction (multiple scattering) that the changes in amplitude are multiplicative. In that case, the total phase shift is just the sum of all the individual phase shifts, so that the individual interactions need not be known. Deviation from the additivity may arise from the presence of three (or more) body interactions. The validity of the hypothesis can be tested by experiment. One necessary, but not sufficient, condition which is satisfied at high energies is that there is little "spreading out" of the incident wave after travelling through the nucleus, ie. if a is the range of interaction of the wave with a target nucleon, then the effects of the diffraction will be wiped out in a distance $\frac{a^2}{\lambda}=ka^2$ past the nucleon. The condition for little "spreading" through a nucleus of radius R is that $R<<ka^2$ since $O(R)\div O(a)$ and ka is large at large energies.

Given a nucleus with A nucleons, fixed at positions $\vec{s}_1, \vec{s}_2, \ldots \vec{s}_A$ relative (and normal) to the axis of collision, given by $\vec{k}$ (Fig. 3.1) the phase shift function for the entire system is $\chi(\vec{b}, \vec{s}_1, \ldots, \vec{s}_A)$ since it will depend on the positions of the target nucleons as well as on $\vec{b}$. The change in amplitude of the wave is then given by

$$e^{i\chi(\vec{b}, s_1, \ldots s_A)} = e^{i\{\chi_1(\vec{b}-\vec{s}_1)+\ldots+\chi_A(\vec{b}-\vec{s}_A)\}} \qquad (3.5)$$

where χ_j is the phase shift function for the j-th target

nucleon. The profile function is then given by

$$\Gamma(\vec{b},\vec{s}_1,\dots,\vec{s}_A) = 1 - e^{i\chi(\vec{b},\vec{s}_1,\dots\vec{s}_A)} \qquad (3.6)$$

A composition law can then be written for the profile functions:

$$\Gamma(\vec{b},\vec{s}_1,\dots,\vec{s}_A) = 1 - \prod_{j=1}^{A}\{1-\Gamma_j(\vec{b}-\vec{s}_j)\} \qquad (3.7)$$
$$= \sum_j \Gamma_j(\vec{b}-\vec{s}_j) - \sum_{j<m}\Gamma_j(\vec{b}-\vec{s}_j)\,\Gamma_m(\vec{b}-\vec{s}_m) + \sum\Gamma\Gamma\Gamma$$

where Γ_j is the profile function for the j-th nucleon, ie. $\Gamma_j = 1 - e^{\chi_j(\vec{b}-\vec{s}_j)}$. It is the alternating signs of the terms in the expansion of Γ that result in a diffraction-type curve. (Fig. 3.2)

One can write the scattering amplitude, then, for collisions in which the nucleus goes from a state $|i\rangle$ to a final state $|f\rangle$. If the nucleon recoil is ignored* then the scattering amplitude can be written as the appropriate matrix element of the profile function, ie.

$$F_{fi}(\vec{q}) = \frac{ik}{2\pi}\int e^{i\vec{q}\cdot\vec{b}}\int \varphi_f^*(\{\vec{r}_j\})\,\Gamma(\vec{b},\vec{s}_1,\dots,\vec{s}_A)\,\varphi_i(\{\vec{r}_j\}) \times \delta(A^{-1}\sum_n \vec{r}_n)\prod_m d\vec{r}_m\, d^2b \qquad (3.8)$$

where φ_i and φ_f are the internal (centre-of-mass) wave functions of the nuclear target particles for the initial and final states, respectively. The δ term arises from the requirement of constraining the centre-of-mass to remain fixed. The scattering amplitude can also be written in terms of the Γ_j's,

---

*This is reasonable if the energies transferred in the elastic scattering are negligible.

or what in practice are better known, the elastic scattering amplitudes of the nucleons:

$$F_{fi}(q) = \frac{ik}{2\pi}\int e^{i\vec{q}\cdot\vec{b}}\int \varphi_f^*(\vec{r}_j)\left[1-\prod_{\ell=1}^{A}\{1-\Gamma_\ell(\vec{b}-\vec{s}_\ell)\}\right]$$
$$\times \varphi_i(\vec{r}_j)\,\delta\Big(A^{-1}\sum_n r_n\Big)\prod_m dr_m\, d^2b$$
$$= \frac{ik}{2\pi}\int e^{i\vec{q}\cdot\vec{b}}\int \varphi_f^*(\vec{r}_j)\left\{1-\prod_{i=1}^{A}\left[1-\frac{1}{2\pi ik}\int e^{-i\vec{q}_i\cdot(\vec{b}-\vec{s}_i)} f_i(q_i)\,d^2q_i\right]\right\} \quad (3.9)$$
$$\times \varphi_i(\vec{r}_j)\,\delta\Big(A^{-1}\sum_n r_n\Big)\prod_m dr_m\, d^2b$$

For elastic scattering, where $\varphi_f = \varphi_i$ and $F_{fi} = F_{ii}$, if the total nucleon density is $A\rho(r)$ then the factor $|\varphi_i(r_j)|^2\delta(A^{-1}\sum_j r_j)$ in the elastic scattering amplitude can be replaced by $\prod_{j=1}^{A}\rho(r_j)$, if correlation effects between the target nucleons are neglected. Using the normalization $\int\rho(r_j)\,dr_j = 1$ and assuming that the scattering amplitudes f_j are the same ($\equiv f$) for all nucleons, then

$$F_{ii} = \frac{ik}{2\pi}\int e^{i\vec{q}\cdot\vec{b}}\left\{1-\left[1-\frac{1}{2\pi ik}\int e^{i\vec{q}'\cdot\vec{b}} f(\vec{q}')S(\vec{q}')\,d^2q'\right]^A\right\}d^2b \quad (3.10)$$

where $S(\vec{q})$ is the form factor of the density function

$$S(\vec{q}) = \int e^{i\vec{q}\cdot\vec{r}}\,\rho(\vec{r})\,d\vec{r} \quad (3.11)$$

The expressions are much simpler than standard multiple scattering in that only one nucleon index occurs in each term of the expansion and the expression is, at most, A-fold.

For light nuclei, Eq. (3.10) can be expanded simply in powers of f, since, in this case, the highest power of A is small.

An effective phase shift function $\chi(\vec{b})$ is defined by $\chi(b) = \frac{A}{2\pi k}\int e^{-i\vec{q}\cdot\vec{b}} f(\vec{q})S(\vec{q})\,d^2q$, so that for heavy nuclei, the

term in Eq. (3.10) which is raised to the power A, can be approximated by

$$\left(1 + i\frac{\chi}{A}\right)^A \sim e^{i\chi}$$

for sufficiently large A so that Eq. (3.10) becomes

$$F_{fi}(\vec{q}) = \frac{ik}{2\pi}\int e^{i\vec{q}\cdot\vec{b}}\left\{1 - e^{i\chi(\vec{b})}\right\} d^2b \qquad (3.12)$$

This is of the same form of the scattering amplitude as obtained by the optical model.

If the range of the scattering interaction is much smaller than the nuclear radius, then the form factor $S(\vec{q})$ is more sharply peaked at $q=0$ than $f(q)$, and thus $f(0)$ may be factored out of $\chi(b)$ to give

$$\chi(b) \sim \frac{1}{2\pi k} f(0)\, T(b) \qquad (3.13)$$

as the effective phase shift function, where

$$T(b) \equiv A\int_{-\infty}^{\infty} \rho\left(\vec{b} + \frac{\vec{k}}{|\vec{k}|} z\right) dz \qquad (3.14)$$

called the thickness function of the target, is the integral of the nucleon density function along the straight path given by the impact parameter (Fig. 3.3).

The elastic scattering gives a diffraction pattern which rapidly drops to negligible intensity for $|\vec{k} - \vec{k}'| >> R^{-1}$.

Of importance to the case of pion production is the inelastic, rather than the elastic scattering. To calculate the inelastic scattering cross section experimentally, one first measures the sum of all the cross sections which

correspond to leaving the nucleus in any possible final state $|f\rangle$, ie. $\sum |F_{fi}|^2$. From this one can subtract the elastic cross section in which the nucleus is left in its ground state which, due to the completeness of all the final states $|f\rangle$ considered, gives the inelastic cross section:

$$\left(\frac{d\sigma}{d\Omega}\right)_{inelastic} = \sum_f |F_{fi}(k-k')|^2 - |F_{ii}(k-k')|^2 \qquad (3.15)$$

which can be evaluated for momentum transfers outside the diffraction region $k-k' \gg R^{-1}$. As before, an independent particle approximation for the nucleus and an interaction range that is small compared with the size of the nucleus are assumed. This gives

$$\left(\frac{d\sigma}{d\Omega}\right)_{inelastic} = \left(\frac{k}{2\pi}\right)^2 \int e^{i(\vec{k}-\vec{k}')\cdot\vec{b}} - \sigma T(\vec{B}) \times \exp\left[\frac{T(\vec{B})}{q^2}\int e^{i\vec{q}\cdot\vec{b}} |f(\vec{q})|^2 d^2q\right] - 1 \Big] d^2b\, d^2B \qquad (3.16)$$

where σ is the cross section for a free nucleon (assumed spin and charge independent). Expanding Eq. (3.16) in terms of gives

$$\left(\frac{d\sigma}{d\Omega}\right)_{inelastic} = |f(k-k')|^2 \int e^{-\sigma T(\vec{B})} T(\vec{B})\, d^2B + \frac{1}{2}\int |f(q)|^2 |f(\vec{k}-\vec{k}'-\vec{q})|^2 \frac{d^2q}{k^2} \int e^{-\sigma T(\vec{B})} T^2(B) d^2B + \cdots \qquad (3.17)$$

which is, again, a multiple scattering expansion in which the n-th term (of order 2n in f) represents an n-fold quasi-elastic scattering.

Ignoring the multiple scattering and considering only the first term which represents quasi-elastic scattering off of a single nucleon, then the number of nucleons which gives rise to this first order scattering is given by N_1 where

$$N_1(A) = \int e^{-\sigma T(\vec{B})} T(\vec{B})\, d^2B. \qquad (3.18)$$

Due to the strong nuclear absorption, it is only the incident nucleons which are on paths which strike the nucleus along its periphery which have an appreciable chance of emerging from the nucleus. It is unlikely that a particle striking the nucleus centrally will re-emerge. For this reason, it is expected that the effective nember of nucleons $N_1(A) << A$. Fig. 3.4 gives a plot for ^{64}Cu of $e^{-\sigma T(B)} T(B)$ showing how the main contribution comes from the nucleons near the nuclear surface in the plane perpendicular to the incident velocity $\vec{k}$. It is also expected that $N_1(A)$ is very sensitive to the surface nuclear density; a plot of $N_1(A)$ vs. A in Fig. 3.5 indicates that the measured values of $N_1(A)$ compare very well with those calculated using a Woods-Saxon nuclear density, in contrast to those obtained using a uniform spherical density.

A calculation of the contributions of the various orders of quasi-elastic scattering to the total inelastic scattering cross section shows that up to high momentum transfers (about 0.5 GeV/c for ^{64}Cu with 19.3 GeV/c protons), it is only the first order term that contributes significantly. (Fig. 3.6)

Figure 3.7 indicates that it is the diffraction pattern which dominates at small momentum transfers, but at high momentum transfers, it is the quasi-elastic (and predominantly the first order term) which dominates. This is verification that this can be used for pion production models at intermediate energies.

3.2 Application to pion production

Margolis (1968) obtained a model for pion production for protons incident on heavy nuclei (A>>1) at intermediate energies by directly applying Glauber's multiple diffraction theory for multi-GeV collisions. The forward peaking of the pion cross section, especially for π^+, encouraged this model. It is assumed that the $\Delta(3/2,3/2)$ is formed by quasi-elastic incoherent proton-nucleon collisions. The cross section for π^+ production is calculated, and the corresponding π^+/π^- ratio is calculated using the prediction of the isobar model. From the isobar model, it is expected that $\pi^+/\pi^- \div (10Z+N)/N$ for collisions with a (Z,N) nucleus (Table II.5); this is $\div 7$-11, which is approximately true for the high energy end of the spectra obtained at 600 MeV by Heer et al. (1966) (Figs. 3.8 and 3.9), but too high for the low energy end since many of the π^- are expected to come from secondary scatterings.

Only single scattering is assumed, so that the first term in Glauber's expression for inelastic scattering, corresponding to quasi-elastic scattering from a single nucleon, is used. It is modified for production of the isobar, and is given by:

$$\frac{d\sigma}{d\Omega} \approx \frac{1}{A}\left(Z + \frac{1}{10}N\right) N_1^I \; |f^*(q)|^2 \qquad (3.19)$$

Compare this with Glauber's expression $|f(q)|^2 N_1$ Eq. (3.17) and (3.18). Again, the factor $\frac{Z+\frac{1}{10}N}{A}$ comes from the isobar model prediction of the π^+ production and $|f^*(q)|^2$ is the differential cross section for isobar production in pp collisions with momentum transfer q . N_1^I is given by

$$N_1^I = \int d^2b \left\{ \frac{\exp[-\sigma_1 T(b)] - \exp[-\sigma_2 T(b)]}{\sigma_2 - \sigma_1} \right\} \quad (3.20)$$

where σ_1 and σ_2 are the nucleon-nucleon and the nucleon-isobar total cross sections, respectively (assumed spin and isospin independent). Note that for $\sigma_1 = \sigma_2$, then $N_1^I = N_1$ from Glauber's paper.

It turns out that the pp and the np cross sections at 600 MeV are approximately equal, as well as being equal to the nucleon-nucleon cross section at 19.3 GeV for which the Glauber calculations were made (Lock and Measday (1970), Figs. 7.2 and 7.8). Thus, it was assumed by Margolis that $\sigma_2 \sim \sigma_1$, so that Glauber's calculation of N_1 at 19.3 GeV could be used for the calculation of N_1^I at 600 MeV; this was a helpful assumption since Margolis lacked information on the isobar-nucleon cross section σ_2 .

Eq. (3.20), integrated over all angles then gives

$$\sigma_{prod} \sim \frac{1}{A} \left(Z + \frac{1}{10} N \right) N_1^I \sigma^I \quad (3.21)$$

where σ_{prod}^I is the total isobar production cross section in a (Z,N) nucleus which results in π^+ production and σ^I is the corresponding cross section for the pp interaction.

Figure 3.10 shows the results of the calculation of N_1 using Eq. (3.19), as well as the results for the Heer (1966) data at 600 MeV and the high energy pp quasi-elastic scattering data at 19.3 GeV (Glauber 1967, p. 311). This

indicates a consistency with the assumption that $\sigma_2 \sim \sigma_1$ which provides a starting point for the estimation of σ_2. This is important since, if a value for σ_2 is found, then either Eq. (3.21) or (3.19) can be evaluated with no free parameters, with the normalization coming from the free pp pion production cross section.

A later paper by Kolbig and Margolis (1968) gives a more detailed calculation for both coherent and incoherent particle production in collisions with nuclei, of which only the latter is of importance at intermediate energies. Large ranges of N_{eff} are tabulated for various values of σ_1 and σ_2. (Table III.1). Detailed calculations of production cross sections are made only for photoproduction of ρ mesons, however, and not for pion production from nucleons; the agreement with experimental data is good.

One major problem with the models of Kolbig and Margolis is that no nuclear corrections are made to the calculations; of particular importance is the neglect of the charge exchange processes and the assumption of only forward production.

CHAPTER 4

CLASSICAL ABSORPTIVE GAS MODEL: BEDER AND BENDIX

Beder and Bendix (1971) were the first to attempt a model for positive pion production from protons incident upon nuclei with nuclear effects taken into account. Theirs is a "classical absorptive gas" model in which the production cross section is the Fermi averaged cross section for single production on a free nucleon, multiplied by an attenuation factor, denoted N_{eff}, to account for absorption of the incident proton and exiting pion. It is, thus, mathematically equivalent to the Glauber formalism for incoherent, quasi-elastic scattering, but it is much simpler to deal with conceptually.

Included in the pion absorption is the absorption due to the charge exchange due to $\pi^+ n \rightarrow \pi^o p$, as well as the absorption on two nucleons given by $\pi NN \rightarrow NN$. It is expected that the nuclear absorption is quite strong, and that the surface nucleons, predominantly, will contribute to the pion production.

The free production cross section used by Beder and Bendix is a modified form of the T-matrix of Mandelstam's (3/2,3/2) resonance model. The range of applicability is thus from above threshold to about 650 MeV. The model obtains reasonable agreement with experimental data from CERN at 600 MeV (Heer et

al. 1969) and data from Lillethun (1962) and Mathie (1976) at 400-500 MeV.

Since the model is concerned with only π^+ production from incident protons, the free nucleon-nucleon interactions which are considered are:

$$pp \rightarrow \pi^+ np \qquad (4.1)$$

where the n and the p are unbound, and

$$pp \rightarrow \pi^+ d \qquad (4.2)$$

where d is a deuteron, and a small contribution due to

$$pn \rightarrow \pi^+ nn \qquad (4.3)$$

is also included. Recall that from the isobar model the Clebsch-Gordon coefficients predict that π^+ production from pn collisions is only 1/10 that from pp collisions. Beder and Bendix use the CERN data at 600 MeV as a guide, and assume that the contribution from the pn collisions is 1/6 that of the 3-body contribution (Eq. 4.1) at T_π=100 MeV, 1/8 for 200 MeV and 1/20 at 250 MeV.

The free production cross section used is discussed first, and then the method of introducing the Fermi-averaging, the nuclear potentials and the Pauli Exclusion Principle is shown. The absorption factor N_{eff} is introduced finally.

From standard scattering theory, the cross section for a nuclear reaction from and initial two particle state i to a final n-particle state f is given by

$$\sigma[\text{particles } i \rightarrow \text{particles } f] = \prod_{i=1}^{2} \rho_i \cdot (\text{flux})^{-1} (2\pi)^4 \int \sum \prod_{f=1}^{n} \left[\frac{d^3k_f}{(2\pi)^3 2E_f}\right] \prod_i \left[\frac{1}{2E_i}\right] \times \delta^4\left(\sum P_f - P_i\right) |T|^2 \qquad (4.4)$$

where ρ_i is the initial target density,

$\vec{k}_f$ are the final 3-momenta,

E_i and E_f are the initial and final energies, respectively,

P_i and P_f are the initial and final total 4-momenta, respectively,

and T is the T-matrix.

Beder and Bendix write the doubly differential free cross section in terms of an invariant matrix element (constant over the energy range considered) and the required phase space factors. In standard notation,

$$\frac{d^2\sigma}{dT\,d\Omega}(NN\to\pi NN) = \frac{p_{\pi,lab}}{\left[p_1\cdot p_2 - p_1^2 p_2^2\right]^{1/2}} \frac{k_N}{W_{NN}} \frac{\int_{-1}^{+1} d(\cos\theta_{NN})\,|T|^2}{514\,\pi^4} \qquad (4.5)$$

where p_1 and p_2 are the 4-momenta of the initial nucleons,

$\left[p_1\cdot p_2 - p_1^2 p_2^2\right]^{1/2}$ is the invariant flux Mp_N^{lab} for the target nucleon at rest. (For the mass shell case, $p_1^2 = p_1\cdot p_1 = M^2$.)

k_N is the 3-momentum of the final nucleon in the centre-of-mass frame and

W_{NN} is the total energy of the two final nucleons in their centre-of-mass frame.

The T matrix used in $|T|^2$ is a modified version of Mandelstam's phenomenological T matrix in which the pion production proceeds via the (3/2,3/2) intermediate resonant state. The T matrix is given by

$$|T|^2 = \eta\, R(\theta_{c.m.})\, g(W) \left| \frac{f_1}{S_{\pi 1} - S_\Delta + i\Gamma_\Delta M_\Delta} - \frac{1}{3}\frac{f_2}{S_{\pi 2} - S_\Delta + i\Gamma_\Delta M_\Delta} \right|^2 \qquad (4.6)$$

where η is a normalization factor,

$R(\theta_{cm})$ accounts for the angular distribution of the outgoing pions,

$g(W)$ is a unitarization factor, and

the quantity being squared, $|\ \ |^2$, accounts for the resonant nature of the πN interaction.

These factors are introduced for various reasons and deserve further explanation.

$R(\theta)$ gives the angular distribution of the outgoing pion in terms of θ, the angle between the pion and the initial proton momenta (measured in the centre-of-mass frame). This is empirically deduced. For low energies, up to about 450 MeV, the $N\Delta$ system is assumed to be in a relative S-state, and the angular distribution is given by

$$R(\theta_{cm}) = 3\cos^2\theta_{cm} + 1 \qquad (4.7a)$$

For higher energies, the angular distribution becomes more isotropic and an expression for $R(\theta)$ which fits the data is given by

$$R(\theta_{cm}) = 2\left[1 + 3\cos^2\theta_{cm}\left(1 - \frac{KE - 450\,MeV}{450\,MeV}\right)\right]\left[2 - \frac{KE - 450\,MeV}{450\,MeV}\right]^{-1} \qquad (4.7b)$$

Note that at 450 MeV, the expressions for $R(\theta)$ are consistent as required. Without this factor, only forward production would be assumed.

$g(W)$, where W is the total centre-of-mass energy, is introduced to maintain unitarity. If $g(W)$ were a constant

function, then the total production cross section, which is normalized to 4.5 mb. at 450 MeV, would violate unitarity for proton energies above 450 MeV, for it is found that with a constant $g(W)$, these total cross sections rise more rapidly as a function of incident proton energies than do the experimental cross sections. Mandelstam avoided the violation of unitarity by treating the T matrix as a K matrix, which neglects the processes due to intermediate real states. In this way, emission and reabsorption of real pions was accounted for, and the cross section did not exceed the maximum allowed. The Beder and Bendix T matrix (T_{BB}) and the Mandelstam T matrix (T_M) are related by

$$T_M \sim \frac{(T_{BB},\ g(W)=1)}{1+\frac{\sigma_{tot}\ (T_{BB}\ \text{treated as actual amplitude})}{\sigma_{tot}\ (\text{unitarity limit})}} \qquad (4.8)$$

$g(W)$ is chosen so that σ_{tot} agrees with the experimental data for $pp \rightarrow \pi^+ np$ and normalized so that σ_{tot^+} (450 MeV)=3 mb. The fit is obtained by setting

$$g(W) = \left[1 + 0.02\,(KE - 450\ MeV)\right]^{-1} \qquad (4.9)$$

Referring again to Eq. (4.5), the πN resonance factor is evident through the factor $(S_{\pi i} - S_\Delta + i\,\Gamma_\Delta M_\Delta)^{-1}$ inside the modulus where $S_{\pi i} = (p_\pi + p_{Ni})^2$ is a four-vector scalar product of the sum of the pion and i^{th} nucleon four-momenta (i=1 refers to the final proton, i=2 refers to the final neutron). $S_\Delta = M_\Delta^2$, the mass of the resonance squared, i.e. $(1238\ MeV)^2$, and Γ_Δ=122 MeV ($=\hbar/\tau_\Delta$). The factor -1/3 in the term for the

neutron arises from isospin invariance: recall Mandelstam's term, $(a-a'/3)^2$. The factors f_i in Eq. (4.6) are P-wave emission factors which are due to the πN resonant state, which causes the pion to be emitted in a predominantly l=1 state (l is the orbital angular momentum). They are given by:

$$f_i = \frac{q_i}{[q_i^2 + (140\,MeV)^2]^{1/2}} \qquad (4.10)$$

where q_i are the 3-momenta in the πN_i centre-of-mass frame of the i^{th} nucleon. The factor q in the numerator comes from the standard P-wave factor, and the denominator is parametrized to fit the $\pi+$ energy spectrum from $pp \rightarrow \pi+np$.

The effect of the resonant structure and the f_i's can be seen in Fig. 4.3 as a strong enhancement of the high energy end of the spectrum. A reasonable fit to the 600 MeV data was obtained by normalizing σ_{tot} to 6.5 mb.

The free particle production cross section is averaged over the possible Fermi momenta of the target nucleons. If a uniform distribution in momentum space is assumed, then the Fermi motion averaged production cross section becomes

$$\rightarrow \frac{1}{\frac{4}{3}\pi k_F^3} \int_0^{k_F} k^2 dk \, d\Omega_k \frac{d^2\sigma}{dE_\pi d\Omega_\pi}^{free}(\vec{p}, \vec{k} \rightarrow \vec{p}_\pi, \ldots) \qquad (4.11)$$

where $\frac{d^2\sigma}{dE_\pi d\Omega_\pi}^{free}$ is given by Eq. (4.4) and k_F is the maximum Fermi momentum of the target nucleons.

The momenta of all the particles, while inside the nucleus, will be affected by the nuclear potentials, which are assumed to be some average optical potential <V>. It is

these modified momenta that are used to calculate $|T|^2$ and the invariant phase space.

The values for the optical potential are from Preston (1962), and are based on the formation of a compound nucleus by the incident proton with the target nucleus. For the incident 600 MeV proton, $\langle V \rangle$ = 20 MeV is used. It is estimated that the final nucleon, since it is of lower energy, feels a potential of about only 10 MeV, which is ignored in the calculation. The optical potential used for the pion is taken to be roughly half that developed by Frank et al. (1956) for πN scattering. Only half the value is taken by Beder and Bendix since, due to the strong nuclear absorption, the pions are produced mainly on the edge of the nucleus where the nuclear density is low. (Figure 4.1)

The various momenta of the particles are calculated using the potentials discussed above, and the following expressions:

$$E_i = E_o = \sqrt{p_o^2 + m^2} = \sqrt{p_i^2 + m^2} + \langle V \rangle \qquad (4.12)$$

where i and o denote inside and outside the nucleus, respectively, m is the rest mass of the particle, and $\langle V \rangle$ is the appropriate potential.

The effect of Fermi averaging and of nuclear potentials on a free body invariant phase space ($\equiv \frac{d^2\sigma}{dE_f d\Omega_f} / |T|^2$) can be seen in Fig. 4.2.

The phase space is enhanced at low energies with the peak also being shifted to a lower energy. This is mainly due to the pion optical potential giving a higher pion momentum (p_π^{lab}), and thus increasing the phase space. At higher energies, the phase space is substantially reduced and a high energy tail is evident.

For the doubly-differential cross section, the effect of the Fermi averaging and the nuclear potentials is qualitatively the same as for the invariant phase space. The degree of change, however, is much larger and the resultant cross section is much reduced in magnitude. (Fig. 4.3)

Fig. 4.4 indicates the sensitivity of the two- and the three-body cross sections to the Fermi momentum chosen.

The 3-body cross section, referred to as $d\bar{\sigma}_3$, was checked for Pauli Exclusion effects, and it was found that it was suppressed by 6% at T_π=100 MeV, and 14% at 300 MeV. (Table 4.1)

The cross section for the two-body final state contribution (Eq. (4.2)), can similarly written down, with the Fermi motion averaging included, as

$$\frac{d^2\sigma}{dE_\pi^L d\Omega_\pi^L}(NN\to\pi^+ d) = \frac{1}{\frac{4}{3}\pi k_F^3}\int_0^{k_F}\frac{k^2\,dk\,d\Omega_p}{[(p-k)^2-(p\cdot p)(k\cdot k)]^{1/2}} \qquad (4.13)$$

$$\times |T(\vec{p},\vec{k}\to\vec{p}_\pi,\ldots)|^2\frac{|p_\pi^{lab}|}{64\pi^2 M_D}\,\delta(E^*-M_D)$$

where $E^* = [(E_p+M-E_\pi^L)^2-(\vec{p}+\vec{k}-\vec{p}_\pi^L)^2]^{1/2}$

and M_D is the rest mass of the deuteron. Note that the absorption is not included in Eq. (4.13).

The matrix $|T|^2$ can be determined from expressions for

the differential cross section $d\sigma/d\Omega$. From the 600 MeV data, the angular distribution of $pp \rightarrow \pi d$ is given by

$$d\sigma/d\Omega_{c.m.} = k_p (A + \cos^2\theta - B\cos^4\theta) \qquad (4.14)$$

where A and B are determined by the observed angular distribution to be $A = 0.255$ and $B = 0.38$ at 600 MeV.

It can also be written that

$$\frac{d\sigma}{d\Omega_{c.m.}} = \left| \frac{q_{\pi D}}{q_{pn}} \right|_{c.m.} \left| \frac{T}{8\pi W} \right|^2 \qquad (4.15)$$

where $q_{\pi D}$ and q_{pn} are the centre-of-mass momenta of the pion and the proton, respectively, and W is the total centre-of-mass energy.

The T matrix can then be written as

$$|T|^2 = |8\pi W|^2 \; K_{eff} (A + \cos^2\theta - B\cos^4\theta) \qquad (4.16)$$

where $K_{eff} \equiv k_p \left| \frac{q_{pn}}{q_{\pi D}} \right|_{c.m.}$

where K_{eff} can also be written as

$$K_{eff} \approx \frac{1200\ \mu b/sr.}{\left(\frac{W - 2155\ MeV}{60\ MeV}\right)^2 + 1} \qquad (4.17)$$

The potentials are evaluated as for the 3-body case. The claculated 2-body cross section is seen in Fig. 4.3.

The Pauli Exclusion effects on the 2-body cross section, referred to as $d\bar{\sigma}_2$, was assumed (somewhat arbitrarily) to be the same as for $d\bar{\sigma}_3$, that is 6% at $T_\pi = 100$ MeV and 14% at 300 MeV. (Table 4.1)

The cross sections for both the two- and the three-body

contributions must be modified to account for the absorption of the exiting pion and the incident proton. Due to the strong nuclear absorption, one can consider that the nucleus contains and "effective number" of target nucleons, given by N_{eff}, which is expected to be much less than A, the total number of target nucleons; N_{eff} is the number of target nucleons with which it is energetically possible for the incident proton to interact to produce a pion which will emerge from the nucleus. N_{eff} is thus a measure of the amount of absorption which occurs in the nucleus.

The expression for N_{eff} is given by

$$N_{eff} = \int d^3r \frac{Z}{A} \rho_{total}(\vec{r}) \exp\left[-\int_{path\ in} \lambda^{-1}_{proton}(\vec{\xi})\, d\vec{\xi}\right] \exp\left[-\int_{path\ out} \lambda^{-1}_{\pi}(\vec{\tau})\, d\vec{\tau}\right] \qquad (4.18)$$

where ρ_{total} is the total nucleon density, and λ^{-1}_{proton} and λ^{-1}_{π} are the inverse mean free paths for absorption of the proton and the pion, respectively. As previously mentioned, it is expected that due to the nuclear absorption, that pion production occurs mainly on the surface target nucleons. It is seen from Eq. (4.18), that for the small path lengths (λ) expected with strong absorption, that $N_{eff} \ll Z$, as expected. Note that N_{eff} corresponds to the expression for T(b) used by Glauber and Margolis.

Most collisions leave the incident proton with insufficient energy for pion production if the nuclear absorption is high enough, and it is assumed that in this case the absorption is complete, and

$$\lambda^{-1}_{proton} \sim \rho_{total}\, \sigma_{NN} \qquad (4.19)$$

where σ_{NN} is averaged over the target nucleons; $\sigma_{NN} \doteq 25$ mb., and is fairly independent of energy at this range.

No attempt is made to account for the "absorption" of the incident proton due to nucleon charge exchange.

The pion absorption is assumed to occur either by pion charge exchange or by absorption of the pion on a nucleon pair, $\pi^+ n \rightarrow \pi^o p$ and $\pi^+ NN \rightarrow NN$, respectively.

The Fermi averaged total cross section for charge exchange of π^-, ie. $\pi^- p \rightarrow \pi^o n$, denoted by $\bar{\sigma}$, is obtained from experimental data (Giacomelli 1969); using isospin invariance this can be related to $\pi^+ n \rightarrow \pi^o p$, so that the π^+ charge exchange is given by

$$\lambda_{CE}^{-1}(r) = \frac{N}{A} \rho_{total}(r)\, \bar{\sigma}(\pi^- p \rightarrow \pi^o n) \qquad (4.20)$$

It is found that the Fermi averaged charge exchange cross section is decreased by $\doteq 15\%$ for $T_\pi \leq 350$ MeV due to the Pauli Exclusion Principle.

Absorption of a pion on a single nucleon implies a momentum transfer of the order of $(2m_N m_\pi)^{1/2} \doteq 625$ MeV, which is too large for nuclear dimensions. Absorption on two nucleons is reasonable, however. In this case, the pion is absorbed on one nucleon, but the momentum transfer is shared with a second nucleon, and this implies a momentum transfer of the order of only $(m_N m_\pi)^{1/2} \doteq 365$ MeV.

The cross section for absorption of low energy pions ($T_\pi < 300$ MeV) on a nucleon pair can be related to nuclear pion

production ($NN \to \pi NN$) by using the invariance of strong interactions under time reversal, which gives

$$\sum_{spins} |T_{\pi NN \to NN}|^2 = \sum_{spins} |T_{NN \to \pi NN}|^2 \qquad (4.21)$$

In as much as the nucleons in the nucleus are independent, it is assumed that the two nucleons which absorb the pion are also independent.

The mean free path for the nuclear pion absorption, $\lambda^{(r)}_{\pi NN \to NN}$ is then given by

$$\lambda^{-1}_{\pi NN \to N_1 N_2}(r) = \rho_1 \rho_2 \frac{1}{M^2 p_\pi^{lab}} \frac{P}{W} \int_{-1}^{1} \frac{d(\cos\theta)\,|T|^2}{128\pi^2} \qquad (4.22)$$

where ρ_i is the density of nucleons of the type N_i.
P is the final nucleon 3-momentum in the centre-of-mass frame, and W is the total centre-of-mass energy.

For convenience $\rho_1 \rho_2$ can be written as $\left(\frac{\eta_1 \eta_2}{A^2}\right) \rho^2_{total}$ where η_i is the total number of nucleons of the type N_i. (Beder 1971). This emphasizes that the absorption is proportional not to ρ but to ρ^2, which has been assumed by other authors.

The two absorption processes are given by $\pi^+ np \to pp$ and $\pi^+ nn \to np$, and using data from Rosenfeld (1954), it is assumed that the latter contributes only about 30%, so that

$$\lambda^{-1}_{\pi NN \to NN}(r) = \rho^2_{total}(r) \cdot a \qquad (4.23)$$

where $$a \sim \frac{ZN + 0.3N^2}{A^2} \frac{1}{M^2 p_\pi^{lab}} \frac{P}{W} \frac{\int_{-1}^{1} d(\cos\theta)\,|T_{pp \to \pi^+ pn}|^2}{128\pi^2}$$

The quantity $\frac{2N+0.3N^2}{A^2}$ is approximately independent of A, ie. for ^{27}Al it is 0.33, and for ^{208}Pb it is 0.35.

The cross section is then Fermi averaged over the momenta of the target protons. To evaluate it over both the protons and the neutrons would be exceedingly lengthy. The resonance model for $\pi^+ pn \to pp$, predicts that the pion resonates mainly with the proton, and thus it is reasonable to average only over the proton motion.

It is not expected that the Pauli Exclusion Principle will affect the pion absorption on a nucleon pair since the absorbed pion imparts such high momentum to the final nucleons.

A Woods-Saxon potential given by

$$\rho_{total}(r) = \rho_0 (1 + e^{r-R/a_0})^{-1} \qquad (4.24)$$

is used in Eqs. (4.20) and (4.22), normalized according to

$$\int \rho_{total}(r)\, d^3r = 1$$

and where $\rho_0 = 1/7$ fm.$^{-3}$, $R = 1.25A^{1/3}$fm., and $a_0 = 0.55$ fm.

The results for the Fermi averaged pion charge exchange cross section, $\bar{\sigma}_{CE}$, (without Pauli Exclusion effects), and the coefficient for absorption on a nucleon pair, a, are given in Fig. 4.5. For 200 MeV protons, $\lambda^{-1}_{\pi^+ pn \to pp} = 0.3$ fm^{-1} and $\lambda^{-1}_{\pi^+ \to \pi^0}(Z=A) = 0.23$ fm, so that $\lambda^{-1}(\text{total absorption}) = 1.9$fm.

Results are tabulated for 600 MeV incident protons (and compared with the 600 MeV data) with Pauli Exclusion Principle effects where applicable and/or calculated in Table 4.1 and

Figs. 4.6 and 4.7. Note that the cross sections for production from protons on target neutrons, denoted $d\bar{\sigma}_{neutron}$, are also given in Table 4.1. As mentioned, these are determined from the experimentally observed ratios of $d\bar{\sigma}_3$ to $d\bar{\sigma}_{neutron}$.

The values of N_{eff} shown in Table 4.2 (multiplied by Z/A) compare well with the literature (Table 3.1). The decrease in the Fermi averaged pion charge exchange of 15% due to the Pauli Exclusion effects, causes a subsequent enhancement of the effective nucleon numbers ($N_{eff} \propto \int \lambda_\pi^{-1} d\tau$) of 10% at $T\pi$= 100 MeV and 18% at 300 MeV.

The total effect of the Pauli Exclusion Principle is to increase the net flux (results of Table 4.1 times Table 4.2) by about 4%.

The doubly differential cross sections, compared with the 21°.5 CERN data agree well for ^{208}Pb (Fig. 4.7), but are low for ^{12}C (Fig. 4.6). For ^{12}C, the model underestimates the low angle (21°.5) π^+ production by about 15%; there is also a tendency to underestimate the low energy relative to the high energy population. Although the ^{208}Pb data produces a better fit, there is still a tendency to underestimate the number of low energy $\pi+$ and overestimate the number of high energy $\pi+$. This seems to be an indication of presence of multiple scattering within the nucleus which has been ignored in the model. The qualitative fits are, however, quite good.

The A-dependence of the cross section is shown for only

the best fit which is for the 100 MeV pions (Fig. 4.8). The curve shows the general fattening of the curve at large A which is expected due to the geometrical dependence of the production cross section on the nuclear structure.

Calculations made for 450 Mev incident protons were compared with available 19°.5 data on ^{12}C (Lillethun 1962). The calculated cross section agreed well with the experimental cross section if the latter were renormalized by a factor of 1/3 (Fig. 4.9). This renormalization was confirmed by Mathie (1976) with data from TRIUMF.

This further experimental data from TRIUMF were for incident protons at 450 MeV and 500 MeV with π^+ emerging at angles of 60°, 100° and 150°. Beder calculated cross sections for comparison with this new large angle data for C and Cu (Figs.5.7-5.12,Mathie 1976). In general, the results were not as favourable as for the 600 MeV case: For 60°, for both 450 MeV and 500 MeV, the number of low energy π^+ is underestimated, while for higher angles the number is either a good fit or is too high. The number of high energy pions is overestimated for 60° and for 100° at both energies, and slightly underestimated for 150°. The peaks in the spectra are also predicted at too high energies for 60°, and in all cases, the predicted peak widths are, at least, too broad. It was not expected, however, that the model would be very reliable at high angles since multiple scattering was ignored.

CHAPTER 5

GEOMETRICAL MODELS

5.1 Importance of the nuclear geometry in pion production

The dependence of the pion production cross section on the geometry of the nucleus, and especially the nuclear surface, has been indicated in the previous models.

Oganesyan (1968) discusses the geometrical nature of pion production from nuclei in relation to data obtained from 600 MeV neutrons on nuclei; ignoring Coulomb effects, if charge symmetry holds, then $\pi^{\pm}$ production from a proton, say, on a nucleus with an equal number of neutrons and protons ($^{12}_{6}C^{6}$) is equivalent to $\pi^{\mp}$ production from a neutron incident on that nucleus. This dependence of the pion spectrum on the geometry of the nucleus is due, of course, to the absorption of the pions by the nucleons in the nucleus, and therefore is a strong function of the distribution of the target nucleons.

This manifests itself through a particular dependence on the atomic number A. Since the πN interaction has a resonant behaviour and shows a strong dependence on the pion energy, it is expected to be that the pion spectrum will show a differential absorption (will show through the A dependence) according to the pion energy. The cross section for the pion interaction with the nucleons increases by a factor of more than 10 between 50 MeV and 200 MeV; a pion created with

an energy of 50 MeV has mean free path which is much larger than that for a 200 MeV pion. For the less energetic pion, then, there may be a contribution to the interaction from the internal nucleons which will lead to a strong A dependence. The more energetic pions, however, are strongly absorbed, and thus little or no contribution for the internal nucleons is expected. The high energy pion spectrum will not have such a strong A dependence since they are produce mainly by the surface nucleons. Note that this argument assumes no nucleon recoil in the production process (Section 5.4). This trend is observed from the data, and 50 MeV pions show an A dependence which is steeper than $A^{2/3}$, while 190 MeV pions have a dependence which is flatter than $A^{2/3}$.

Comparing dependences for the different angles available at several fixed pion energies indicates that there is no variation in the A dependence. The only trend is a general softening (shift to lower energies) of the spectrum with increasing angle.

There is also support indicated in the data for a neutron excess in the nuclear surface, especially for heavy nuclei. This surface neutron excess would contribute to an enhancement of the π^-/π^+ ratio for nuclei with such an excess. This would occur due to two contributions; the π^- will be increased due to the relative increase of neutron population in the nuclear surface to enhance the reaction $nn \rightarrow \pi^- pn$, and also

the π^+ production will be diminished due to the shielding of the target protons required for the π^+ production via np π^+nn. This effect is seen in comparing relative π^- yields in Carbon and Beryllium, in which a relatively higher π^- yield is expected in Beryllium which has a neutron excess of 1. It is found that

$$\sigma_C \pi^- / \sigma_{Be} \pi^- = 1.02 \pm 0.05$$

while

$$\sigma_C \pi^+ / \sigma_{Be} \pi^+ = 1.72 \pm 0.14$$

which is higher than the ratio of the number of protons in the two nuclei.

For heavier nuclei, it is not sufficient to consider that the large surface neutron excess simply will decrease the relative π^+ population (for neutron-nucleus collisions). Charge exchange becomes increasingly important with increasing atomic number, and tends to increase the relative π^+ population (for neutron collisions). This is because more π^- are charge exchanged to π^o than vice versa, and similarly the charge exchange of π^o to π^+ dominates over the inverse process due to the original large populations of π^-, and small number of π^+ relative to the π^o. This reduction in relative population of π^- to π^+ is most evident for the nuclei Al and Cu; for the heavier nuclei, ie. Pb, the opposing action of the neutron shell effect results in a decrease in the relative difference of the π^+ and π^- yields.

For the case of protons incident on nuclei, the neutron shell effect and the charge exchange act together to both result in the relative increase in the π^- population. For nuclei where the neutron shell effect is unimportant, i.e. C to Cu, the A dependence of the π^+ spectrum from incident proton collisions is very close to that of the π^- spectrum from incident neutron collisions. A large difference in the relative yields of π^- from neutron collisions and of π^+ from proton collisions on ^{208}Pb is an indication of the validity of these two opposing forces.

Section 5.2 Geometrical Model with no nuclear corrections

Extensive measurements were reported by Cochran et al. (1972), which included both π^+ and π^- production from protons incident on eleven nuclei ranging in size from H to Th. The emerging pions were measured at eleven angles from 15° to 150°, and at twelve energies from 25 to 550 MeV for all nuclei. The paper was published concurrently with the first of two papers by Sternheim and Silbar (1972) which proposed a phenomenological model for pion production which could make use of these new data at 740 MeV.

The Cochran et al. data provided valuable information for constructing a simple theoretical model of the pion production. The wide range of energies and of angles enabled reliable total cross sections to be determined. This is extremely valuable, since the models considered assume only single scattering so that the total cross sections are expected to be most reliable; this is true, in fact, whenever angular integrations are performed. The wide range of nuclei provides a good means of investigating the dependence of the cross section on the size of the nucleus. Of special importance is that both the π^+ and the π^- cross sections were measured. The isobar model predicts the ratio for π^+/π^- for free nucleon-nucleon collisions and experimental measurement of this will offer an indication of the role of the nuclear effects on the different charge states of the pions; it will be shown that the pion charge exchange has a much stronger effect on the π^- than on the π^+.

The Sternheim and Silbar models (1972) and (1973), like the Beder and Bendix model, are mathematically equivalent to the Glauber formalism for incoherent, quasi-elastic scattering. They use, however, a quasigeometrical approach motivated by the 740 MeV data which shows that $d\sigma/d\Omega$ and $d^2\sigma/dT d\Omega$ are quite smooth and slowly varying functions of atomic number.

Consider first the model of Sternheim and Silbar (1972) in which the Fermi averaging, the nuclear potentials and the effects of the Pauli Exclusion Principle are ignored.

The incident proton and the exiting pion are assumed to make straight line trajectories within the nucleus (Fig. 5.1). The proton penetrates the nucleus a distance d_p and it then interacts with a target nucleon to produce a pion at that point (if it has sufficient energy after undergoing attenuation by the nucleus) given by $\vec{r} = (b, z, \phi)$. The pion production ratios are again given by the (3/2,3/2) isobar model. This is not inconsistent with the production at a point since the width of the Δ implies a decay length $\leq$1fm. which is less than the typical internucleon distances. The pion is produced with a kinetic energy T at and angle θ to the original proton momentum. The pion undergoes both attenuation due to the nuclear medium and charge exchange. It then leaves the nucleus after travelling a distance d_π. Treatment of the angular distribution of the emerging pion is important so that the total cross sections may be compared, as well

as to account for the large angle contributions, especially of the π^- due to secondary scattering (charge exchange).

Since Sternheim and Silbar allow for production of pions of all three charge states, it is convenient to construct a set of transport equations to allow for the attenuation of the incident proton and the exiting pion, as well as the charge exchange of these pions.

If $N_i(0)$ pions, where $i = +, 0, -$, are produced at $\vec{r}$, then at a distance s, say, from $\vec{r}$, the populations $N_i(s)$ are given by standard transport equations, for a nucleus of atomic number A=Z+N,

$$\frac{dN_+}{ds} = -(\lambda_a + \lambda_{x,n})N_+ + \lambda_{x,p} N_0 \qquad (5.1a)$$

$$\frac{dN_0}{ds} = -(\lambda_a + \lambda_{x,n} + \lambda_{x,p})N_0 + \lambda_{x,n} N_+ + \lambda_{x,p} N_- \qquad (5.1b)$$

$$\frac{dN_-}{ds} = -(\lambda_a + \lambda_{x,p})N_- + \lambda_{x,p} N_0 \qquad (5.1c)$$

where λ_a is the inverse mean free path for pion absorption, assumed to be the same for all pions.*

$\lambda_{x,n}$ is the inverse mean free path for pion charge exchange given by $\pi^+ n \to \pi^0 p$ and $\pi^0 n \to \pi^- p$.

$\lambda_{x,p}$ is the inverse mean free path for pion charge exchange given by $\pi^0 p \to \pi^+ n$ and $\pi^- p \to \pi^0 n$.

ρ is the nuclear density.

---

* λ_a is assumed to be the same for pions of all three charges. The charge dependence of λ_a is predicted by the isobar model ($\pi NN \to NN$ is just the inverse of the production process $NN \to \pi NN$) for when N,Z>>1 as: $\lambda_{a+} : \lambda_{a0} : \lambda_{a-} = A^{-2}(2N + \tfrac{1}{2}N^2) : 1 : A^{-2}(2N + \tfrac{1}{2}Z^2)$ For N=Z, this gives 1.375:1:1.375. For ^{208}Pb, it is 1.38:1:1.28. For heavier nuclei, the π^+/π^- would be lowered.

Sternheim and Silbar assume a constant nuclear density $\mathcal{C}$,

$$\mathcal{C} = \frac{4}{3}\pi R^3 \tag{5.2}$$

where R is the nuclear radius.

The solutions for Eq. (5.1) are obtained by the standard method; for a single attenuation the transport equations would be of the form $\frac{dN(s)}{ds} = -\lambda N(o)$ and the solution would be of the form $N(s) = e^{-\lambda s} N(o)$ so that the solution of Eq. (5.1) can be written as

$$N_i(s) = \sum_{j=1}^{3} M_{ij}(s,T)\, N_j(o) \tag{5.3}$$

where

$$M_{ij}(s,T) = \exp(-\lambda_a d_\pi)\left[C_{ij}^{(1)} + C_{ij}^{(2)} \exp(-\lambda_s d_\pi) + C_{ij}^{(3)} \exp(-\lambda_+ s)\right] \tag{5.4a}$$

$$\lambda_{s,L} = \lambda_{x,n} + \lambda_{x,p} \pm (\lambda_{x,n}, \lambda_{x,p})^{1/2} \tag{5.4b}$$

and $$C_{ij} = C_{ij}\left(\frac{z}{N}\right) \tag{5.4c}$$

Eq. (5.3) is solved for $s = d_\pi$ which can be determined , ie. $d_\pi = -\ell + (\ell^2 + R^2 - b^2 - z^2)^{1/2}$ where $\ell = b\cos\phi \sin\theta + z\cos\theta$

It is also necessary to calculate the number of protons arriving at $\vec{r}$. Some will have sufficient energy, after attenuation by the nucleus to produce a pion; this cross section is given by $\sigma_{p,prod}$. Others will have insufficient energy to produce a pion and this will be represented by $\sigma_{p,abs}$. The number of protons arriving at $\vec{r}$ is thus proportional to

$$P(r) = \exp\left(-A\mathcal{C} \int \sigma_p \, dp\right) \tag{5.5}$$

where

$$\sigma_p = \sigma_{p,prod} + \sigma_{p,abs} \tag{5.6}$$

and $d_p = (R^2 - b^2)^{1/2} + z$

The probability of producing a pion of charge i is proportional to the probability of producing a pion of charge j at a point $\vec{r}$, which is, in turn, proportional to the production cross section on free nucleons times the density, ie.

$$\frac{d^2\sigma}{dT d\Omega}(\pi^i) = \sum_j I_{ij}\left(Z\frac{d^2\sigma}{dT d\Omega}(pp\to\pi^j NN) + N\frac{d^2\sigma}{dT d\Omega}(pn\to\pi^j NN)\right) \tag{5.7}$$

where

$$I_{ij} = \int d^3r\, P(d_p) \rho\, M_{ij}(d_\pi, T)$$

There are therefore 5 cross sections to be evaluated in the model: They are:

$\sigma_{p,prod}$ the cross section for producing a pion of any charge,

$\sigma_{p,abs}$ the absorption cross section which includes all those processes which leave the proton with insufficient energy to produce a pion,

$\sigma_{\pi,ch}$ the cross section for the pion charge exchange reactions,

$\sigma_{\pi,abs}$ " " " " " absorption,

$d^2\sigma/dT d\Omega\,(pN\to\pi^i NN)$ which is the free proton-nucleon production cross section.

Note that $\sigma_p = \sigma_{p,prod} + \sigma_{p,abs}$ from Eq. (5.6).

In this first paper the above cross sections are not modified for nuclear effects.

The free proton-nucleon cross section involves six cross sections for the six possible π production reactions, for

which experimental evidence was available for one, ie. $pp \rightarrow \pi^+np$. The isobar model is used to express the other five cross sections in terms of this one. Evaluating the Clebsch-Gordon coefficients, and assuming incoherence between the various contributions to a given final state gives

$$\begin{aligned} d\sigma(pp\rightarrow\pi^+np) &= 5/6\, d\sigma_{iso} \\ d\sigma(pp\rightarrow\pi^0pp) &= 1/6\, d\sigma_{iso} \\ d\sigma(pp\rightarrow\pi^-NN) &= 0 \\ d\sigma(pn\rightarrow\pi^+nn) &= 1/2\, d\sigma_{iso} \\ d\sigma(pn\rightarrow\pi^0pn) &= 1/3\, d\sigma_{iso} \\ d\sigma(pn\rightarrow\pi^-pp) &= 1/2\, d\sigma_{iso} \end{aligned} \qquad (5.8)$$

where $d\sigma_{iso}$ is the cross section for $NN \rightarrow N\Delta$, and where from experimental data it is known that $\sigma(pp\rightarrow\pi^+np) \approx 13.5$ mb for 740 MeV incident protons (Cochran et al. 1972).

The cross section for π production is then written as

$$\frac{d^2\sigma}{dT d\Omega}(\pi^+) = \frac{6}{5} A \frac{d^2\sigma(pp\rightarrow\pi^+np)}{dT d\Omega} \sum_j I_j \eta_j \qquad (5.9)$$

where

$$\begin{aligned} \eta_+ &= (10Z+N)/12A \\ \eta_0 &= (Z+2N)/6A \\ \eta_- &= N/12A \end{aligned}$$

Experimentally it is known that $\sigma(\pi^+)/\sigma(\pi^-)$ is approximately 5 for light (N=Z) nuclei and approximately 2 for heavy nuclei, but from the above isobar model predictions, the ratios are expected to be much higher, ie. for N=Z, $\eta_+ : \eta_0 : \eta_- = 11:6:1$, and for ^{208}Pb, $\eta_+ : \eta_0 : \eta_- \div 7.5:5.3:1$. This discrepancy is due to the effects of the nucleus, as well

as to the assumption of incoherence of the different amplitudes, as pointed out by Mandelstam (1958).

From the isobar model, it is also expected that, adding up the 6 contributions from Eq. (5.8), gives

$$\sigma_{p,prod} = (Z + \tfrac{1}{2}N)\,\sigma_{iso}/A \qquad (5.10)$$

$$\sigma_{iso} = \tfrac{6}{5}\,\sigma(pp \to \pi^+ np)$$

and $\sigma_{iso} \doteq 16$ mb. for a 740 MeV proton.

The three input cross sections still required are thus $\sigma_{\pi,exch}$, $\sigma_{\pi,abs}$ and $\sigma_{p,abs}$.

$\sigma_{\pi,exch}^{(T)}$ can be determined directly from experimental data by assuming that the πN system is in a pure (3/2,3/2) state; in a (3/2,3/2) resonant state, it is seen from Appendix B that the scattering amplitude in the absence of a T=1/2 state, for each of the two charge exchange processes is equal, and they can easily be related to the elastic cross section for π^+p scattering which is a pure T=J=3/2 state. Sternheim and Silbar thus use the relation that,

$$\sigma_{\pi,exch}^{(T)} = \tfrac{2}{9}\,\sigma(\pi^+ p) \qquad (5.11)$$

which is obtained numerically from Giacomelli et al. (1969).

To obtain the two remaining cross sections, less direct methods are used since little direct experimental information was available to the authors. An empirical fitting procedure is used in which $\sigma_{p,abs}$ and $\sigma_{\pi,abs}$ are chosen to the $\sigma(\pi^+)$ and the $\sigma(\pi^+)/\sigma(\pi^-)$ data.

For proton absorption, an upper limit can be determined by using

$$\sigma_{p,abs} \leq \frac{Z\sigma_{pp} + N\sigma_{pn}}{A} - \sigma_{p,prod.} \qquad (5.12)$$

where σ_{pp} and σ_{pn} are the total free proton-nucleon scattering cross sections, and where $\sigma_{p,prod}$ is known from Eq. (5.10). Pion absorption is dominated by absorption on nucleon pairs, so that an upper limit cannot be obtained for it, and Sternheim and Silbar claim that using the semi-analytical value for $\sigma_{\pi,abs}$ obtained by Beder and Bendix (Eq. 4.23) gave them poor results.

The fitting procedure was motivated by several factors: Increasing either $\sigma_{\pi abs}$ or $\sigma_{p,abs}$ decreases the production cross section, or for a fixed production cross section, an increase in $\sigma_{\pi,abs}$ requires a corresponding decrease in $\sigma_{p,abs}$, and vice versa. It is also noted that variations in $\sigma_{p,abs}$ do not directly affect the π^+/π^- ratio although the ratio is strongly dependent on $\sigma_{\pi,exch}$, ie. if $\sigma_{\pi,abs}$ is small compared with $\sigma_{\pi,exch}$, then large numbers of $\pi^{+,o}$ produced in the primary reaction ($NN \rightarrow NN\pi^{+,o}$) tend to be charge exchanged into π^- rather than be absorbed, thus decreasing the π^+/π^- ratio. With this in mind, Sternheim and Silbar choose their values to reproduce the observed π^+ production cross section and π^+/π^- ratio.

Several fitting procedures were attempted, but one in particular gave the best results: The absorption cross sections are fitted to heavy nuclei where absorption is expected to be largest, and to small angles where the multiple

scattering effects are expected to be small. The choice made is the fitting of $\frac{d^2\sigma(\pi^+)}{dT d\Omega}$ for ^{208}Pb at 15°. The differential cross sections were calculated for several values of σ_{pabs} and fitted to the above data by appropriate adjustment of $\sigma_{\pi abs}$ (Fig. 5.2). For each σ_{pabs} and corresponding $\sigma_{\pi abs}(T)$, the π^+/π^- ratios were calculated, and the best fit was chosen. This gave a value of $\sigma_{pabs} = 30$ mb which is very close to the theoretical maximum of 33 mb. Figure 5.2 shows and increase in $\sigma_{\pi abs}(T)$ with increasing T, which is in direct contrast to the results of Beder and Bendix. This disagreement in results is ,however, greatly reduced by the introduction of Fermi averaging which decreases the pion absorption for $T_\pi > 200$ MeV; this is seen in the second paper by Sternheim and Silbar (Section 5.3). The nuclear absorption is also reduced by the nuclear corrections. This method of fitting the two cross sections does, however, mask many errors which might be hidden in the model, and good fits with the data may be meaningless.

All the cross sections are then substituted into Eq. (5.7), and the production cross sections are determined.

In the results of this model, the values for $\sigma(\pi^+)$ were only slightly high, and the $\sigma(\pi^-)$ values were only slightly low for small Z nuclei, while for large Z nuclei both cross sections were 15-30% too high. The $\sigma(\pi^+)/\sigma(\pi^-)$ ratios compared well for all nuclei. (Table V.1)

In order to decrease the calculated values for $\sigma(\pi^\pm)$, the amount of absorption for large A must be increased which seems

impossible with only $\sigma_{p,abs}$ and $\sigma_{\pi,abs}$ as free parameters, since $\sigma_{p,abs}$ is close to the maximum allowed value, and any increase in $\sigma_{\pi,abs}$ will tend to increase the π^+/π^- ratio. One method of overcoming this would be to include the charge dependence of the pion absorption coefficient, as was previously mentioned. It is also expected that the inclusion of the charge exchange of the incident proton would lower the π^+/π^- ratio, since by the isobar model more π^- would be produced in pn and nn collisions. In this model, the value of $\sigma_{\pi,abs}$ is very small (since $\sigma_{p,abs}$ is large), but if $\sigma_{\pi,abs}$ were increased then a better fit might be expected; again, this larger $\sigma_{\pi,abs}$ is obtained in the following model.

A strong dependence on the nuclear radius is found: $\sigma(\pi^+) \propto R^{5/2}$, $\sigma(\pi^-) \propto R^2$ and thus $\pi^+/\pi^- \propto R^{1/2}$. This strong dependence on the nuclear radius implies that the use of a constant nuclear density, rather than a more realistic diffuse-edged Woods-Saxon density, may be quite important.

This strong R dependence, and thus A dependence since $R \propto A^{1/3}$, is an indication of the validity of a geometrical model of pion production. Figs. 5.3 and 5.4 show the comparison of the experimental and the theoretical geometrical dependences of $\sigma(\pi^+)$ and $\sigma(\pi^-)$; the experimental data shows that $\sigma(\pi^+) \propto Z^{1/3}$ and that $\sigma(\pi^-) \propto N^{2/3}$ but the theoretical predictions only matches the data for small nuclei, while for heavy nuclei the predictions are too high due to the

high cross sections for these nuclei.

The power law dependences observed are consistent with large nuclear absorption: Due to the high absorption, it is expected that the π^+'s are formed near the rim of the nuclear disc and the main contribution will thus be an R or an $A^{1/3}$ dependence. Since most of the π^+ production is due to collisions with target protons, there is also a Z/A factor, which gives a $Z/A^{2/3}$, or $Z^{1/3}$, dependence for $\sigma(\pi^+)$. For the case of the π^- production, however, the loss due to absorption is nearly balanced by the charge exchange of π^0 to π^-. It is thus expected that there is a stronger R, or A, dependence, ie. proportional to the area $R^2 \propto A^{2/3}$. Since the π^- (and π^0) are mainly produced from neutrons in the disk, there is an N/A contribution giving, finally, that $\sigma(\pi^-) \propto N/A^{1/3}$, or $N^{2/3}$.

To study the angular distributions, $d^2\sigma/dT d\Omega^{(\pi^i)}$ in Eq. (5.9), is numerically integrated over T.

From Fig. 5.5, it is seen that $d\sigma/d\Omega^{(\pi^+)}$ fits very well for the C and Cu but not for Pb for which is generally too high; this leads to a high total cross section for Pb.

Fig. 5.6 gives the results for $d\sigma/d\Omega^{(\pi^-)}$. The fit is again better for C and Cu than for Pb, but in all cases the results are worse than for π^+. The cross sections tend to underestimate the high angle π^- population, and overestimate the number at small angles. This is expected to be mainly

due to the neglect of multiple scattering. As mentioned, this is more evident in the π^- predictions than in the π^+ predictions since the π^- population is strongly enhanced by secondary, ie. charge exchange, processes.

Calculations of the doubly differential cross sections also tend to be more agreeable with the data for the lighter nuclei (Figs 5.7 and 5.8). For π^+ production at small angles (30^o) there is a tendency to be too small at low energies and too high at high energies; again, this is a result of the neglect of multiple scattering which would tend to shift and smear out the energy spectrum due to the degrading of the pion energy. As one might expect, the peak becomes sharper and goes to lower energies as one goes to large angles.

The π^- spectra have the same general features as the π^+ spectra, and the comparisons of the calculated spectra with the observed spectra are similar. For the π^- case, however, the calculated and the experimental spectra are even more disparate. This is a result of the neglect of the multiple scattering being more important for the π^- than for the π^+.

The inclusion of the prediction of pions of all charges has seen to be very beneficial. In the next paper reviewed, Sternheim and Silbar (1973) continue with basically the same format but nuclear effects are included.

Section 5.3 Geometrical model with nuclear corrections

In their second paper, Sternheim and Silbar (1973) extend their semiclassical geometrical model to include the important modifications due to the nuclear effects, ie. Fermi motion of the target nucleons, the Pauli Exclusion Principle and the nuclear potentials. Also included are the charge exchange of the incident proton and a more realistic diffuse edged nuclear density. The latter necessitates a numerical integration of Eq. (5.7).

Four cross sections from the original paper, ie. $\sigma_{N,abs}$, $d^2\sigma_{150}/dT d\Omega$, $\sigma_{\pi,exch}$, and $\sigma_{\pi,abs}$, and $\sigma_{N,exch}$, the nucleon charge exchange cross section introduced in this paper are adjusted according to the nuclear effects mentioned; the appropriate correction which is required is not always easy to determine, nor is it always unique. The corrections are often included in an ad hoc manner.

It was hoped by the authors that inclusion of the nuclear corrections would improve the accuracy of the results, and that more information could be obtained about the nuclear surface, however, due to the uncertainties in the corrections, this was not possible. The comparisons of the total cross sections with the data are not improved, and, in fact, the π^+/π^- ratios are worse. Much, however, is learned about the role of the nuclear medium through the effects of the nuclear corrections on the various cross sections.

The basic formalism of the model is the same as for Sternheim and Silbar (1972) and the setting up of the production cross section is equivalent to Eq. (5.9). Icluded in this model are transport equations, modified to include the nucleon charge exchange of the incident proton.

The number of protons and neutrons arriving at the productions point $\vec{r}$ is determined by

$$N_p' = -(\lambda_a^N + \lambda_{x,n}^N + \lambda_{\Delta,p}) N_p + \lambda_{x,p}^N N_n \qquad (5.13a)$$

$$N_n' = -(\lambda_a^N + \lambda_{x,p}^N + \lambda_{\Delta,n}) N_n + \lambda_{x,n}^N N_p \qquad (5.13b)$$

where λ_a^N is the inverse mean free path for nucleons, which is assumed the same for neutrons and protons, for absorption. λ_{xn}^N and λ_{xp}^N are the inverse mean free path lengths for nucleon charge exchange, ie. pn→np and np→pn, respectively and $\lambda_{\Delta,p}$ and $\lambda_{\Delta,n}$ are the inverse mean free path lengths for pion production as given by the isobar model:

$$\lambda_{\Delta,p} = (Z + \tfrac{1}{2}N)\rho\sigma_{iso} \quad \text{and} \quad \lambda_{\Delta,n} = (N + \tfrac{1}{2}Z)\rho\sigma_{iso}$$

The nuclear density is now given by

$$\rho(\vec{r}) = \rho_0 \left[1 + \exp(r - r_0)/a\right]^{-1} \qquad (5.14)$$

normalized to $\int \rho \, d^3r = 1$.

The transport equations are solved as for the pions, and N_p and N_n are given as functions of $\sigma_{N,abs}$, $\sigma_{N,exch}$, σ_{iso}, N and Z. A final expression, equivalent to Eq. (5.7), for the cross section for production of pions of charge i, at a point $\vec{r}$, is given by

$$\frac{d^2\sigma(\pi^+)}{dT\,d\Omega} = \frac{d^2\sigma_{iso}}{dT\,d\Omega} \sum_j \int d^3r\, \rho(\vec{r})\, M_{ij}(r,T)\left[N_p(r)\, p_j + N_n(r)\, n_j\right] \quad (5.15)$$

where the weight factors p_j and n_j are given by the Clebsch-Gordon coefficients of the isobar model:

$$\begin{aligned} p_+ &= \tfrac{5}{6}Z + \tfrac{1}{12}N \\ p_0 &= \tfrac{1}{6}Z + \tfrac{1}{3}N \\ p_- &= \tfrac{1}{12}N \\ n_+ &= \tfrac{1}{12}Z \\ n_0 &= \tfrac{1}{3}Z + \tfrac{1}{12}N \\ n_- &= \tfrac{1}{12}Z + \tfrac{5}{6}N. \end{aligned} \quad (5.16)$$

The absorption, charge exchange and production cross sections are then evaluated with the appropriate nuclear corrections. An improvement is made in the evaluation of the pion and nucleon absorption cross sections. An empirical fitting procedure is used only in the determination of $\sigma_{\pi,abs}$, and the nucleon absorption is evaluated separately using a small angle exponential fit to the pp cross section; a more meaningful fit is expected using this method.

To determine $\sigma_{N,abs}$, an empirical fit of the elastic pp cross section* is used, ie.

$$\frac{d\sigma}{dt} = 25.9\, e^{-c|t|}\ mb\left(\frac{GeV}{c}\right)^{-3}$$

* At 740 MeV, the total pp cross section is 46 mb (Benary et al. 1970). From Cochran et al. (1972), $\sigma(pp \to \pi^+ np) \div 2.7$mb., and from the isobar model, the π^0 production is $1/5(\sigma(pp\ \pi^+ np)) \div 2.7$ mb. This leaves 30 mb. as elastic pp scattering.

where C = 4.1 and 4.98 $(GeV/c)^{-2}$ at 705 and 788, respectively. Now, $\sigma_{N,abs}$ at 740 MeV is assumed to correspond to an energy loss of >180 MeV, implying a laboratory scattering angle of $>26^0$, since this is one half width below the threshold for pp $N\Delta$. (It is found by experiment, that at 560 MeV, the π^+ and π^0 production have been reduced by 64% and 74%, respectively (Benary et al 1970).) Now, an energy loss of 180 MeV by a nucleon corresponds to a momentum transfer of $-2m\,\Delta E = t_{max} = 0.388(GeV/c)^2$. An estimate of $\sigma_{N,abs}$ is thus given by

$$\sigma_{N,abs} = \int_{-\infty}^{t_{max}} \left(\frac{d\sigma}{dt}\right) dt$$

$$= \begin{cases} 6.5 \text{ mb at } 705 \text{ MeV} \\ 4.8 \text{ mb at } 788 \text{ MeV} \end{cases}$$

which gives an average of

$$\sigma_{N,abs} = 5.6 \text{ mb at } 740 \text{ MeV}. \qquad (5.17)$$

Note that this value is much smaller than the previous value of 30 mb. This smaller value of nucleon absorption implies that in the fitting procedure for $\sigma_{\pi,abs}$, a larger value for $\sigma_{\pi,abs}$ is possible. Margolis and Beder and Bendix also use a large value ($\sigma_{N,abs} \div \sigma_{NN}^{(elastic)} \div 25$ mb.). Such a large value of $\sigma_{N,abs}$ indicates that pion production is mainly on the nuclear surface, and thus a strong dependence on the nuclear surface results. With the new, lower value of $\sigma_{N,abs}$, the results are not expected to be so dependent on the surface effects. Since there is little dependence of $\sigma_{N,abs}$ on energy,

and there is little energy lost so that the final energies are large, there are no corrections made for the Pauli Principle, Fermi motion or nuclear potentials.

$\sigma_{N,exch}$ is the cross section for an incident proton scattering off a neutron, with the neutron emerging with most of the momentum. This can be related, in the nuclear case, to the free nucleon charge exchange $d\sigma/d\Omega(pn \rightarrow np)$, but a factor must be included to account for the angular dependence. Recall that if the proton is scattered through more than 26°, it has insufficient energy to create a pion, so that to obtain the total cross section for nucleon exchange, the differential cross section needs to be integrated only form 0° to 26°. To account for the Pauli Principle, Sternheim and Silbar include a multiplicative factor denoted by $R(\theta)$, which reduces the contribution to the cross section $d\sigma/d\Omega$ for small angle scattering. The form of $R(\theta)$ is deduced from an argument from Bethe (1973) which is based on the treatment of the nucleus as a Fermi gas with Fermi momentum $\vec{k}_F$. If the struck neutron has an initial laboratory momentum $\vec{k}$ ($|\vec{k}| \leq |\vec{k}_F|$) then the final proton has a momentum $\vec{k}' = \vec{k} + \vec{q}_L$ where $\vec{q}_L$ is the 3-momentum transfer. In momentum space, both $\vec{k}$ and $\vec{k}'$ lie within spheres of radius k_F with the centres of the two spheres displaced by a distance q_L. Thus, the overlap of the two spheres gives the region of momentum space excluded by the Pauli Principle. $R(\theta)$ is given by

$$R(\theta) = \frac{3}{4}\frac{q_\perp}{k_F}\left(1 - \frac{q_\perp^2}{12 k_F^2}\right) \qquad (5.18)$$

Note that $R(\theta)$ reduces the cross section more for small momentum transfers , ie. small angles, than for large momentum transfers, ie. large angles. This is in accordance with the Pauli Principle which restricts the "occupancy" of the energy levels in the Fermi gas model nucleus. As with $\sigma_{N,abs}$, due to the weak energy dependence of $d\sigma/d\Omega$, the effects of Fermi motion averaging and nuclear potentials. With k_F = 250 MeV/c and using the average of the data for at 649 Mev and 816 MeV which are 3.4 mb. and 2.8 mb., respectively, gives for 740 MeV,

$$\sigma_{N,exch} = 3.1 \text{ mb.} \qquad (5.19)$$

Without the Pauli Exclusion effects, this value would be approximately 4.3 mb. (÷ 40% change)

For $d^2\sigma_{iso}/dT d\Omega$, Silbar and Sternheim use a phase space model to determine the factor, called $F(T,\theta)$, which corrects the free $pp \rightarrow \pi^+ np$ for the nuclear effects. The effect of the Pauli Principle is small for even the fastest pions, ie. the slowest nucleons, and therefore it is neglected. Included in $F(T,\theta)$ are corrections for Fermi motion and for the nucleon-nucleus and the pion-nucleus potentials. $F(T,\theta)$ is given by

$$F(T,\theta) = \frac{(d^2\sigma/dT d\Omega)_{ave}}{(d^2\sigma/dT d\Omega)_{free}} \qquad (5.20)$$

where the denominator is obtained from experiment, and where the numerator is the Fermi averaged free cross section, ie.

$$\left(\frac{d^2\sigma}{dT\,d\Omega}\right)_{ave} = \frac{3}{4\pi k_F^3}\int_0^{k_F} d^3k \left(\frac{d^2\sigma(\vec{k})}{dT\,d\Omega}\right)_{free} \qquad (5.21)$$

The right side of Eq. (5.21) is determined using standard relativistic quantum mechanics:

$$\left(\frac{d^2\sigma(\vec{k})}{dT\,d\Omega}\right)_{free} = \frac{p_{\pi,lab}}{\left[p_1\cdot p_2 - p_1^2 p_2^2\right]^{1/2}} \frac{k_{NN}}{W_{NN}} |M|^2 \qquad (5.22)$$

where $\vec{k}$ is the 3-momentum of the struck nucleon,

p_1 and p_2 are the initial 4-momenta,

k_{NN} is the 3-momentum of one of the nucleons in the final 2-nucleon centre-of-mass frame,

$W_{NN}^2 = p_1' + p_2'$ is the invariant mass squared of the final NN system, and $p_{\pi,lab}$ is the pion laboratory momentum.

In the formulation of Silbar and Sternheim, $|M|^2$ is constant, and only the phase space factor is considered. Since $|M|^2$ is in both the numerator and denominator of Eq. (5.2), it is argued that the energy and angle dependence of $|M|^2$ will tend to cancel out.

The kinematical quantities on the right side of Eq. (5.22) are modified to include the effects of the nuclear potentials.

The incident proton, with 4-momentum $p^\mu = (E_{in}, \vec{p}_{in})$, enters the nucleus which is represented by a repulsive optical potential with a real part $V_1 \div 26$ MeV (Benary 1970). For a free particle entering a constant potential, the 3-momentum is changed while the energy is unchanged, so that for the 4-momentum

of the proton inside the nucleus, $p^{\mu}_{1,in} = (E_{1,in}, \vec{p}_{1,in})$ it is known that

$$E^2_{1,in} \equiv E^2_{1,out} = p^2_{1,out} + m^2 \tag{5.23}$$

$$p^2_{1,in} = (E_{1,in} - V_1)^2 - m^2 \tag{5.24}$$

The initial bound nucleon, with a 3-momentum $\vec{k}$, has an energy

$$E_2 \equiv k_0 = (m^2 + k^2)^{1/2} + V_2 \tag{5.25}$$

where $V_2 (<0)$ is such that the "last" nucleon, ie. the nucleon for which $|\vec{k}| = k_F$, is bound by B=8 MeV, ie.

$$V_2 = m(-m^2 + k_F^2)^{1/2} - B \approx -\frac{k_F^2}{2m} - B \tag{5.26}$$

The optical potential felt by the final nucleons is ignored, arguing that it will be negligible compared with V_1 or V_2, ie. $V_2 < V < V_1$, and $V_2 < 0$ and $V_1 > 0$, so that $V \div 0$.

In determining the optical potential felt by the emerging pion, it is argued by Silbar and Sternheim that no modification of $p_{\pi,lab}$ is necessary. They argue that since the range of the p-wave πN interaction is only 0.4 fm., and the internucleon distance is about 1.8 fm., then, at the moment of creation, the pion interacts only with the 2 nucleons which contributed directly to its cration. It is admitted by the authors that this is "rough at best". A calculation using the pion optical potential of Goldberger and Watson (1964), as did Beder and Bendix, apparently resulted in a very wild behaviour of $\sigma_{\pi abs}$.

It is also required, for $\left(\frac{d^2\sigma(\vec{k})}{d\tau d\Omega}\right)_{free}$, to calculate W_{NN} and thus

$$k_{NN} = \left(\frac{1}{4} W_{NN}^2 - m^2\right)^{1/2} \qquad (5.27)$$

where $$W_{NN}^2 = (p_1' + p_2')^2$$

and where $$p_1 = (E_1, \vec{p}_{1,in})$$
$$p_2 = (E_2, \vec{p}_{2,in}) \equiv (k_0, \vec{k})$$
$$p_\pi = (E_\pi, \vec{p}_\pi)$$

are all measured in the laboratory frame. Using conservation of energy and momentum, and using the impulse approximation so that the momentum of the nuclear residua is the same before and after the pion production, gives

$$W_{NN}^2 = (p_1 + p_2 - p_\pi)^2 \qquad (5.28)$$

In all cases, the Coulomb potentials are ignored. $F(T,\theta)$ is then the same for all nuclei and for pions of all charges. The error in neglecting the Coulomb interactions is, at most, 15% which is for ^{208}Pb, the heaviest nucleus considered.

The effects on the phase space spectrum of the Fermi averaging and the inclusion of the optical potential V_1 on the incident nucleon are indicated in Fig. 5.9. The Fermi averaging, as discussed in Beder's and Bendix's paper, decreases the cross section in the region of phase space accessible to the free nucleon case, and gives the spectrum a high energy tail. The further inclusion of V_1, a repulsive potential, increases the cross section due mainly to a

decrease in the invariant flux factor $[(p_1 \cdot p_2)^2 - p_1^2 p_2^2]^{\frac{1}{2}}$, also the high energy tail is extended out to a further cutoff, since a smaller incident nucleon momentum implies that the heavy nucleons are not required to carry away such high momenta to balance the conservation requirements. This results in more kinetic energy being available for the pion.

$F(T,\theta)$ is then given by the ratio of curve (c) to curve (a) in Figure 5.9, and is arbitrarily set to 1 for the high energy tail.

$\sigma_{\pi,exch}^{(T)}$ is determined from the free pion charge exchange cross section, and since $\sigma_{\pi,exch}^{(T)}$ is a strong function of energy, Fermi averaging on the free cross section is required, giving

$$(\sigma_{\pi,exch})_{ave} = \frac{3}{4\pi k_F^3} \int d^3k \int d\Omega \left(\frac{d\sigma_{\pi,exch}}{d\Omega}\right)_{free} \Theta \qquad (5.29)$$

where Θ incorporates the Pauli Principle, ie.

$$\Theta = \begin{cases} 1 & |\vec{k}'| > k_F \\ 0 & |\vec{k}'| \leq k_F \end{cases} \qquad (5.30)$$

where $\vec{k}'$ is the final nucleon momentum in the laboratory. From before, $|\vec{k}'| = (k^2 + 2\vec{k}\cdot\vec{Q}_L + Q_L^2)^{\frac{1}{2}}$ where Q_L is the laboratory momentum transfer. Q_L is obtained by a Lorentz transformation, given by $\beta = \frac{\vec{p}_{\pi in} + \vec{k}}{E_\pi + k_0}$, of the centre-of-mass momentum transfer $Q_{c.m.}$. $Q_{c.m.}$ is given by $Q_{c.m.}^\mu = (q - q')^\mu = (0, \vec{Q}_{c.m.})$ and $Q_{c.m.}^2 = 2q^2(1 - \cos\theta_{c.m.})$. For the expression for the free pion charge exchange, it is again assumed that the (3/2,3/2) interaction dominates the πN system, so that

$$(\sigma_{\pi,exch})_{free} = \frac{2}{9}\,\frac{\sin^2\delta(q)}{q^2}\,(1+3\cos^2\theta_{c.m.}) \qquad (5.31)$$

where q is the centre-of-mass momentum and $\theta_{c.m.}$ is the scattering angle in the πN centre-of-mass system. The angular distribution is that of a p-wave and the expression for $\delta(q)$ is given by using a Breit-Wigner shape for the resonance:

$$\tan\delta(q) = \frac{M_\Delta\,\Gamma(q)}{M_\Delta^2 - W^2}$$

where

$$W^2 = (p_\pi + p_N)^2$$

$$q^2 = [(p_\pi \cdot p_N)^2 - p_\pi^2 p_N^2]\,/\,W^2$$

and where p_π and p_N are 4-vectors.

To calculate $p_\pi = (E_\pi, \vec{p}_{\pi,in})$, knowledge is required about V_π, and $f_{\pi N}(0)$, the appropriate resonance amplitude. A dispersion relationship is used:

$$p_\pi^2 - 4\pi C f_{\pi N}(p_\pi, E_\pi) = p_\pi^2 = E_\pi^2 - \mu^2 \qquad (5.32)$$

where $p_{\pi,in} = Re\,p_\pi$ and $\mu^2 = E_\pi^2 - p_{\pi,in}^2$. A Chew-Low expression is used for the scattering amplitude:

$$f_{\pi N}(p_\pi, E_\pi) = \frac{C p_\pi^2}{(E_R - E_I - i\Gamma/2)} \qquad (5.33)$$

where C and Γ are assumed to be constants, used to fit the total averaged πN cross section. From this, $p_{\pi,in}$ is given by

$$p_{\pi,in}^2 = p_\pi^2\, f(x) \qquad (5.34)$$

where

$$f(x) = \frac{1}{2}\left[1 + \frac{\alpha x}{1+x^2} + \left(1 + \frac{\alpha(2x+\alpha)}{1+x^2}\right)^{1/2}\right],$$

$$x = \frac{E_R - 4\pi\rho C - E_\pi}{\Gamma/2}$$

$$\alpha = \frac{4\pi\rho C}{\Gamma/2}$$

Figure 5.10 shows $f(x)$, p_π, $p_{\pi,in}$ and μ^{*2}/μ^2 as a function of pion kinetic energy. It is seen that the pion potential is attractive below resonance, in that the $p_{\pi,in}$ curve crosses over the curve for p_π. The cross-over is also shifted $4\pi\rho C$ =76 MeV before the free resonance peak due to the simplicity of the model. The final expression for $(\sigma_{\pi,excl.})ave$ is given in Figure 5.11, with the effects of the inclusion of the Fermi-averaging, the Pauli Exclusion Principle and the pion potential indicated.

Only $\sigma_{\pi,abs}^{(T)}$ remains to be calculated. Whereas in the previous paper, $\sigma_{\pi,abs}$ and $\sigma_{N,abs}$ were adjusted to fit the π+ data, in this paper $\sigma_{N,abs}$ is calculated indepently, and it is required to fit only $\sigma_{\pi,abs}$ to the data. Again, the cross section is fitted to the data for $d^2\sigma(\pi^+)/d\Omega d\Omega$ for Pb at 15°. This fit gives a broad resonance shape for $\sigma_{\pi,abs}^{(T)}$ centred about 200 MeV. It is interesting to note the energy dependence of the calculated $\sigma_{\pi,abs}^{(T)}$ for various models and cases of models (Figure 5.12). The dependence varies greatly for the models considered. It is also pointed out, but not indicated in Fig. 5.12 that a fit for $\sigma_{\pi,abs}^{(T)}$ for V_π=0 gave a curve that varied from curve (a) by less than 7% (so that hopefully the rather arbitrary choice for V_π will not be too important in the calculation). It is seen that the pion absorption cross section obtained by Beder is not in such sharp disagreement with the new value obtained by Silbar and Sternheim. The effect of the nuclear effects, especially through $F(T,\theta)$,

can be seen quickly through comparison of curves (b) and (c), where $\sigma_{N,abs}$ in both of the Sternheim and Silbar models has been set to 25mb; this peak in the pion absorption cross section is not unreasonable since it seems to be a reflection of the πN interaction.

The results are tabulated for Al, Cu and Pb in Table V.1 . Only the total cross sections are included; it is found that with the nuclear corrections included, the comparison of the results for the energy spectra and the angular distributions with the data, are qualitatively little different from the first model with no nuclear corrections. For the total cross sections, it is seen that $\sigma(\pi^+)$ is improved over the simpler model for Pb, but the agreement worsens with decreasing Z, for which cases, $\sigma(\pi^+)$ is too low. This contrasts with the earlier model in which the calculated $\sigma(\pi^+)$ is in agreement with the Al data, but is too high for higher Z. The $\sigma(\pi^-)$ is too low in all cases, with agreement worst for Al. (In the previous paper, $\sigma(\pi^-)$ is too large for Pb.)

The result of this is that the ratio π^+/π^- is too high for the heavy elements.

An interesting calculation is made to investigate the geometrical nature of the pion production by dividing the target nucleus into eight bins, as indicated in Fig. 5.13 with the results in Table V.2 . It is found that 75% of the π^+ production does come from the annulus, and especially from bins 2. In fact, 50% of π^+ is produced in the region

where $\rho < 0.7\rho_0$. For π^-, there is relatively more production throughout the nucleus, and 34% originates in the denser core region ($\rho > 0.3\rho_0$). This supports the fact that much of the π^- production occurs via secondary reactions.

Although the results of the production cross sections have not been improved with the inclusion of the nuclear corrections, it is informative to consider the quantitative effects of the nuclear corrections on the various cross sections, as indicated in Table V.3. It is seen that the largest effect is due to the Fermi averaging and the nucleon potentials; it is pointed out by Sparrow, Sternheim and Silbar (1974) that the Fermi averaging of the $d^2\sigma_{iso}/d\tau d\Omega$ was incorrect and it has only an 18% effect in the isobar paroduction cross section. Note also that the inclusion of nucleon charge exchange has a +25% change to $\sigma(\pi^-)$. The nuclear density chosen also has a large effect, about 15% for $\sigma(\pi^+)$; this again indicates that the π^+ production is more sensitive to the surface nuclear density.

The introduction of the nuclear effects has not improved the numerical results of the model; this may not just be a reflection of the ambiguities of the nuclear corrections, but it also might be due to the fitting of the first model to the data which could have resulted in a meaningless fit, and thus an unwarranted confidence in the results.

Sparrow, Sternheim and Silbar (1974) extended the model to account for pion production from neutron collisions with nuclei. These results are related simply to the proton collision results by charge independence; for an N=Z nucleus, the "roles" of the π^+ and the π^- production are interchanged when comparing proton and neutron induced collisions with the nucleus. Of particular interest is a check of the isobar model, as well as further investigation of the pion absorption cross section. Data was used from Oganesyan (1968) for 600 MeV neutron collisions, and from Cochran et al. (1972).

The procedure of the model was the same as for Silbar and Sternheim (1973), except that the nuclear corrections were not included. The effect of these corrections was determined by turning them on, one by one. The results are seen in Table V.4. It is again pointed out that the Fermi averaging of $d^2\sigma/d\tau d\Omega$ was incorrectly calculated in the previous paper.

Sparrow, Sternheim and Silbar also include in the nucleon absorption, an angular dependence which increases the absorption from 5.6 mb. to 8.0 mb. A further correction is included to allow for small angle multiple scattering of the nucleon which is expected to strongly affect the nucleon absorption; this further increases the cross section to 11.2 mb. for an N=Z nucleus, and 10.6 mb for ^{208}Pb.

It is also shown that the Fermi averaging of the pion absorption cross section is very important for high energy

pions (Fig. 5.14), for while the Fermi averaging decreases $\sigma_{\pi abs}$ by only 18%, the effect is mainly felt at the high energy end of the spectrum.

The authors also find that their $\sigma_{\pi,exch}$ is twice as sensitive to nuclear corrections as the value in the previous paper. This is a result of a different $\sigma_{\pi abs}$, since there is a strong coupling between the energy dependences of $\sigma_{\pi,exch}$ and $\sigma_{\pi abs}$. The coupling exists because both cross sections increase rapidly between 100 MeV and 200 MeV. If the energy loss of the pion during charge exchange were considered, the strong coupling would not be expected.

Section 5.4 Extension to include multiple scattering with and without nucleon recoil

The Sternheim and Silbar model has been extended to include multiple scattering by Adler (1974) and Adler, Nussinov and Pascho (1974). In this improved model, straight line propogation is again assumed, but the incident and outgoing particles are allowed to scatter back and forth several times off target nucleons before leaving the nucleus. The scattering in the forward hemisphere is treated as 0° scattering, while that in the backward hemisphere is treated as 180° scattering. This is reasonable for πN scattering at intermediate energies, since at these energies, the πN scattering is predominantly p-wave with a characteristic angular distribution proportional to $(1+3\cos^2\theta)$, which is peaked at $\theta = 0^{\circ}$ and 180°. Adler, in discussing the πN scattering, assumes that the target nucleon is fixed within the nucleus, thus ignoring nucleon recoil; a pion can lose more than half of its kinetic energy in a large angle scattering, so the recoil effect may be substantial.

Adler's model results in a series that can be summed exactly, so that all orders of multiple scattering are included. Taking the series term by term, the nucleon recoil effects are simply included; this is accomplished by Yang, Sparrow, Holstein and Sternheim (1976).

The inclusion of multiple scattering is expected to

increase the predicted number of large angle pions, particularly π^-'s, which is underestimated in the simpler models. Inclusion of the nucleon recoil is expected to account also for the number of pions, again particularly π^-'s, which are produced at low energies.

Using Adler's series, Yang, Sparrow, Holstein and Sternheim account for the energy loss due to the nucleon recoil in each multiple scattering, in each term of the series. The expressions for the production cross sections used in the Sternheim and Silbar and Adler models are then seen to be particular cases of the more general recoil, multiple scattering model.

In the model, the incident nucleon enters the nucleus in a straight line path, and a pion is produced at some target nucleon, via the reaction $NN \rightarrow \pi NN$, with kinetic energy T, at an angle θ to the path of the incident nucleon. Due to backscattering, the direction of the pion's path can be reversed several times before leaving the nucleus. The production mechanism is dominated by the (3/2,3/2) isobar model, and the pion and the incident nucleon both undergo attenuation by the nucleus and charge exchange.

Transport equations for the nucleons are, as before, given by Eq. (5.13), and transport equations, equivalent to Eq. (5.1), for the pions are given by

$$\frac{dN_+}{dx} = -\left\{\sigma_{abs} A + \sigma_{\pi p}\left[\frac{2}{9} N + \mu_- \left(2 + \frac{1}{9} N\right)\right]\right\} \rho N_+ + \sigma_{\pi p} \frac{2}{9} \mu_+ 2 \rho N_0 \quad (5.35a)$$

$$\frac{dN_0}{dx} = \sigma_{\pi p} \frac{2}{9} \mu_+ A \rho N_+ - \left[\sigma_{abs} A + \sigma_{\pi p}\left(\frac{2}{9} + \mu - \frac{4}{9}\right) A\right] \rho N_0 + \sigma_{\pi p} \frac{2}{9} \mu_+ \cdot 2 \rho N_- \quad (5.35b)$$

$$\frac{dN_-}{dx} = \sigma_{\pi p}\frac{2}{9}\mu_+ z\rho N_0 - \{\sigma_{abs}A + \sigma_{\pi p}[\frac{2}{9}z + \mu_-(N+\frac{1}{9}z)]\}\rho N_- \qquad (5.35c)$$

where σ_{abs} is the absorption cross section (same for all pions), $\sigma_{\pi p}$ is the π+p cross section at energy T, and where μ_+ and μ_- are the probabilities that a pion striking a nucleon will be forward or backward scattered, respectively.

The transport equations are solved by diagonalizing the matrix elements to give

$$N(x) = P_0(x,T)\,N(0) \qquad (5.36)$$

where $P_0(x,T)_{ij} = \sum_k S^{-1}_{ik} e^{-A\rho\lambda_{kk}} S_{kj}$. S is a similarity transformation, and λ_{kk} are the eigenvalues of the matrix.

A pion leaves the nucleus at an angle θ without backscattering and this is described by

$$N^{(0)}(\theta,T) = P_0(L,T)\,N_i(\theta,T) \qquad (5.37)$$

where N_i is the population of π^i at the production point with energy T at an angle θ . A pion may also leave the nucleus at an angle θ , if it is produced at an angle $\pi-\theta$, and then undergoes a single backscatter. This is given by

$$P_1(L,T) = \int_0^L dx\, P_0(x+L,T)\,\beta(T_1)\,P_0(x,T_1) \qquad (5.38)$$

where T_1 is the pion energy at which the pion is produced. After the backscatter, it is at an energy of T , and β is

the backscatter matrix:

$$\beta(T) = \mu_- \rho\, \sigma_{\pi p}(T) \begin{pmatrix} Z+\frac{1}{9}N & \frac{2}{9}Z & 0 \\ \frac{2}{9}N & \frac{4}{9}A & \frac{2}{9}Z \\ 0 & \frac{2}{9}N & N+\frac{1}{9}Z \end{pmatrix} \tag{5.40}$$

This gives a contribution to $N(\theta,T)$ of

$$N^{(1)}(\theta,T) = P_1(L,T)\, N_i(\pi-\theta, T_1) \tag{5.41}$$

This can be extended to n-backscatters. The cross section for producing a pion of charge i, at an angle θ and energy T, is

$$\frac{d^2\sigma(\theta,T)_i}{dT\,d\Omega} = \sum_{\substack{n=0 \\ n\ \text{even}}}^{\infty} \frac{d^2\sigma^{iso}(\theta,T_1)}{dT\,d\Omega} \sum_j \int d^3r\, \rho(\vec{r})\, P_{ji}(L(\vec{r}),T)_{ij}\, (N_p(\vec{r})\rho_j + N_n(\vec{r})\eta_j)$$

$$\sum_{\substack{n=0 \\ n\ odd}}^{\infty} \frac{d^2\sigma^{iso}(\pi-\theta,T_1)}{dT\,d\Omega} \sum_j \int d^3r\, \rho(\vec{r})\, P_{ji}(L(\vec{r}),T)_{ij}\, (N_p(\vec{r})\rho_j + N_n(\vec{r})\eta_j) \tag{5.42}$$

where ρ_j and η_j are given in Eq. (5.16)

Now, for the Adler model energy losses due to recoil are ignored so that $T_1 = T_2 = \cdots = T_n = T$, so that Eq. (5.42) reduces to

$$\frac{d^2\sigma(\theta,T)_i}{dT\,d\Omega} = \frac{d^2\sigma^{iso}(\theta,T_n)}{dT\,d\Omega} \sum_j \int d^3r\, \rho(r)\,(N_p(\vec{r})\rho_j + N_n(\vec{r})\eta_j) \sum_{\substack{n=0 \\ n\ even}}^{\infty} P_{ji}(L(\vec{r}),T)_{ij}$$

$$+ \frac{d^2\sigma^{iso}(\pi-\theta,T_n)}{dT\,d\Omega} \sum_j \int d^3r\, \rho(r)\,(N_p(\vec{r})\rho_j + N_n(\vec{r})\eta_j) \sum_{\substack{n=0 \\ n\ odd}}^{\infty} P_{ji}(L(\vec{r}),T)_{ij} \tag{5.43}$$

which can be summed exactly.

Finally, the Sternheim and Silbar models are obtained by ignoring the backscatter, ie. set $\mu_+ = 1, \mu_- = 0$ in Eq. (5.43) to get:

$$\frac{d^2\sigma(\theta T)}{dT\,d\Omega} = \frac{d^2\sigma^{150}(\theta T)}{dT\,d\Omega} \sum_j \int d^3r\, \rho(\vec{r}) \left(N_p(\vec{r}) p_j + N_n(\vec{r}) n_j\right) P_0(L(\vec{r}), T). \quad (5.44)$$

which can be compared with Eq. (5.15).

Nuclear effects are included by Yang, et al. for only the production cross section and the pion charge exchange; both are corrected for Fermi averaging, and the latter is also corrected for the Pauli Exclusion Principle: these are the corrections predicted by Sparrow et al. The nucleon absorption and the charge exchange cross sections are taken from Sparrow et al, and a fit is again used to obtain $\sigma_{\pi abs}$. The fit is, however, obtained by fitting the $d\sigma^+/dT$ spectrum for Pb, rather than the cross section $d^2\sigma/dT\,d\Omega$ at 15^0.

It is interesting and informative to compare the results of the multiple scattering models, with and without nucleon recoil, and the single scattering model without recoil, using common parameters.

The most marked difference between the models is in the calculation of the fitted value of $\sigma_{\pi abs}$. Although both the Sparrow et al. and Adler calculations are similar (Fig. 5.15), showing a peak about 200 MeV, the nucleon recoil model gives a pion absorption which becomes very small at the resonance. This is due to the large elastic scattering cross sections

at resonance; many pions are thus backscattered with a resultant energy loss.

In the production cross sections, the Adler and the Sparrow et al. models do not significantly vary, although the former does reduce the forward angle scattering, and increase the large angle scattering (Figs. 5.16, 5.17, 5.18 and 5.19); the total number of pions is about the same for each, as expected. Only when nucleon recoil, and pion energy loss, is allowed do the number of pions in a given energy bin change; they are then degraded to lower energies.

The Yang et al. model with the nucleon recoil, although it does show an increase in the number of low energy pions over the earlier models, the increase is still not sufficient to account for the low energy, large angle π^- population. (Fig. 5.20).

CHAPTER 6

SUMMARY AND CONCLUSIONS

Fairly good fits with experimental data have been obtained with the simple models discussed. At first, the success of such simplistic models may seem surprising, but it is a result of the dominance of only a few physical features of the interaction. These have been mentioned previously in the text, but they can now be more fully discussed in terms of the models introduced.

The intermediate energy range allows the convenient application of two basic assumptions: the energies are high enough to justify the impulse approximation for nucleon collisions with nuclei, and low enough for an angular momentum analysis of the individual nucleon-nucleon interaction. These lead to the formulation of the isobar model for the T=J=3/2 resonance and its application to pion production from nucleon-nucleus collisions.

The models are expected to be valid for complex, or large, nuclei. This eliminates the need to account for the correlation of the target nucleons which is required for low Z nuclei. The simple geometrical nature of the production reaction for complex nuclei is seen in Figs. 5.3 and 5.4, in which the plots of $\sigma(\pi^+)/Z^{1/3}$ and $\sigma(\pi^-)/N^{2/3}$ versus A flatten out for A>12.

In all cases, a semiclassical model is used, in which the nucleus is treated as a Fermi gas in which the positions and the momentum distribution of the target nucleons are treated simultaneously. An alternative expression for the cross section which is formally consistent with quantum mechanics is derived by Beder (1971); he remarks, however, that the expression is prohibitive to assess numerically, so that it is difficult to evaluate the comparative validity of the classical expression. It is expected, however, that since there are large momentum transfers involved in intermediate energy collisions, there will be a large number of final states of the nucleus. From quantum mechanics, it is predicted that the interference effects from so many final states will tend to cancel each other out, and a semiclassical approximation will be valid.

Although the inclusion of only single scattering within the nucleus is supported by the assumption of strong nuclear absorption, it will tend to overestimate the number of low energy, large angle pions produced. This is expected, and seen, especially in the π^- differential cross sections, since their production is strongly enhanced by secondary interactions. This can be seen from the Sternheim and Silbar results in Figs. 5.6 and 5.8 in which the number of high energy, low angle π^-'s (ie. result of single or low order scattering) is overestimated, and the number of low energy, large angle

π^-'s (result of higher order scattering) is underestimated. This is less pronounced in the π^+'s since they are produced relatively more abundantly than the π^-'s from single scatterings, although a slight tendency can be seen in the results of Sternheim and Silbar (Figs. 5.5 and 5.7) and of Beder and Bendix (Fig.3.6). The π^- population is enhanced through charge exchange at the expense of the π^+ population, which will tend to deplete the high energy, low angle π^+'s and augment the low energy, high angle π^-'s.

The effect in the π^+ data may be reduced further, since in all cases, the models are fitted to the small angle $pp \Rightarrow \pi^+$ data; this will tend to reduce (or "hide") the effects of the single scattering approximation.

It is expected that, although the differential cross sections at low energies are underestimated, the total cross sections will be more reliable. This is verified by comparison with experiment. In fact, this is expected whenever angular integrations are performed, as long as energy loss is ignored. This is found in the more sophisticated multiple scattering model by Adler, in which the multiple scattering is included in a Sternheim and Silbar-type model; there is a small improvement (ie. increase) in the predicted low energy cross sections, but when angular integrations are performed, the final cross sections show no improvement over the simpler models. With the further introduction of nucleon recoil, and

pion energy loss, by Yang et al., there is a healthy improvement in the prediction of low energy pions, and an improvement also in the total cross sections, but, unfortunately, not enough to fit the observed π^- data.

The single scattering models do have the strong advantage over multiple scattering models in that the computation time is greatly reduced in the former. Introduction of a secondary scattering within the nucleus would be most easily accomplished in the Sternheim and Silbar models by introduction of a nucleon-nucleon scattering at a second point $\vec{r}'$ in the nucleus. The additional time required for the extra integrations would acutely decrease the ease of calculation.

One strong advantage of the Sternheim and Silbar models of Chapter 5, is that they account for the production of pions of all three charge states, with the greatest emphasis on the π^+ and the π^-, which gives a more complete picture of the production processes. This is important, in particular, for it offers both a quantitative and a qualitative understnading of the charge exchange processes which play a dominant role in the scattering off nuclei. Accounting for all pion charge states, of course, also introduces further complications and the need for further simplifying assumptions. For example, the pion absorption coefficient λ_a, used by Sternheim and Silbar is assumed to be the same for the three different pions, but as indicated in Section 5.2, the three

appropriate coefficients are predicted by applying the isobar model to the $\pi NN \rightarrow NN$ reaction. This tends to decrease the π^+/π^- ratio for nuclei of increasing Z, which would be beneficial to lowering the predicted ratio for Pb in Sternheim and Silbar (1972), but would not be at all good for Silbar and Sternheim (1973).

It is the cross sections of the various processes involved, ie. nucleon and pion absorption, charge exchange, etc., that are the major inputs to the calculations. The values used for these cross sections are often very different for the various models and deserve closer attention. The amount of nucleon and pion absorption within the nucleus especially varies in the models.

The nucleon (ie. incident proton) absorption in both the Beder and Bendix and the Kolbig and Margolis models is assumed to be very strong and is set equal to the nucleon-nucleon cross section; at 600 MeV, this is approximately equal to 25 mb. For Sternheim and Silbar (1972), the proton absorption is determined using a fitting procedure with σ_{inabs}, and a value of 30 mb. results; this is close to the maximum possible value of 33mb., the nucleon-nucleon cross section at 740 Mev. In Sternheim and Silbar (1973), however, a more empirical value for the nucleon absorption is obtained independently of the pion absorption, by an exponential fit to the medium angle elastic pp scattering cross section. This

results in a much lower nucleon absorption, ie. 5.6 mb. compared with 30 mb. This lower nucleon absorption leads, however, to possible contradictions with the basic assumption that the single scatterings only would dominate. Such low nucleon absorption also implies that the pion production processes could occur deeper within the nucleus, but this is in contradiction with the observed geometrical dependence of the cross section which indicats surface production. Indeed, this value of 5.6 mb. is surprisingly low, and Sparrow et al. indicate that an error was made in the Fermi averaging of the cross section in the previous paper; a recalculation which also includes a double scattering term and an improved angular dependence, gives and absorption which is double the original value. It is not indicated, however, whether this larger value, while more reasonable than the earlier one, is large enough to be consistent with the observed surface production. Figure 5.13 indicates that it is at least partially consistent.

A different method of evaluation is required for the pion absorption since there is little experimental data that can be used directly to determine it. This would require experiments in which a pion enters the nucleus but does not emerge. Also, no upper bound can be obtained for the pion absorption, as is possible for nucleon absorption; this is because most of the pions are absorbed on two nucleons via $\pi NN \rightarrow NN$. These factors lead to conflicting values for the

absorption for the different models (Figs. 5.12 and 5.15).

To attempt to overcome the difficulties in determining the pion absorption, the Sternheim and Silbar models in Chapter 5 resort to fitting the models to the data to obtain $\sigma_{\pi,abs}^{(T)}$. Sternheim and Silbar (1972) contains the least reliable (or meaningful) method, fitting both the $\sigma_{\pi,abs}^{(T)}$ and $\sigma_{\pi,abs}$ to the data. This is an ambiguous procedure which tends to cover up errors which might occur in the model. The predicted absorption is an increasing function of T. In Silbar and Sternheim (1973) and Sparrow et al, the nucleon absorption is determined directly from experiment, and the pion absorption alone, is fitted to give the 15° Pb data. The result is a cross section which indicates a peak at 200 MeV - 275 MeV for the two papers, and which drops off fairly gradually at higher and lower energies. It is pointed out by Sparrow et al. that it is the inclusion of the Fermi motion averaging of the absorption cross section (excluded in Sternheim and Silbar (1972)) that causes the decrease in the pion absorption at higher pion energies.

In contrast, Beder and Bendix obtain a cross section for pion absorption which is a decreasing function of T, which at high energies only, is in qualitative agreement with the above calculations, but opposes the low energy results. Beder and Bendix use a semi-analytical method for obtaining their cross section which is based on a density-squared dependence of the cross section on the nucleon density since the pion

absorption occurs, mainly, on nucleon pairs via $\pi NN \rightarrow NN$; the time reversal invariance of strong interactions is also used to relate the T-matrix for the absorption to the T-matrix for the production process. This increasing energy dependence, however, is also in contradiction to the predictions of the quasi-deuteron absorption model for pions on nucleons, which predicts an increase with energy.

Due to the resonant nature of the πN interaction, it would be expected that the pion absorption should reflect this peak at about 200 MeV (assuming no nucleon recoil), since the pion absorption reaction is dominated by the inverse of the production reaction. There is slight evidence in the Beder and Bendix curve that there are contributions, perhaps, from two sources, one which is monotonically decreasing with energy, and one that is a broad resonance-type curve. Beder and Bendix may also have ignored other important absorptive channels.

The assumption of nucleon recoil by Yang et al., however, results in a very different pion absorption cross section compared to the earlier geometrical models. In the recoil model, the pion absorption becomes very small at resonance; this is because, at resonance, the elastic scattering cross section is large, and many pions are backscattered to lower energies. In all other models, the pions remain at their original energies, and this does not occur.

It is difficult, in the absence of further experimental data, to determine the true nature of the pion absorption, however, the latter value seems to be the most consistent with indirect experimental evidence.

It has been mentioned that Beder and Bendix, in treating the pion absorption, assume a ρ^2 dependence for absorption on two nucleons; this has been ignored by other authors who have assumed only a ρ dependence. The ρ^2 dependence implies that absorption takes place nearer the nuclear centre; assumption of a ρ dependence weights the surface regions too heavily. Too much absorption is thus predicted for light nuclei, relative to heavy nuclei. This is reflected in the geometrical models, for which the sum of the total cross sections for π^+ and π^- is too high for large nuclei.

The pion charge exchange cross section is based on the π^+p elastic cross section (valid for a pure (3/2,3/2) state). The models in Sections 5.3 and 5.4 include the nuclear corrections to the cross section which affect it by 10-30% and affect the π^+ and π^- total cross sections by about 5 and 15%, respectively.

Nucleon charge exchange is dealt with only in Sections 5.3 and 5.4 and is obtained from the large angle nucleon-nucleon scattering; this gives an additional contribution of 3.1 mb. of absorption.

While the semiclassical models give reasonable fits to the data, they are lacking in the prediction of the low energy

pions, and especially for the π^- production. Even with the addition of multiple scattering and, more strikingly, nucleon recoil, the model still underestimates the low energy π^-'s. It would, perhaps, seem best to abandon this approach, however, a Monte Carlo calculation by Harp (1974) based on the same basic assumptions, has been successful in predicting pion spectra in good agreement with experiment. Since a Monte Carlo model represents a complete semiclassical calculation, this would imply that corrections to the inputs of the models considered here would give results comparable to Harp's. Unfortunately, it is difficult to directly compare the inputs of the two models. Since the Sternheim and Silbar calculations require orders of magnitude less computing time, and are conceptually much simpler than the Monte Carlo calculations, it would seem worthwhile to further compare the two approaches in order to obtain better agreement of the simpler models with experiment.

An entirely new approach, however, is expected to be more productive. This is a result of recent experimental data for pion production obtained for protons on nuclei, in which some of the final states have been measured. Much of the original data was obtained by the Uppsala group (Dahlgren et al. 1971, 1973a, 1973b) for threshold pion production from ^{12}C and ^{9}Be with pion energy spectra and angular distributions for the nuclei left in the ground state and the first few excited states. More recently, similar data (Gabathuler et

al. 1971, Dollhopf et al. 1973) has been obtained at incident energies of up to 600 MeV for various nuclei, thus providing a broader basis on which to construct the models. These models necessarily have a more quantum mechanical formulation (Reitan 1971, Fearing 1975).

One omission in all models considered, is a spin dependence in the cross section. TRIUMF has produced the first polarized beam, and has found a large (÷90%) left-right asymmetry with the exiting pions; not even the most recent final state models have included a spin dependence. Such a strong effect certainly is worth further investigation.

TABLE II.1

PARTIAL WAVE ANALYSIS OF $pNN \rightarrow NN\pi^i$

Reaction	Isotopic Reaction	Class	Partial Wave Analysis
$pp \rightarrow \pi^+ np$	$\sigma_{10} + \sigma_{10}(np)$	Ss	$^3P_1 \rightarrow {}^3S_1 s_1$
		Sp	$^1S_0 \rightarrow {}^3S_1 p_0$
			$^1D_2 \rightarrow {}^3S_1 p_2$
$pp \rightarrow \pi^+ d$	$\sigma_{10}(d)$	Ss	$^3P_1 \rightarrow {}^3S_1 s_1$
		Sp	$^1S_0 \rightarrow {}^3S_1 p_0$
			$^1D_2 \rightarrow {}^3S_1 p_2$
$pp \rightarrow \pi^0 pp$	σ_{11}	Ss	$^3P_0 \rightarrow {}^1S_0 s_0$
		Sp	FORBIDDEN
$pn \rightarrow \pi^+ nn$	$\frac{1}{2}(\sigma_{11} + \sigma_{01})$	Ss	$^3P_0 \rightarrow {}^1S_0 s_0$
$\rightarrow \pi^- pp$		Sp	$^3S_1 \rightarrow {}^1S_0 p_1$
			$^3D_1 \rightarrow {}^1S_0 p_1$
$pn \rightarrow \pi^0 pn$	$\frac{1}{2}[\sigma_{01} + \sigma_{10}(pn)]$	Ss	$^3P_1 \rightarrow {}^3S_1 s_1$
		Sp	$^3S_1 \rightarrow {}^1S_0 p_1$
			$^3D_1 \rightarrow {}^1S_0 p_1$
			$^1S_0 \rightarrow {}^3S_1 p_0$
			$^1D_2 \rightarrow {}^3S_1 p_2$
$pn \rightarrow \pi^0 d$	$\frac{1}{2}[\sigma_{01} + \sigma_{10}(d)]$	Ss	$^3P_1 \rightarrow {}^3S_1 s_1$
		Sp	$^3S_1 \rightarrow {}^1S_0 p_1$
			$^3D_1 \rightarrow {}^1S_0 p_1$
			$^1S_0 \rightarrow {}^3S_1 p_0$
			$^1D_2 \rightarrow {}^3S_1 p_2$

TABLE II.2

REACTIONS FOR $NN \rightarrow NN\pi$ IN TERMS OF ISOTOPIC SPIN CROSS SECTIONS

Isotopic Reaction	Class	Partial Wave Analysis
σ_{10}	Ss	$^3P_1 \rightarrow {}^3S_1 s_1$
	Sp	$^1S_0 \rightarrow {}^3S_1 p_0$
		$^1D_2 \rightarrow {}^3S_1 p_2$
		$\text{—} \rightarrow {}^3S_1 p_1$
σ_{01}	Ss	$\text{—} \rightarrow {}^1S_0 s_0$
	Sp	$^3S_1 \rightarrow {}^1S_0 p_1$
		$^3D_1 \rightarrow {}^1S_0 p_1$
σ_{11}	Ss	$^3P_0 \rightarrow {}^1S_0 s_0$
	Sp	$\text{—} \rightarrow {}^1S_0 p_1$
	Ps	$^1S_0 \rightarrow {}^3P_0 s_0$
		$\text{—} \rightarrow {}^3P_1 s_1$
		$^1D_2 \rightarrow {}^3P_2 s_2$
	Pp	$^3P_{0,1} \rightarrow {}^3P_0 p_1$
		$^3P_{0,1,2} \rightarrow {}^3P_1 p_{0,1,2}$
		$^3F_2 \rightarrow {}^3D_1 p_2$
		$^3P_{1,2} \rightarrow {}^3P_2 p_{1,2}$
		$^3F_{2,3} \rightarrow {}^3P_2 p_{2,3}$

TABLE II.3

EXPERIMENTAL RESULTS FOR π PRODUCTION ON FREE NUCLEONS AND COMPLEX NUCLEI

Free nucleons	Cross Sections(10^{28}cm^3)		Complex nuclei	
$pp \rightarrow \pi^+$(allowed)	3.0 ± 1.0[a]	3.3 ± 1.0	$p+(p,n)$	π^+(allowed)[c]
$pn \rightarrow \pi^+$(unobserved)	-	0.8 ± 0.4	$p+(p,n)$	π^-(allowed)[c]
$np \rightarrow \pi^-$(unobserved)	-	0.8 ± 0.4	$p+(p,n)$	π^o(allowed)[b]
$np \rightarrow \pi^o$(unobserved)	-	1.7 ± 0.9		
$pp \rightarrow \pi^o$(forbidden)	0.1 ± 0.1[b]	?		

a Cartwright et al. (1950)

b Bjorkland et al. (1950)

c Richamn and Wilcox (1950)

TABLE II.4

THE ISOBAR MODEL FOR $pN \rightarrow NN\pi$

$pp \rightarrow \Delta^+ p$	
$\rightarrow \pi^+ n$	$\pi^+ np$
$\rightarrow \pi^o p$	$\pi^o pp$
$\rightarrow \Delta^{++} n$	
$\rightarrow \pi^+ p$	$\pi^+ pn$
$pn \rightarrow \Delta^o p$	
$\rightarrow \pi^o n$	$\pi^o np$
$\rightarrow \pi^- p$	$\pi^- pp$
$\rightarrow \Delta^+ n$	
$\rightarrow \pi^+ n$	$\pi^+ nn$
$\rightarrow \pi^o p$	$\pi^o pn$

For the pp collisions, using the Clebsch-Gordon Coefficients:

$$|pp\rangle = |1,1\rangle = \sqrt{\tfrac{3}{4}}\,|\underbrace{\tfrac{3}{2}, -\tfrac{1}{2}}_{|\Delta^{++} n\rangle}\rangle - \sqrt{\tfrac{1}{4}}\,|\underbrace{\tfrac{1}{2}, \tfrac{1}{2}}_{|\Delta^{+} p\rangle}\rangle$$

$$\Delta^{++} \equiv |\tfrac{3}{2}, \tfrac{3}{2}\rangle = |\pi^+ p\rangle$$

$$\Delta^{+} \equiv |\tfrac{3}{2}, \tfrac{1}{2}\rangle = \sqrt{\tfrac{1}{3}}\,|\pi^+ n\rangle + \sqrt{\tfrac{2}{3}}\,|\pi^o p\rangle$$

thus, ignoring interference, $\pi^+ : \pi^o : \pi^- = (3/4 \cdot 1 + 1/4 \cdot 1/3) : 1/4 \cdot 2/3 : 0$

$= 5/6 : 1/6 : 0$

Similarly for the pn collisions:

$$|pn\rangle = |1,0\rangle = \sqrt{\tfrac{1}{2}}\,|n\Delta^+\rangle - \sqrt{\tfrac{1}{2}}\,|p\Delta^o\rangle$$

$$|\Delta^o\rangle = |\tfrac{3}{2}, -\tfrac{1}{2}\rangle = \sqrt{\tfrac{2}{3}}\,|\pi^o n\rangle + \sqrt{\tfrac{1}{3}}\,|\pi^- p\rangle$$

therefore $\pi^+ : \pi^o : \pi^- = 1/2 \cdot 1/3 : (2/3 \cdot 1/2 + 1/2 \cdot 2/3) : 1/2 \cdot 2/3$

$= 1/6 : 2/3 : 1/6$

TABLE II.5

THE ISOBAR MODEL AND FERMI STATISTICAL WEIGHTS FOR $PN \rightarrow NN\pi$

Reaction	Isobar model		Statistical Weight	
	T=0	T=1	T=0	T=1
$pp \rightarrow np\pi^+$		5/6		3/4
$pp \rightarrow pp\pi^o$		1/6		1/4
$np \rightarrow pp\pi^-$	-	1/6	1/3	1/4
$np \rightarrow nn\pi^+$	-	1/6	1/3	1/4
$np \rightarrow np\pi^o$	-	2/3	1/3	1/2

TABLE II.6

PARTIAL WAVE ANALYSIS OF $pp \to \pi NN$ FOR THE MANDELSTAM MODEL

ppstate	(ΔN)state	$(NN\pi)$ state	
		σ_{10}	σ_{11}
$^1S_0$	—	$(^3S_1 p)_0$	$(^3P_0 S)_0$
$^1D_2$	$(\Delta_{\frac{3}{2}}, S_2)_2$	$(^3S_1 p)_2$	$(^3P_2 S)_2$
$^3P_0$	$(\Delta_{\frac{3}{2}}, P_1)_0$	$(^1P_1 p)_0$	$(^1S_0 S)_0, (^3P_1 p)_0$
$^3P_1$	$(\Delta_{\frac{3}{2}}, P_1)_1 (\Delta_{\frac{3}{2}} P_2)_1$	$(^3S, S)_1, (^1P, p)_1$	$(^3P_{0,1,2} p)_1$
$^3P_2, {}^3F_2$	$(\Delta_{\frac{3}{2}}, P_1)_2, (\Delta_{\frac{3}{2}} P_2)_2$	$(^1P_1 p)_2$	$(^3P_{1,2,} p)_2$
$^3F_3$	$(\Delta_{\frac{3}{2}}, P_2)_3$		$(^3P_2 p)_3$

TABLE III.1

EFFECTIVE NUCLEON NUMBER FOR VARIOUS TARGETS FOR VARIOUS σ

σ_1=0mb.

σ_2 (mb)	0	10	20	30	40	50	60
$N(^{20}Ne)$	20.0	16.2	13.4	11.5	9.98	8.83	7.93
$N(^{27}Al)$	27.0	21.0	17.0	14.3	12.2	10.7	9.55
$N(^{40}Ca)$	40.0	29.6	23.1	18.8	15.9	13.7	12.1
$N(^{64}Cu)$	64.0	44.0	32.8	26.0	21.5	18.4	16.1
$N(^{108}Ag)$	108	67.9	48.1	36.9	30.0	25.3	22.0
$N(^{140}Ce)$	140	83.9	57.8	43.8	35.3	29.7	25.6
$N(^{208}Pb)$	208	115	76.3	56.7	45.2	37.7	32.5

σ_1=17mb.

σ_2 (mb)	0	10	20	30	40	50	60
$N(^{20}Ne)$	14.2	11.3	9.34	7.93	6.88	6.09	5.47
$N(^{27}Al)$	18.1	13.9	11.1	9.24	7.91	6.92	6.18
$N(^{40}Ca)$	24.7	17.8	13.7	11.1	9.32	8.07	7.14
$N(^{64}Cu)$	35.6	23.6	17.2	13.4	11.1	9.50	8.35
$N(^{108}Ag)$	52.8	31.1	21.3	16.2	13.1	11.2	9.76
$N(^{140}Ce)$	63.9	35.3	23.4	17.5	14.2	12.0	10.5
$N(^{208}Pb)$	85.1	42.2	26.7	19.7	15.8	13.3	11.7

σ_1=26mb.

σ_2 (mb)	0	10	20	30	40	50	60
$N(^{20}Ne)$	12.2	9.70	7.99	6.77	5.88	5.21	4.69
$N(^{27}Al)$	15.3	11.6	9.31	7.73	6.62	5.81	5.19
$N(^{40}Ca)$	20.3	14.6	11.2	9.02	7.59	6.59	5.85
$N(^{64}Cu)$	28.4	18.6	13.5	10.6	8.77	7.54	6.67
$N(^{108}Ag)$	40.7	23.7	16.2	12.3	10.1	8.64	7.62
$N(^{140}Ce)$	48.5	26.4	17.5	13.2	10.8	9.20	8.12
$N(^{208}Pb)$	63.2	30.8	19.5	14.5	11.8	10.1	8.93

σ_1=39mb.

σ_2 (mb)	0	10	20	30	40	50	60
$N(^{20}Ne)$	10.1	8.02	6.60	5.60	4.87	4.32	3.90
$N(^{27}Al)$	12.4	9.43	7.53	6.26	5.38	4.73	4.25
$N(^{40}Ca)$	16.1	11.5	8.80	7.14	6.04	5.27	4.70
$N(^{64}Cu)$	21.9	14.2	10.4	8.18	6.83	5.92	5.27
$N(^{108}Ag)$	30.6	17.7	12.1	9.35	7.75	6.71	5.97
$N(^{140}Ce)$	36.0	19.5	13.0	9.96	8.24	7.14	6.36
$N(^{208}Pb)$	46.2	22.4	14.4	10.9	9.05	7.85	7.01

TABLE IV.1

AVERAGED PRODUCTION RATES IN μb/MeV.sr

KE_π(MeV)	100		150	200	250	300		350
$d\bar{\sigma}_3$	5.9	(5.5)	9.0	9.9	6.9	2.4	(2.1)	0.2
$d\bar{\sigma}_2$	0.1	(0.1)	0.6	2.2	4.0	2.6	(2.2)	0.7
$d\bar{\sigma}_{neutron}$	1.0	(0.9)	1.1	1.2	0.4	0.1	(0.1)	
$d\bar{\sigma}_{total}$	7.0	(6.5)	10.7	13.3	11.3	5.1	(4.4)	0.9

Note that the quantities in brackets are those with the Pauli Exclusion effects included.

TABLE IV.2

EFFECTIVE NUCLEON NUMBER

KE_π(MeV)	100		200	300	
Carbon:N_{eff}	2.7	(3.0)	2.5	2.8	(3.3)
Lead:N_{eff}	6.8	(7.5)	6.0	7.5	(8.9)

Note, again, that the quantities in brackets are those with the Pauli Exclusion effects included.

TABLE V.1

RESULTS FOR TOTAL $\pi^{\pm}$ PRODUCTION CROSS SECTIONS (mb)

Nucleus	R (fm)	$\sigma(\pi^+)$ calc	$\sigma(\pi^+)$ exp	$\sigma(\pi^-)$ calc	$\sigma(\pi^-)$ exp	$\sigma(\pi^+)/\sigma(\pi^-)$ calc	$\sigma(\pi^+)/\sigma(\pi^-)$ exp
^{9}Be	3.12	28.8	27.3±1.4	5.99	6.49±0.37	4.8	4.3
^{12}C	3.205	36.1	35.0±1.8	6.54	6.64±0.41	5.4	5.3
^{27}Al	3.78	50.9	53.1±2.9	12.5	13.2 ±0.9	4.1	4.0
^{48}Ti	4.69	74.0	67.0±3.6	21.6	21.2 ±1.6	3.4	3.2
^{63}Cu	4.97	82.0	77.3±4.3	25.4	25.2 ±2.0	3.2	3.1
^{108}Ag	5.72	97.3	91.6±5.1	37.5	35.0 ±3.0	2.6	2.6
^{181}Ta	7.10	136.2	101.0±5.6	62.4	51.4 ±4.7	2.2	2.0
^{208}Pb	7.11	128.9	104.2±5.8	64.3	53.7 ±4.9	2.0	1.95
^{232}Th	7.37	134.9	107.9±5.9	70.0	60.4 ±5.5	1.9	1.9

Note that experimental values from Cochran et al. (1972).

TABLE V.2

ORIGINS OF PRODUCED PIONS SORTED INTO SIX NUCLEAR BINS ACCORDING TO FIGURE 5.13

Bin	$\sigma_i(\pi^+)$	% of π^+	$\sigma_i(\pi^-)$	% of π^-
1	27.2	25.1	8.4	18.5
2	48.7	45.0	17.8	39.0
3	6.1	5.6	3.7	8.1
4	11.1	10.3	5.4	11.7
5	12.3	11.4	7.8	17.1
6	2.9	2.7	2.5	5.5
Totals	108.3	100.1	45.6	99.9

TABLE V.3

EFFECTS OF THE VARIOUS NUCLEAR CORRECTIONS (ONE AT A TIME ON PRODUCTION CROSS SECTIONS FOR PR

$\sigma(\pi^+)$	% Change	$\sigma(\pi^-)$	% Change	$\sigma(\pi^+)/\sigma(\pi^-)$	% Change
(a) Experiment, taken from Ref. 2.					
104.2 ± 5.8	...	53.7 ± 4.9	...	1.94 ± 0.21	...
(b) "Standard calculation," Saxon-Woods density with $r_0 = 6.66$ fm and $a = 0.50$ fm, nucleon charge exchange, and all nuclear corrections of Sec. III.					
108.2	...	45.6	...	2.373	...
(c) Same as (b) but without Fermi averaging, Pauli principle, and pion-potential corrections for $\sigma_{\pi,\mathrm{exch}}$.					
105.2	−2.8	49.8	+9.2	2.113	−11.0
(d) Same as (b) but without Fermi averaging and nucleon-potential corrections for $d^2\sigma_{\mathrm{iso}}/dTd\Omega$.					
193.1	+78.5	62.0	+35.9	3.116	+31.3
(e) Same as (b) but without Pauli-principle correction for $\sigma_{N,\mathrm{exch}}$, i.e., $\sigma_{N,\mathrm{exch}} = 3.8$ mb.					
107.2	−1.0	47.9	+5.0	2.238	−5.7
(f) Same as (b) but with no nucleon exchange at all, $\sigma_{N,\mathrm{exch}} = 0$.					
114.0	+5.4	34.1	−25.2	3.341	+40.9
(g) Same as (b) but with sharp-edged uniform sphere density of radius $R = 7.11$ fm					
92.4	−14.6	43.6	−4.4	2.117	−10.8

TABLE V.4

EFFECTS OF NUCLEAR CORRECTIONS

σ^+	% change	σ^-	% change	Ratio	% change
Experiment					
104.2 ± 5.8	...	53.7 ± 4.9	...	1.94 ± 0.21	...
Standard					
148.7	...	56.6	...	2.63	...
$\sigma_{\pi,\mathrm{exch}}$ corrected for Pauli principle					
156.2	+5.1	47.6	−15.8	3.28	+24.8
$d^2\sigma_{\mathrm{iso}}/d\Omega dT$ corrected for Fermi motion					
121.5	−18.3	46.4	−18.0	2.62	−0.4
$\sigma_{N,\mathrm{exch}}$ corrected for Pauli principle					
150.9	+1.5	53.6	−5.3	2.81	+7.1

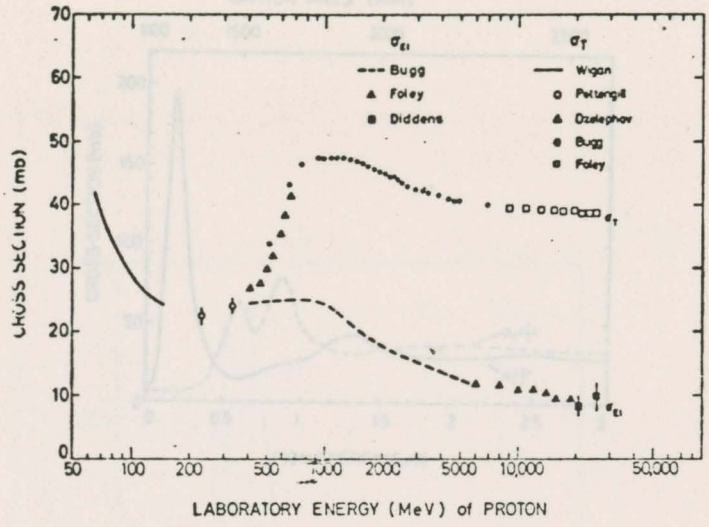

FIGURE 1.1

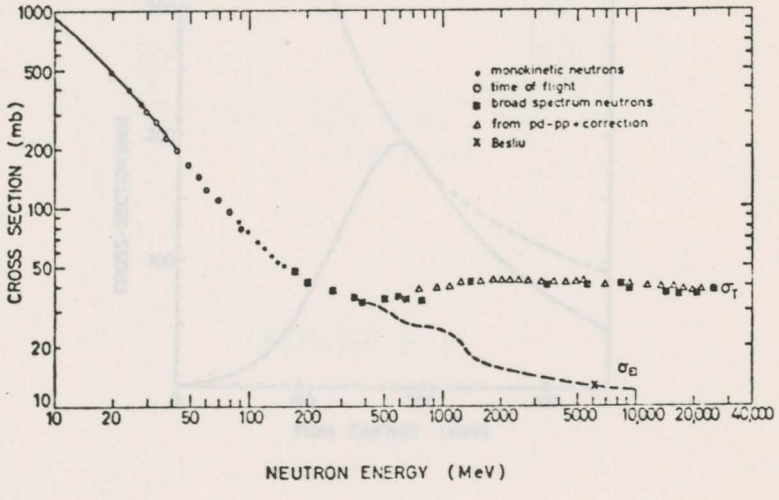

FIGURE 1.2

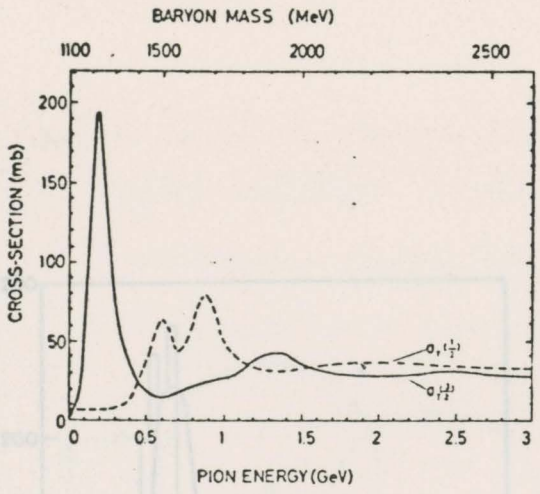

FIGURE 2.1

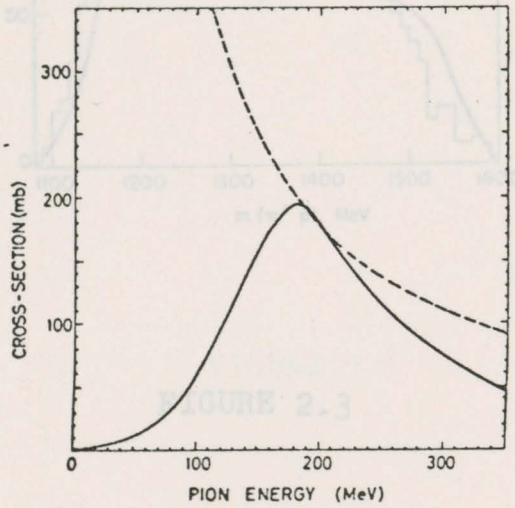

FIGURE 2.2

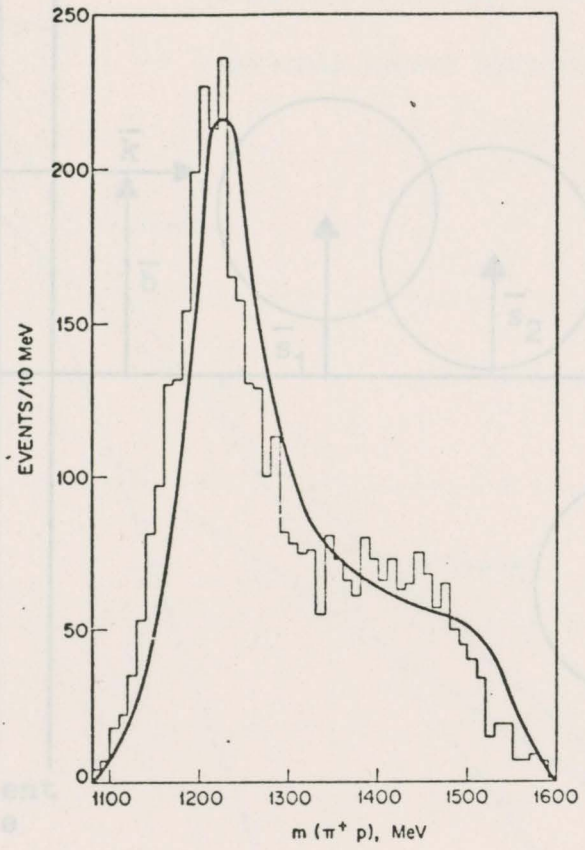
250
200
150
100
50
0
EVENTS/10 MeV
1100
1200
1300
1400
1500
1600
m (π⁺ p), MeV

FIGURE 2.3

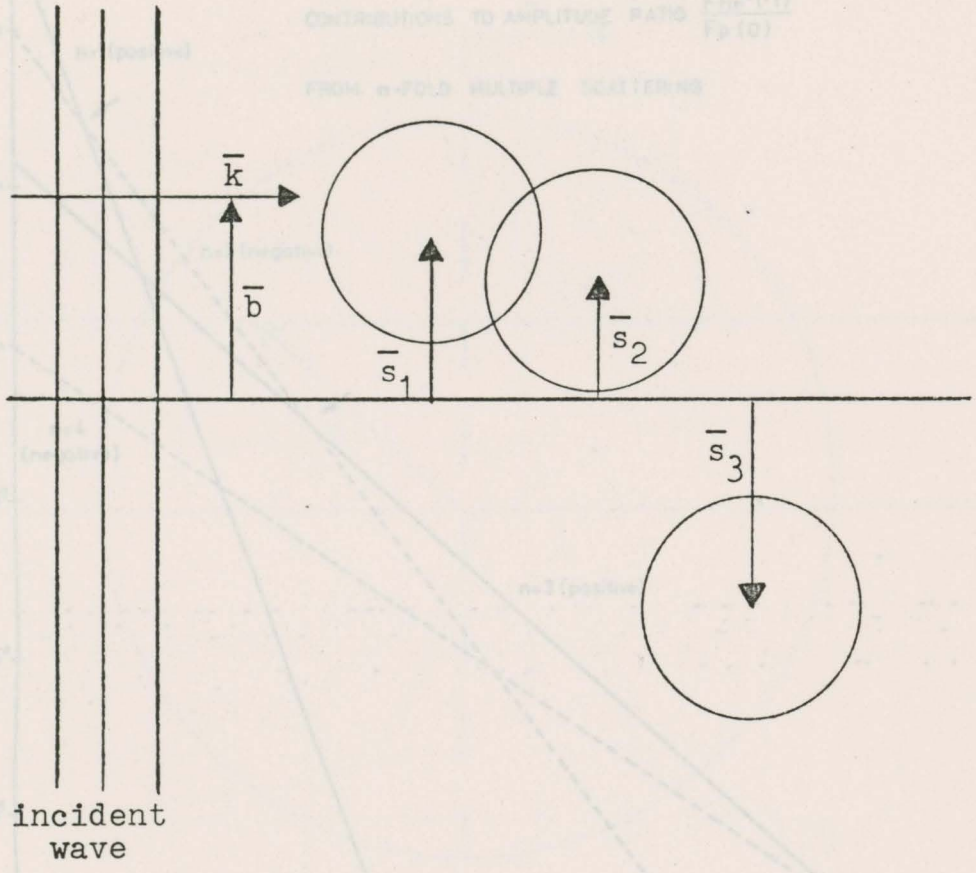

FIGURE 3.1

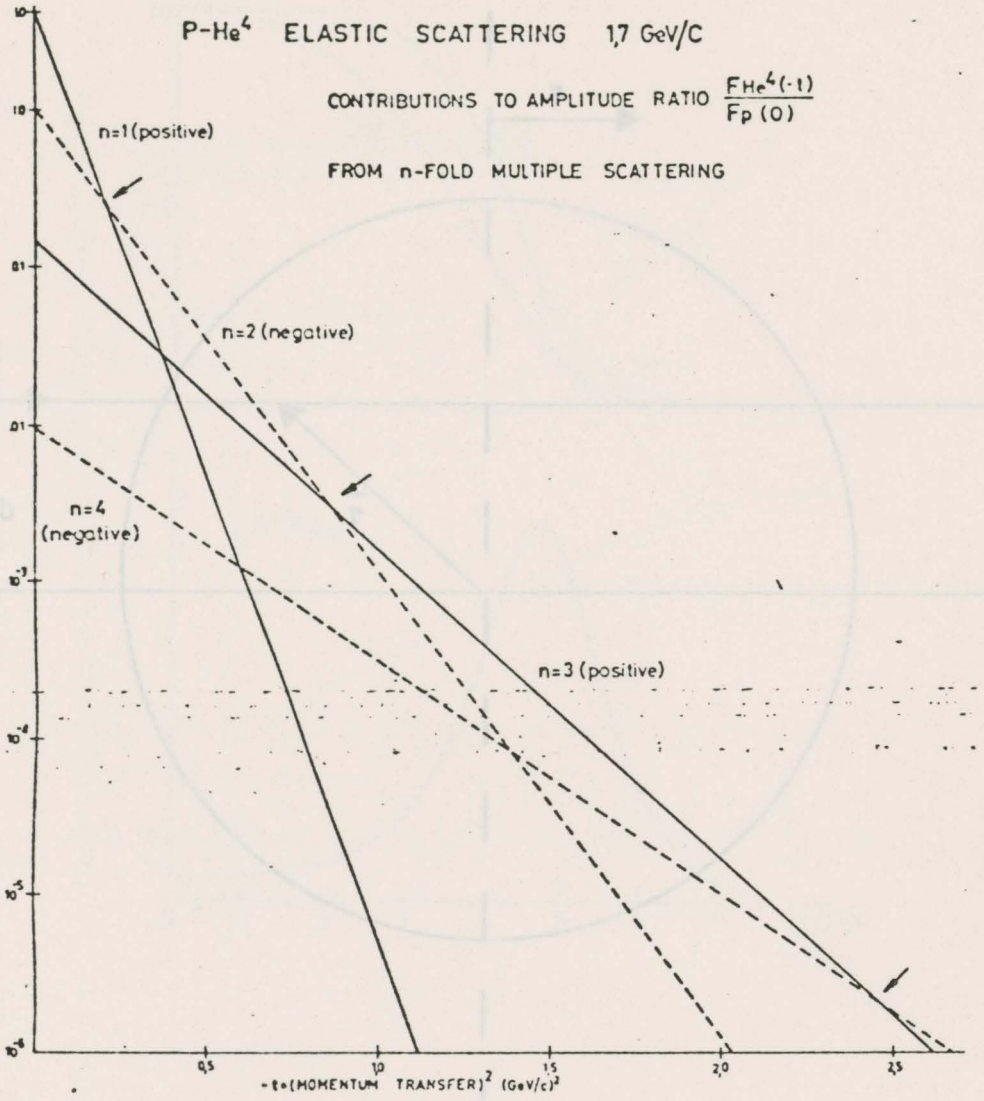
P-He⁴ ELASTIC SCATTERING 1,7 GeV/C
CONTRIBUTIONS TO AMPLITUDE RATIO $\frac{F_{He^4}(-t)}{F_p(0)}$
FROM n-FOLD MULTIPLE SCATTERING
n=1 (positive)
n=2 (negative)
n=4 (negative)
n=3 (positive)
0,5
1,0
1,5
2,0
2,5
-t=(MOMENTUM TRANSFER)² (GeV/c)²

FIGURE 3.2

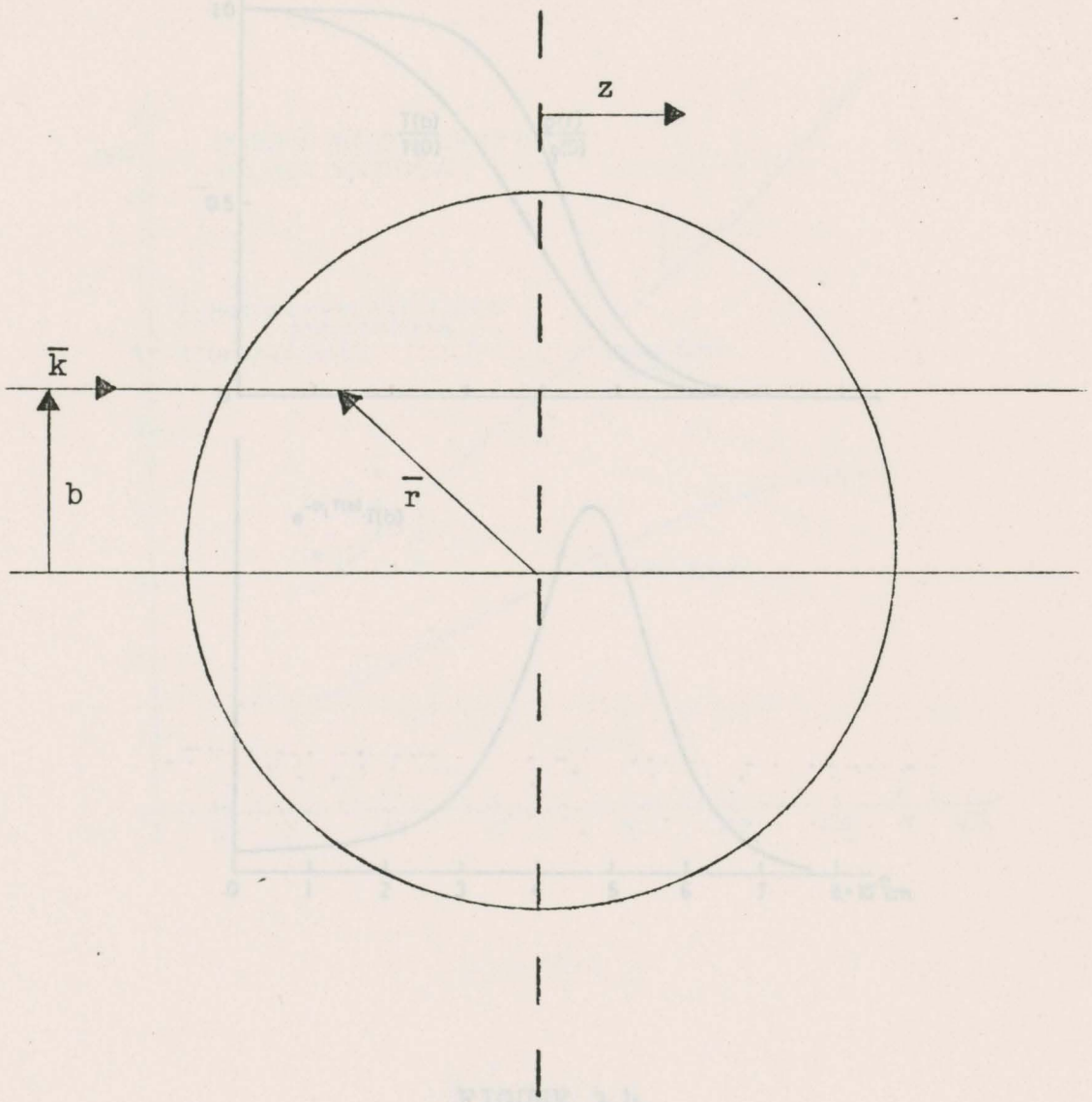

FIGURE 3.3

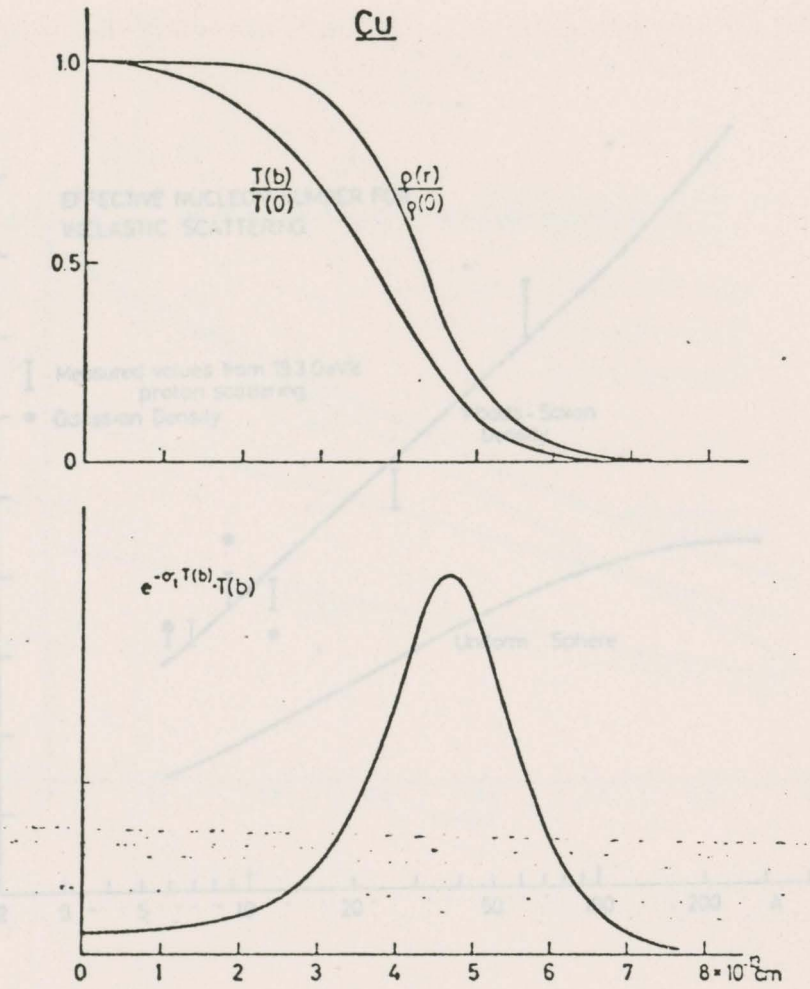

FIGURE 3.4

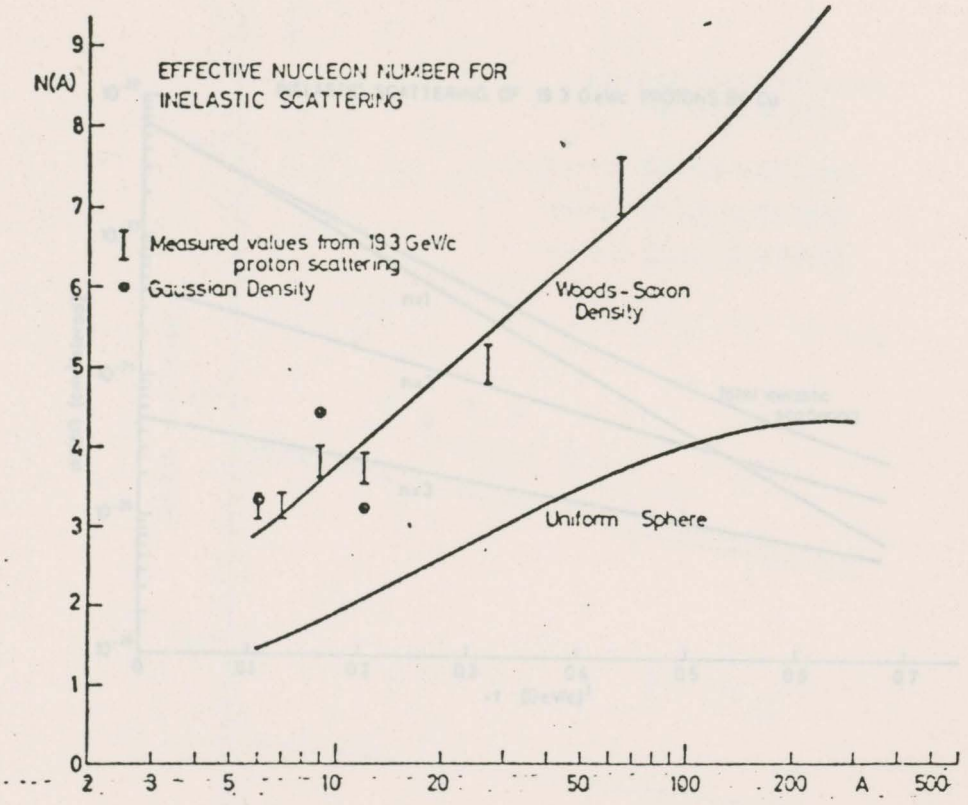
EFFECTIVE NUCLEON NUMBER FOR
INELASTIC SCATTERING
N(A)
Measured values from 19.3 GeV/c
proton scattering
Gaussian Density
Woods-Saxon
Density
Uniform Sphere
A

FIGURE 3.6

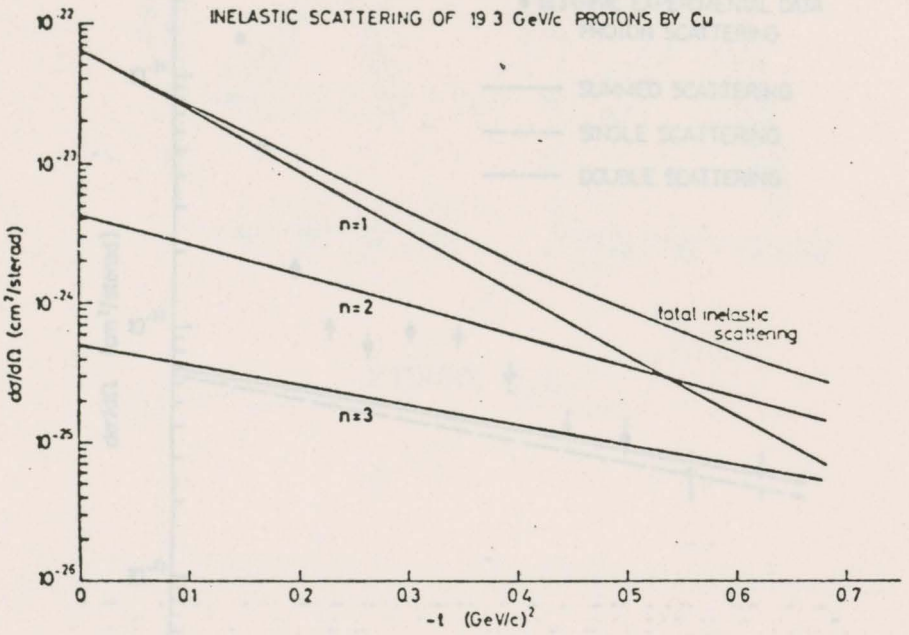
INELASTIC SCATTERING OF 19 3 GeV/c PROTONS BY Cu
dσ/dΩ (cm²/sterad)
10⁻²²
10⁻²³
10⁻²⁴
10⁻²⁵
10⁻²⁶
n=1
n=2
n=3
total inelastic scattering
0
01
02
03
04
05
06
07
-t (GeV/c)²

FIGURE 3.5

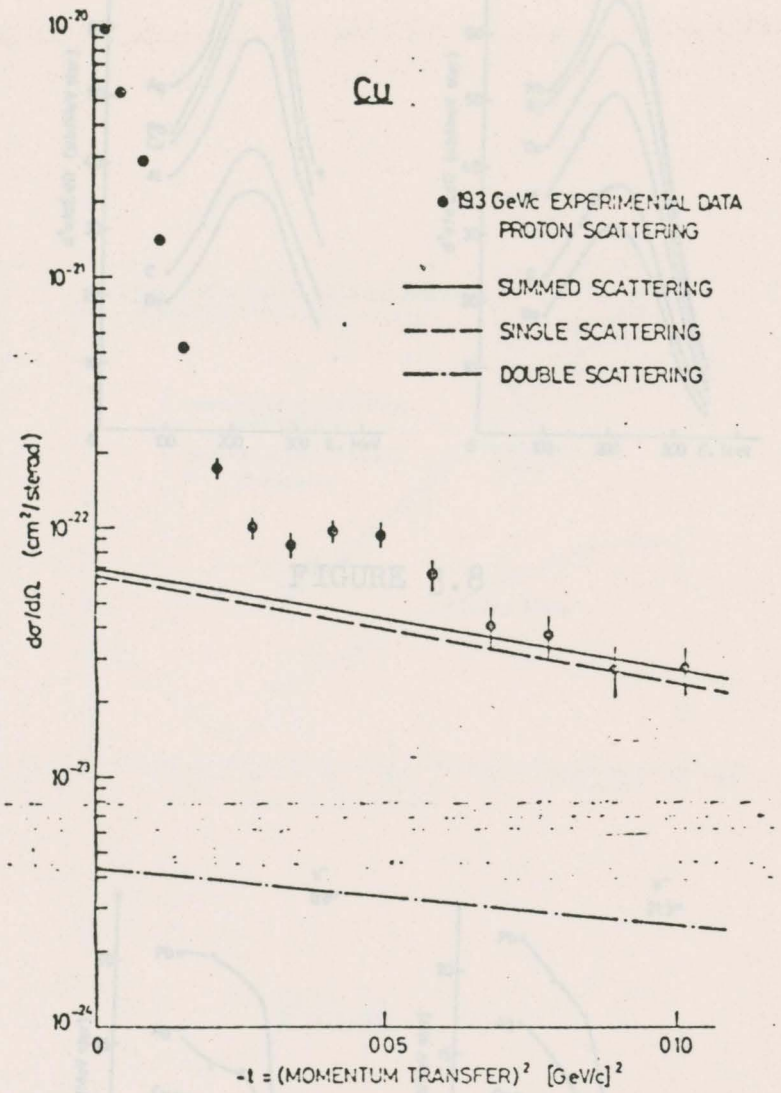
Cu
• 193 GeV/c EXPERIMENTAL DATA
PROTON SCATTERING
SUMMED SCATTERING
SINGLE SCATTERING
DOUBLE SCATTERING
dσ/dΩ (cm²/steradian)
10⁻²⁰
10⁻²¹
10⁻²²
10⁻²³
10⁻²⁴
0
005
010
-t = (MOMENTUM TRANSFER)² [GeV/c]²

FIGURE 3.7

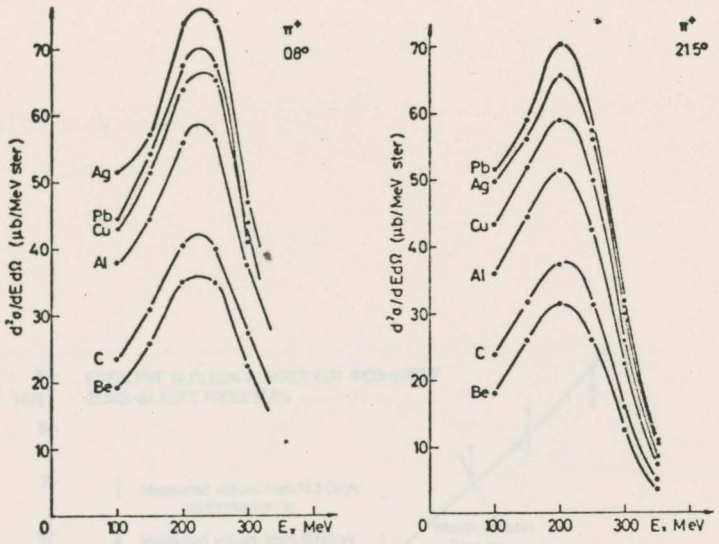

FIGURE 3.8

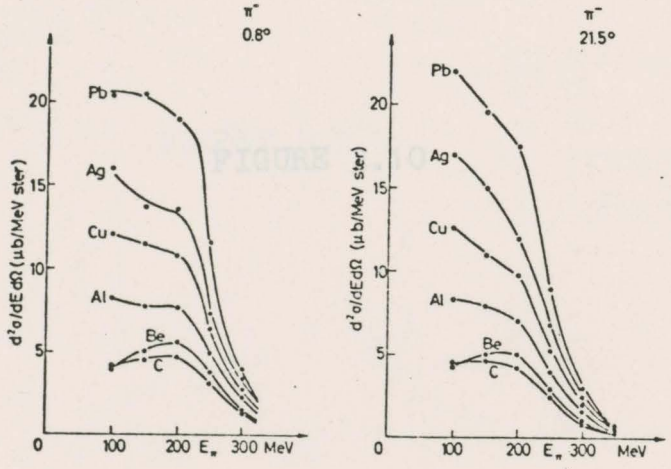

FIGURE 3.9

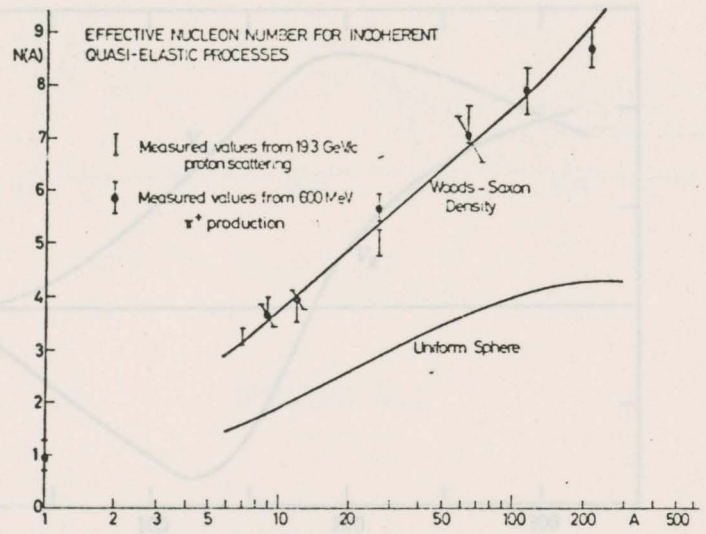
EFFECTIVE NUCLEON NUMBER FOR INCOHERENT
QUASI-ELASTIC PROCESSES
N(A)
Measured values from 19.3 GeV/c
proton scattering
Measured values from 600 MeV
π⁺ production
Woods - Saxon
Density
Uniform Sphere
A

FIGURE 3.10

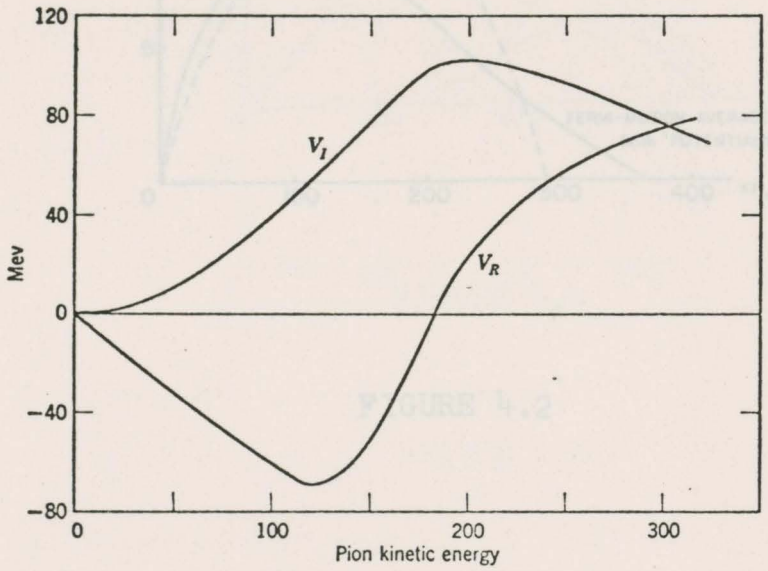

FIGURE 4.1

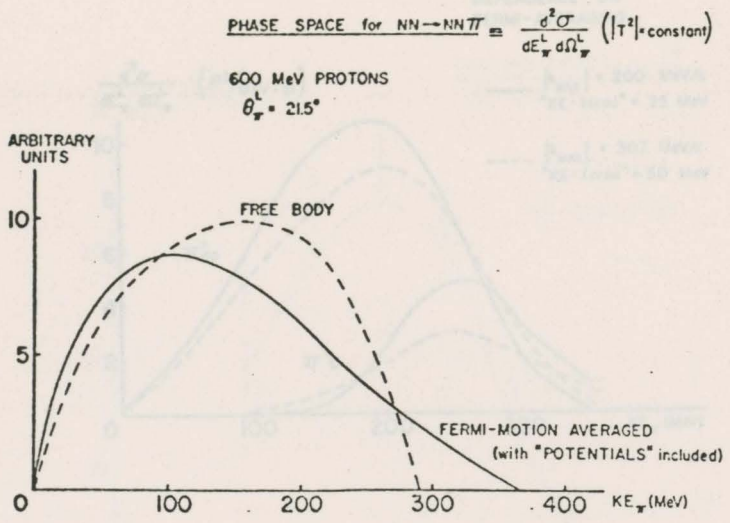

FIGURE 4.2

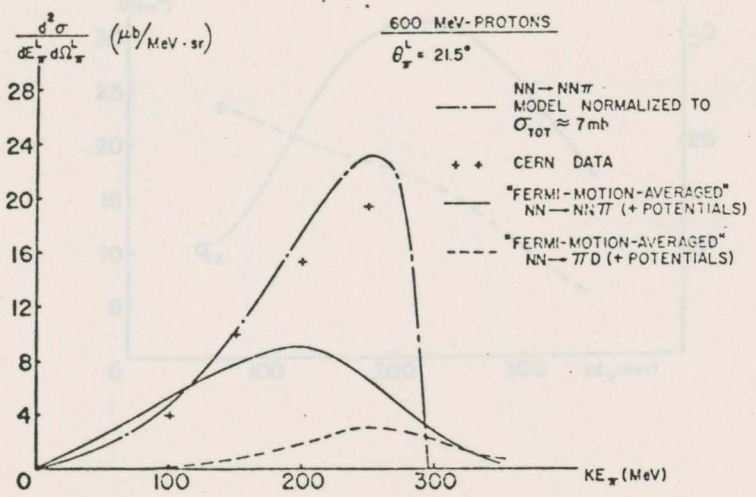

FIGURE 4.3

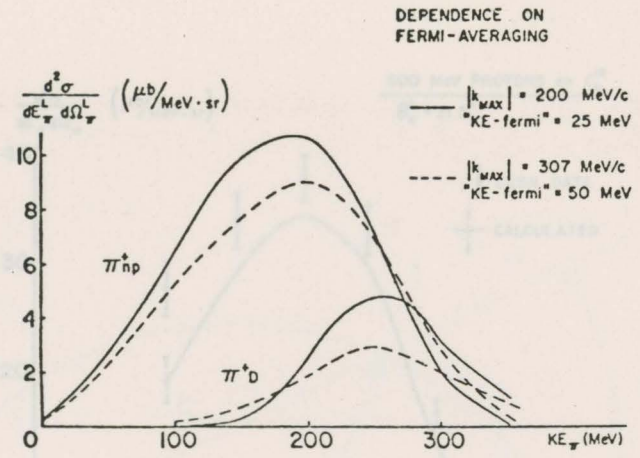

FIGURE 4.4

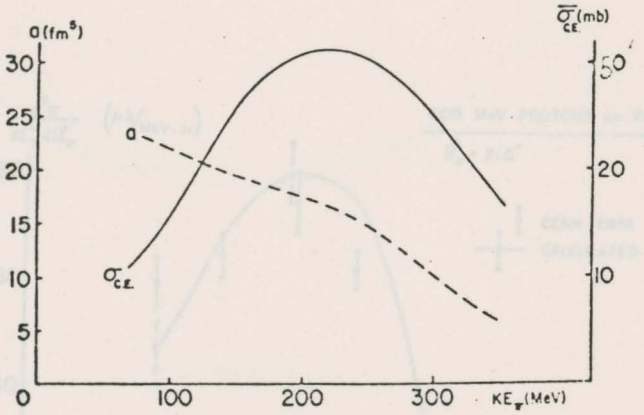

FIGURE 4.5

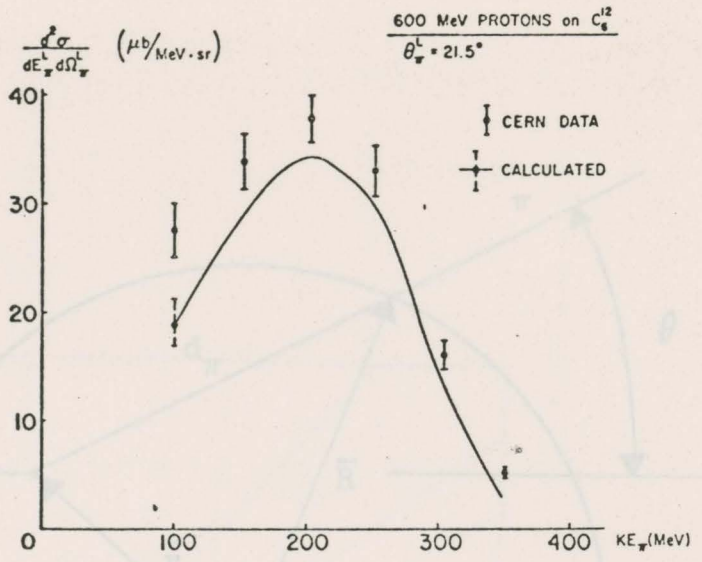

FIGURE 4.6

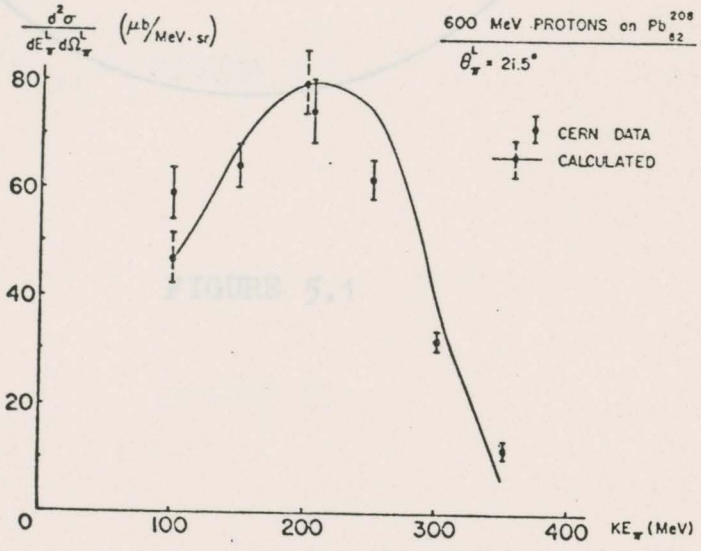

FIGURE 4.7

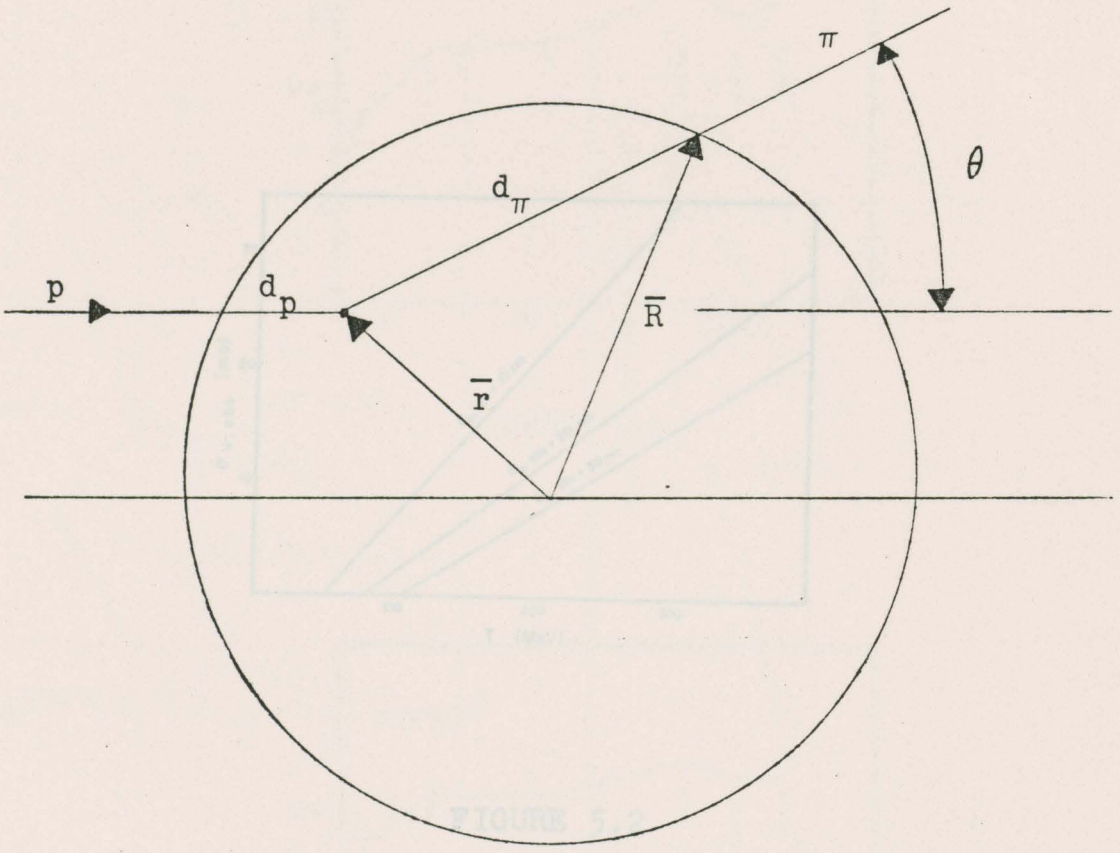

FIGURE 5.1

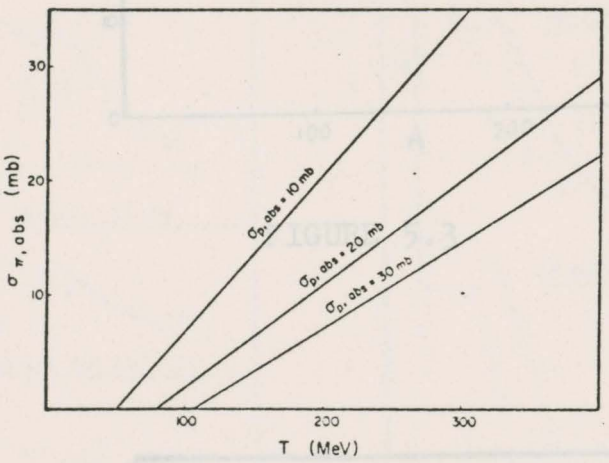
30
20
10
σ π, abs (mb)
σp, abs = 10 mb
σp, abs = 20 mb
σp, abs = 30 mb
100
200
300
T (MeV)

FIGURE 5.2

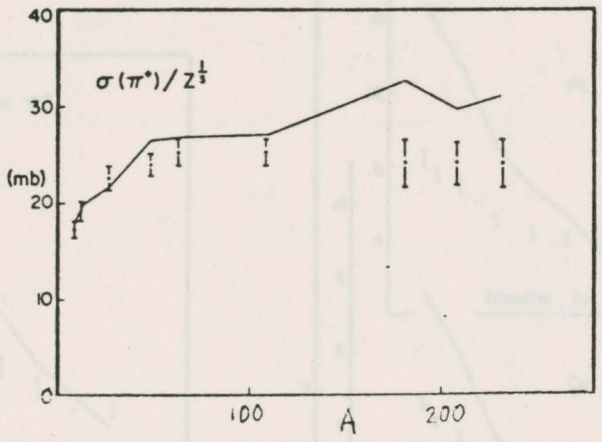

FIGURE 5.3

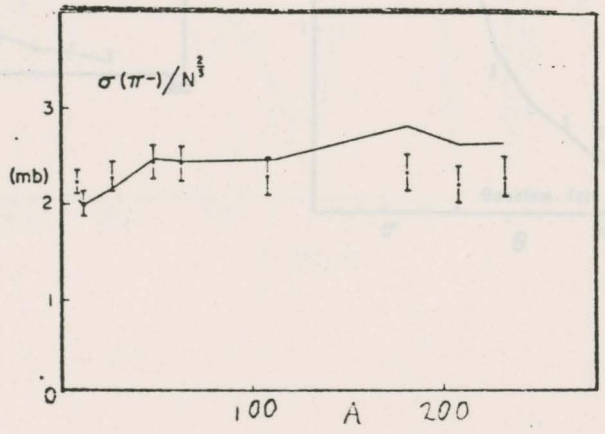

FIGURE 5.4

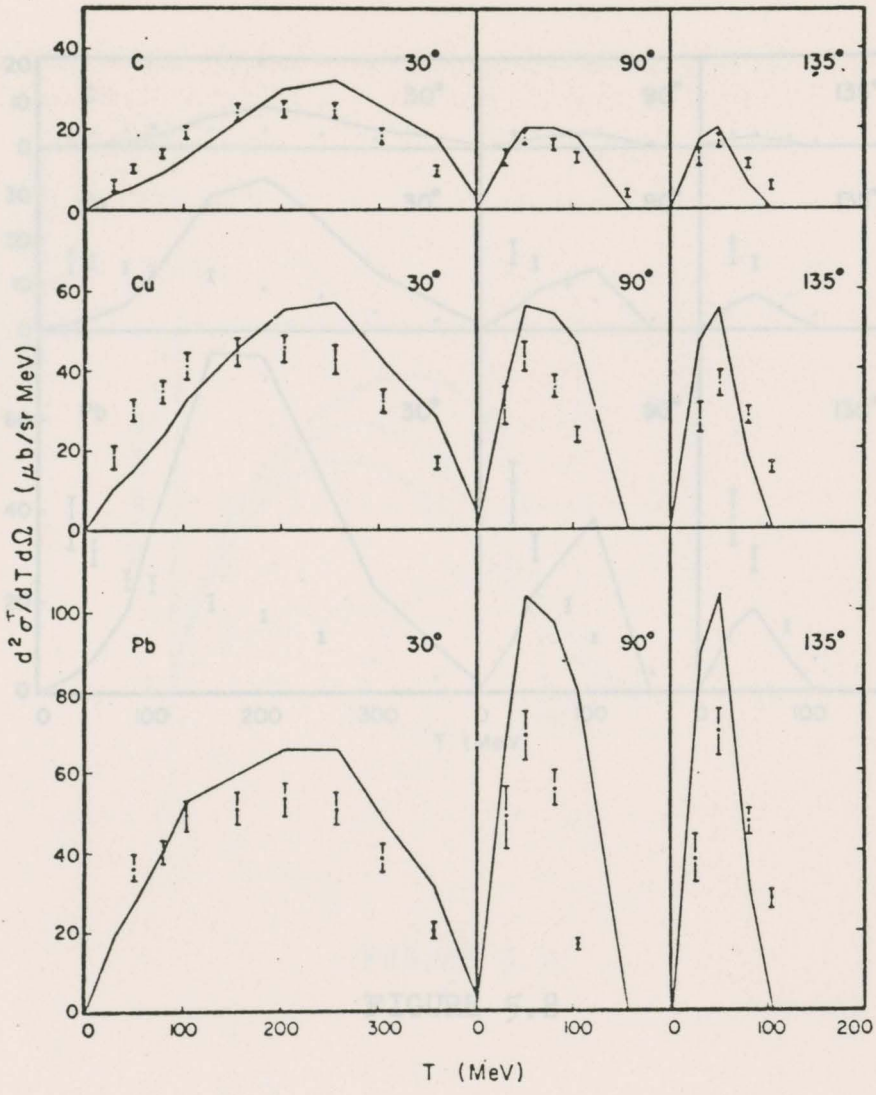
C
30°
90°
135°
Cu
30°
90°
135°
Pb
30°
90°
135°
$d^2\sigma/dT\,d\Omega$ (μb/sr MeV)
T (MeV)

FIGURE 5.7

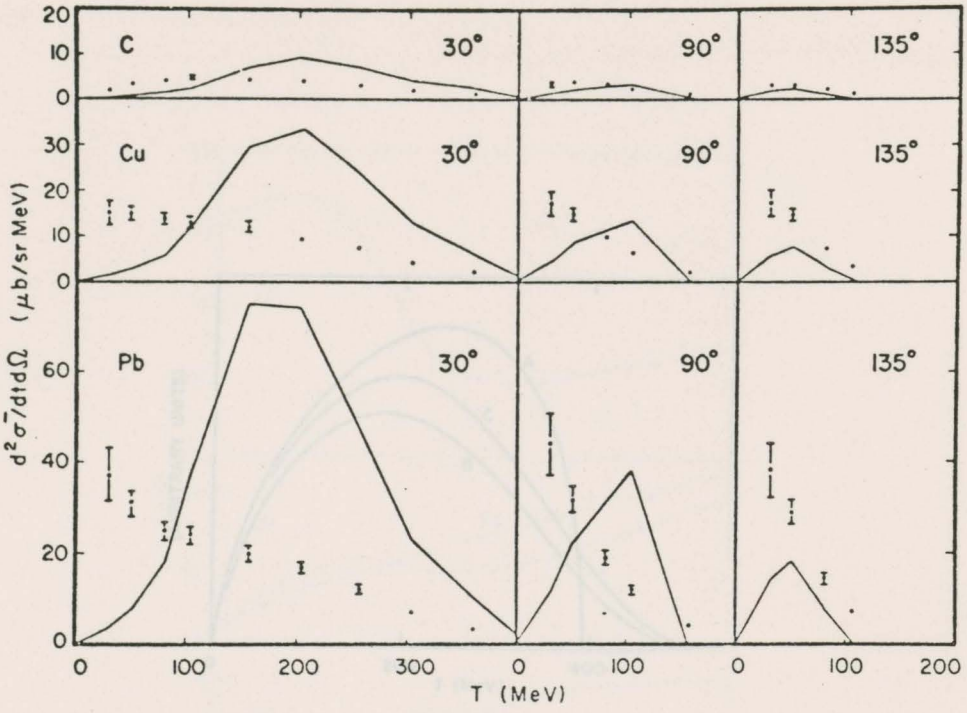

FIGURE 5.8

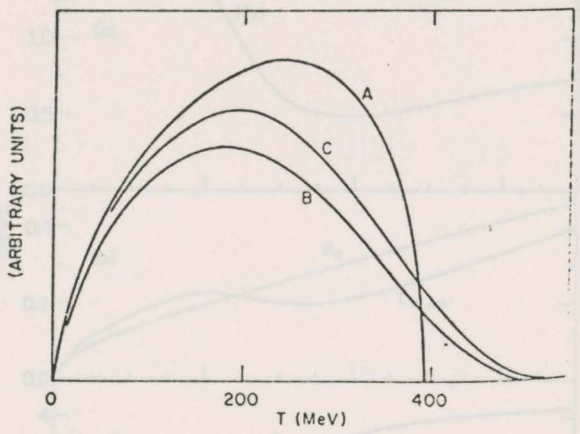

FIGURE 5.9

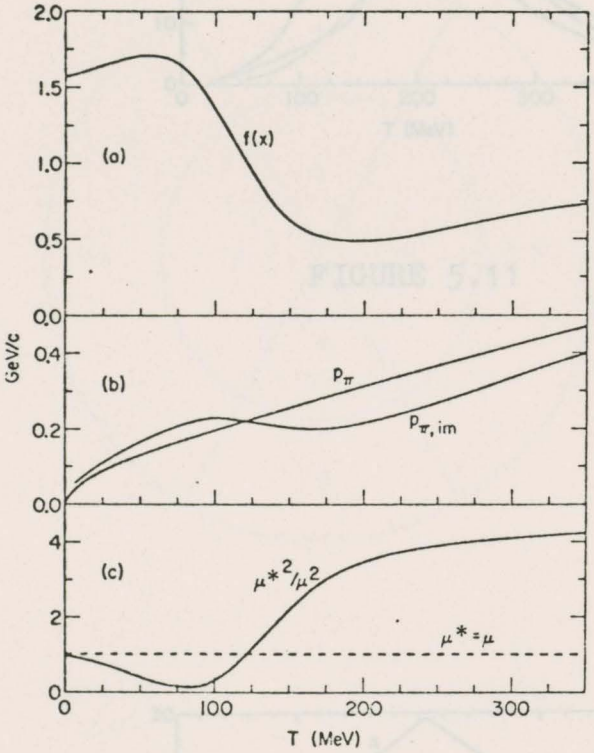
2.0
1.5
1.0
0.5
0.0
(a)
f(x)
GeV/c
0.4
0.2
0.0
(b)
p_π
$p_{\pi,im}$
4
2
0
(c)
μ^{*2}/μ^2
$\mu^* = \mu$
0
100
200
300
T (MeV)

FIGURE 5.10

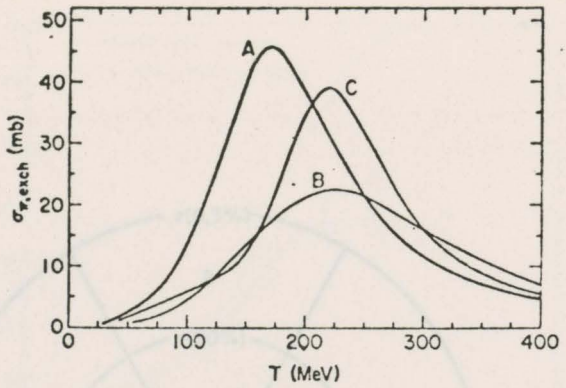

FIGURE 5.11

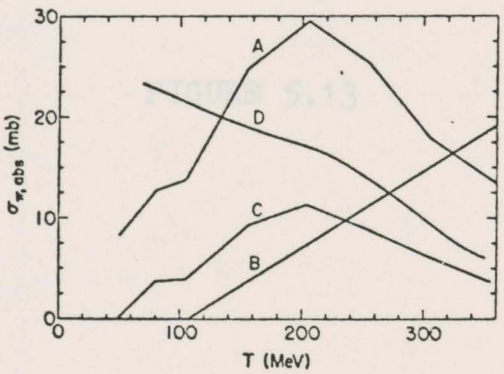

FIGURE 5.12

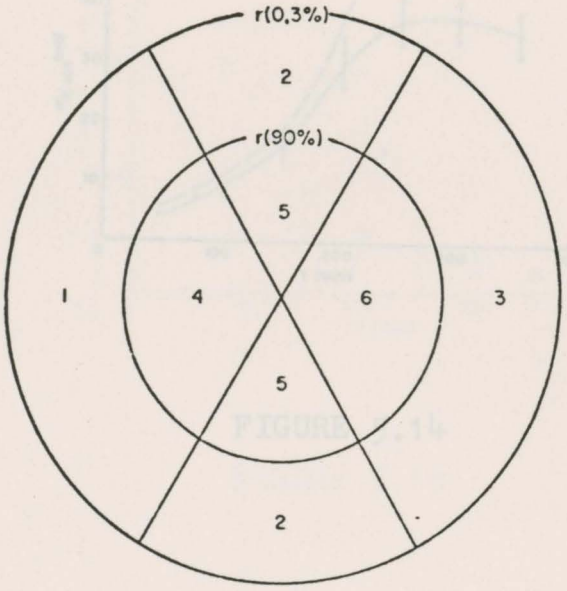

FIGURE 5.13

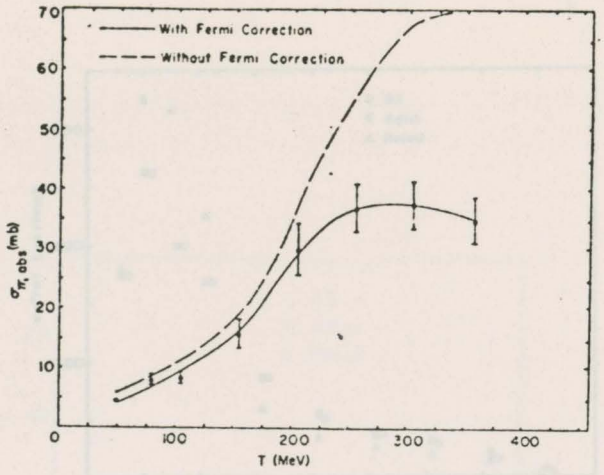

FIGURE 5.14

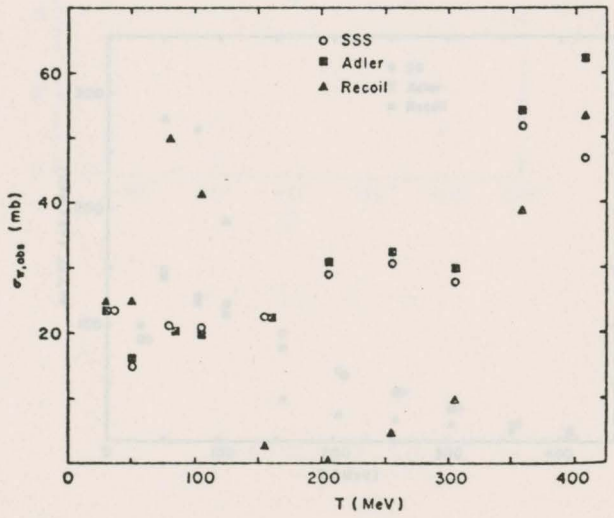

FIGURE 5.15

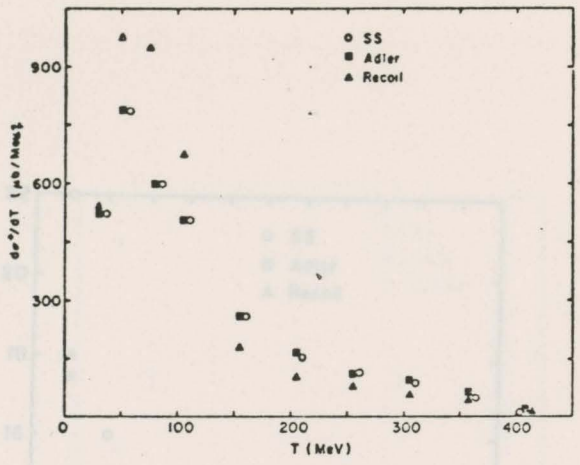

FIGURE 5.16

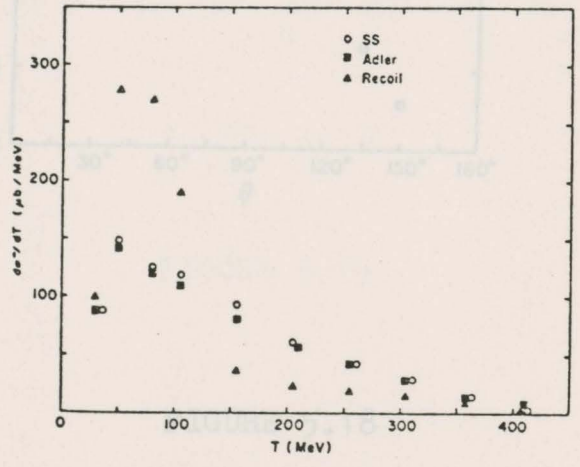

FIGURE 5.17

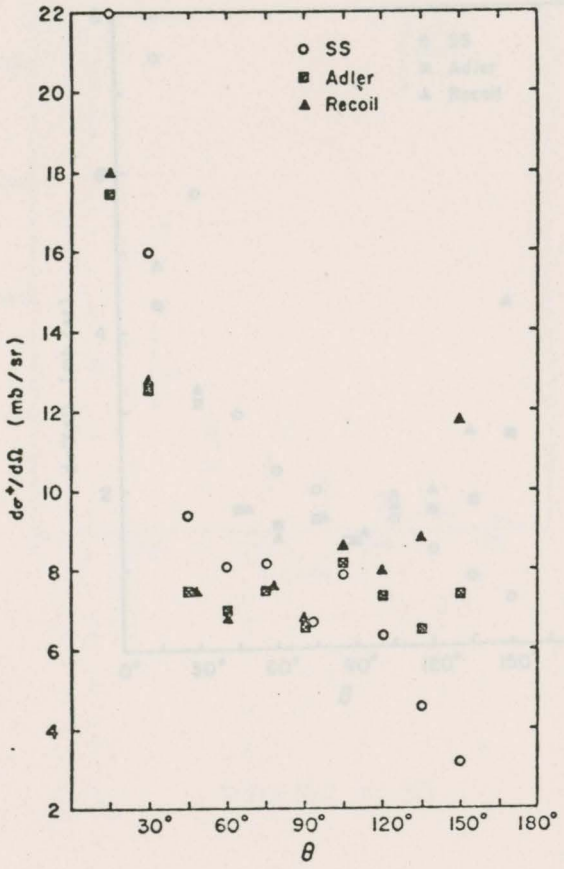
SS
Adler
Recoil
dσ⁺/dΩ (mb/sr)
θ
22
20
18
16
14
12
10
8
6
4
2
30°
60°
90°
120°
150°
180°

FIGURE 5.18

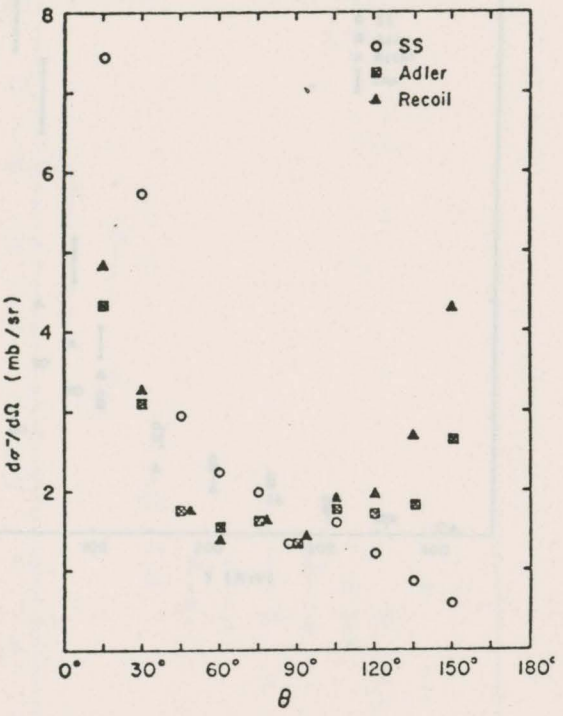

FIGURE 5.19

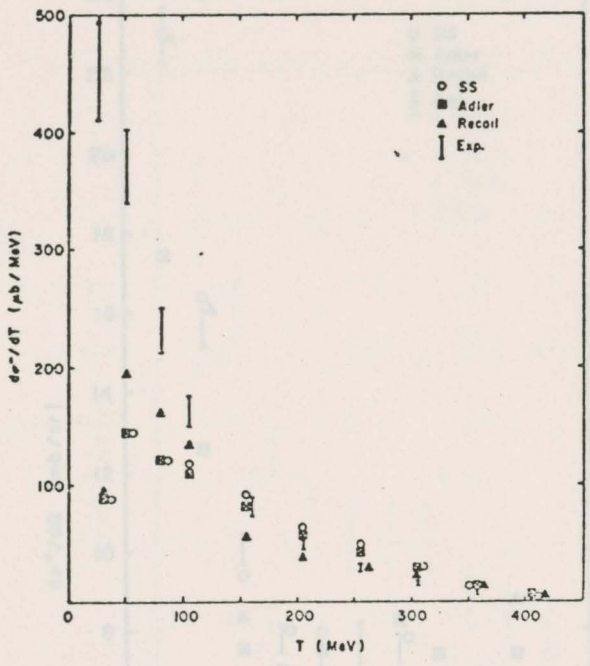
SS
Adler
Recoil
Exp.
dσ/dT (μb/MeV)
T (MeV)
500
400
300
200
100
0
100
200
300
400

FIGURE 5.20

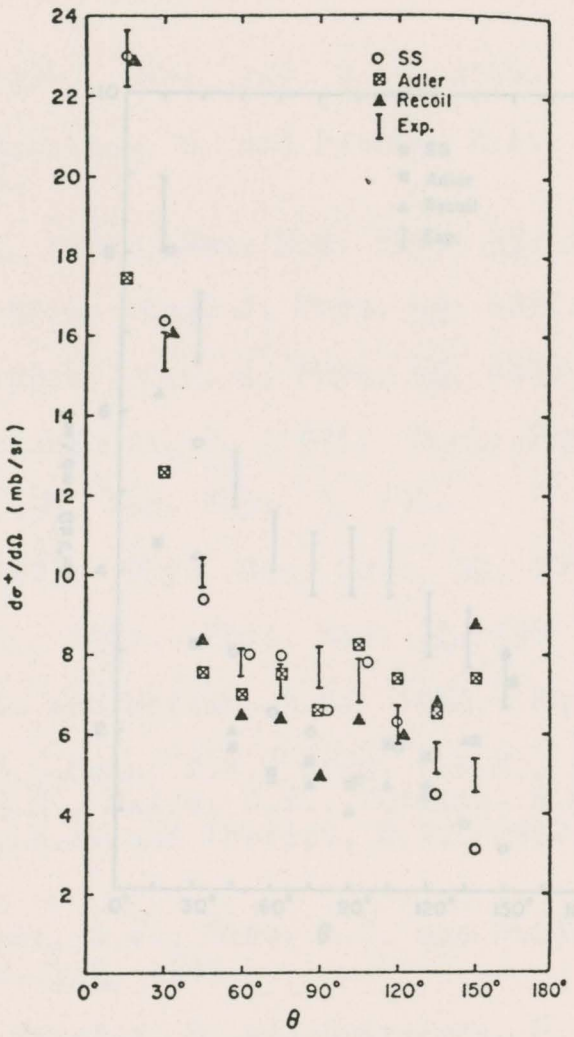
SS
Adler
Recoil
Exp.
24
22
20
18
16
14
12
10
8
6
4
2
0°
30°
60°
90°
120°
150°
180°
θ
dσ⁺/dΩ (mb/sr)

FIGURE 5.21

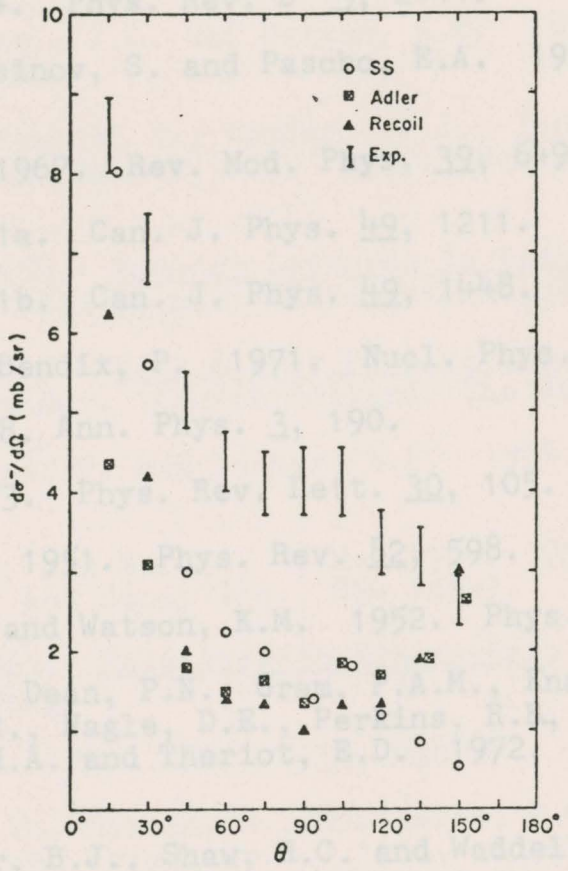

FIGURE 5.22

REFERENCES

Adler, S.L. 1974. Phys. Rev. D 9, 2144.

Adler, S.L., Nussinov, S. and Pascho, E.A. 1974. Phys. Rev. D 9, 2125.

Almadi Jr., U. 1967. Rev. Mod. Phys. 39, 649.

Beder, D.S. 1971a. Can. J. Phys. 49, 1211.

Beder, D.S. 1971b. Can. J. Phys. 49, 1448.

Beder, D.S. and Bendix, P. 1971. Nucl. Phys. B 26, 597.

Bethe, H.A. 1958. Ann. Phys. 3, 190.

Bethe, H.A. 1973. Phys. Rev. Lett. 30, 105.

Brueckner, K.A. 1951. Phys. Rev. 82, 598.

Brueckner, K.A. and Watson, K.M. 1952. Phys. Rev. 86, 923.

Cochran, D.R.F., Dean, P.N., Gram, P.A.M., Knapp, E.A., Martin, E.R., Nagle, D.E., Perkins, R.B., Schlaer, W.J., Thiessen, H.A. and Theriot, E.D. 1972. Phys. Rev. D 6, 3085.

Cohen, D., Moyer, B.J., Shaw, H.C. and Waddell, C.N. 1963. Phys. Rev. 130, 1505.

Dahlgren, S., Höistad, B. and Grafström, P. 1971. Phys. Lett. 35B, 219.

Dahlgren, S., Höistad, B., Grafström, P. and Åsberg, A. 1973a. Nucl. Phys. A 204, 53.

Dahlgren, S., Höistad, B., Grafström, P. and Åsberg, A. 1973b. Nucl. Phys. A 211, 243.

Dollhopf, W., Lunke, C., Perdisat, C.F., Roberts, W.K., Kitching, P., Olsen, W.C. and Priest, J.R. 1973. Nucl. Phys. A 217, 381.

Domingo, J.J., Allardyce, B.W., Ingram, C.H.Q., Rohlin, S., Tanner, N.W., Rohlin, J., Rimmer, E.M., Jones, G. and Giradeau-Montaut, J.P. 1970. Phys. Lett. 32, 309.

Eisenberg, J.M., Guy, R., Noble, J.V. and Weber, H.J. 1973. Phys Lett. 45, 93.

Fearing, H.W. 1975. Phys. Rev. C 11, 1210.

Fermi, E. 1950. Prog. Theor. Phys. (Japan) 5, 570.

Frank, R.M., Gammel, J.L. and Watson, K.M. 1956. Phys. Rev. 101, 891.

Gabathuler, K., Rohlin, J., Domingo, J.J., Ingram, C.H.Q., Rohlin, S. and Tanner, N.W. 1972. Nucl. Phys. B 40, 32.

Glauber, R.J. 1958. Boulder Lectures in Theoretical Physics. ed. W.E. Brittin et al. (Interscience, New York).

Glauber, R.J. 1967. High Energy Physics and Nuclear Structure. ed. G. Alexander. (North-Holland, The Netherlands).

Grossman, Z., Lenz, F. and Locher, M.P. 1974. Ann. Phys. 84, 348.

Goldberger, M.L. and Watson, K.M. 1964. Collision Theory. (John Wiley and Sons, Inc., New York).

Hagedorn, R. 1963. Relativistic Kinematics. (W.A. Benjamin, Inc., New York).

Harp, G.D. 1974. Phys. Rev. C 10, 2387.

Heer, E., Hirt, W., Martin, M., Michaelis, E.G., Serré, C., Skarek, P. and Wright, B.T. 1969. European Organization for Nuclear Research Report CERN 69-24.

Humble, S. 1974. Introduction to Particle Production in Hadron Physics. (Academic Press, New York).

Ingram, C.H.Q., Tanner, N.W., Domingo, J.J. and Rohlin, J. 1971. Nucl. Phys. B 31, 331.

Kolbig, K.S. and Margolis, M. 1968. Nucl. Phys. B 6, 85.

Lillethun, E. 1962. Phys. Rev. 125, 665.

Lindenbaum, S.J. and Sternheimer, R.M. 1957. Phys. Rev. 105, 1874.

Lindenbaum, S.J. and Sternheimer, R.M. 1958. Phys. Rev. 106, 1107.

Lock, W.O. and Measday, D.F. 1970. Intermediate Energy Physics. (Methuen and Co., Ltd., London).

Mandelstam, S. 1958. Proc. Roy. Soc. (London). A244, 491.

Margolis, B. 1968. Nucl. Phys. B 4, 433.

Mathie, E.L. 1976. Low Energy Pion Production by Protons with Incident Energies from 400 to 500 MeV. University of Victoria Master's thesis.

McMillin, D., Bhargava, P., Lam, L. and Vogt, E.W. 1968. Can. J. Phys. 46, 1141.

Oganesyan, K.O. 1968. Soviet Phys. JETP 27, 679.

Olsson, M.G. and Yodh, G.B. 1966. Phys. Rev. 145, 1309.

Omnès, R. 1970. Introduction to Particle Physics. (Wiley-Interscience, Toronto).

Peaslee, D.C. 1954a. Phys. Rev. 94, 1085.

Peaslee, D.C. 1954b. Phys. Rev. 95, 1580.

Reitan, A. 1971. Nucl. Phys. B 29, 525.

Reitan, A. 1972. Nucl. Phys. B 50, 166.

Reitan, A. 1976. Nuclear and Particle Physics at Intermediate Energies. ed. J.B. Warren. (Plenum Press, New York).

Rosenfeld, A.H. 1954a. Phys. Rev. 96, 130.

Rosenfeld, A.H. 1954b. Phys. Rev. 96, 139.

Ruderman, M. 1952. Phys. Rev. 87, 383.

Schillaci, M.E., Silbar, R.R. and Young, J.E. 1969. Phys. Rev. 179, 1539.

Schillaci, M.E. and Silbar, R.R. 1970. Phys. Rev. D 2, 1220.

Sokolov, A.A. 1964. Elementary Particles. (Pergamon Press, London).

Sparrow, D.A., Sternheim, M.M. and Silbar, R.R. 1974. Phys. Rev. C 10, 2215.

Sternheim, M.M. and Silbar, R.R. 1972. Phys. Rev. D 6, 3117.

Sternheim, M.M. and Silbar, R.R. 1973. Phys. Rev. C 8, 492.

Sternheimer, R.M. and Lindenbaum, S.J. 1961. Phys. Rev. 123, 333.

Vovchenko, V.G. 1966. Sov. J. Nucl. Phys. 3, 803.

Watson, K.M. 1952. Phys. Rev. 88, 1163.

Watson, K.M. 1953. Phys. Rev. 89, 575.

Watson, K.M. 1958. Rev. Mod. Phys. 30, 565.

Watson, K.M. and Brueckner, K.A. 1951. Phys. Rev. 83, 1.

Wick, G.C. 1955. Rev. Mod. Phys. 27, 339.

Wilkin, C. 1966. Phys. Rev. Lett. 17, 561.

Williams, W.S.C. 1961. An Introduction to Elementary Particles. (Academic Press, New York).

Yang, K.H., Sparrow, D.A., Holstein, B.R. and Sternheim, M.M. 1976. Phys. Rev. C 14, 1083.

Yuan, L.C.L. and Lindenbaum, S.J. 1956. Phys. Rev. 103, 404.

APPENDIX A

THE NUCLEON-NUCLEON INTERACTION

From the extended Pauli Principle, the 2-nucleon system must be in an overall antisymmetric state with respect to space, spin and isospin.

Symmetry			Spectroscopic	Interacting
Space	Spin	Isospin	Classification	System
s	s	a	$^3S_1$ $^3D_{1,2,3}$	np
s	a	s	$^1S_0$ $^1D_2$	pp, nn, np
a	s	s	$^3P_{0,1,2}$ $^3F_{2,3,4}$	pp, nn, np
a	a	a	$^1P_1$ $^1F_3$	np

where a denotes antisymmetric and s denotes symmetic, and where for isospin: T=1 $\Rightarrow$ s and T=0 $\Rightarrow$ a, for spin: S=1 $\Rightarrow$ s and S=0 $\Rightarrow$ a, for space: l even $\Rightarrow$ s and l odd $\Rightarrow$ a.

The nucleon-nucleon system can also be classified in terms of isospin:

Spectroscopic Classification	Interacting System	Total Isospin T	T_3
$^1P_1$ $^1F_3$ $^3S_1$ $^3D_{1,2,3}$	np	0	0
$^1S_0$ $^1D_2$ $^3P_{0,1,2}$ $^3F_{2,3,4}$	pp	1	1
	np	1	0
	nn	1	-1

The allowed partial waves in nucleon-nucleon scattering are easily calculated for given T, J:

J	T=0	T=1
0	-	$^1S_0$, $^3P_0$
1	$^1P_1$, $^3S_1$ ε_1 $^3D_1$	$^3P_1$
2	$^3D_2$	$^1D_2$, $^3P_2$ ε_2 $^3F_2$
3	$^1F_3$, $^3D_3$ ε_3 $^3G_3$	$^3F_3$
4	$^3G_4$	$^1G_4$, $^3F_4$ ε_4 $^3H_4$

where the ε_J are mixing parameters due to two states having the same J and the same parity, ie. l is not a constant of the motion although J is.

VITA

Surname: LIM Given Names: DIANA JOYCE

Place of Birth: THUNDER BAY, ONT. Date of Birth: November 25, 1948

Educational Institutions Attended, with Dates of Entering and Leaving:

UNIVERSITY OF WESTERN ONTARIO, LONDON 1967 to 1971

UNIVERSITY OF VICTORIA, VICTORIA 1973 to 1977

____ to ____

Degrees, Diplomas, Etc., Awarded, with Dates and Names of Institutions:

B.Sc. (Honours) 1974 University of Western Ontario, London

Honours and Awards:

Ontario Student Award, 1967/68

Steel Company of Canada Bursary, 1967/68, 1968/69, 1969/70, 1970/71

PARTIAL COPYRIGHT LICENCE

I hereby grant the right to lend my thesis or dissertation (the title of which is shown below) to users of the University of Victoria Library, and to make single copies only for such users or in response to a request from the library of any other university, or similar institution, on its behalf or for one of its users. I further agree that permission for extensive copying of the thesis for scholarly purposes may be granted by me or a member of the University designated by me. It is understood that copying or publication of this thesis for financial gain shall not be allowed without my written permission.

Title of Thesis/Dissertation

A REVIEW OF PHENOMENOLOGICAL MODELS FOR PION PRODUCTION ON NUCLEI WITH PROTONS INCIDENT AT INTERMEDIATE ENERGIES

Author [redacted]

Diana J. Lim

Sept. 15, 1977.